ANATOMY

CARSTEN LÜTER
[Museum für Naturkunde der Humboldt-Universität zu Berlin]

INTRODUCTION

The following chapter contains new findings on brachiopod anatomy since the publication of volume 1 of the revised *Treatise* (WILLIAMS & others, 1997). The chapter's structure follows that of the anatomy section in volume 1. Where necessary, new subheadings were introduced. Some new results not only update the anatomy section but also contradict former interpretations given by WILLIAMS and others (1997). Whenever new results have led to new interpretations, the qualified section in volume 1 is cited. This gives the reader the opportunity for comparison and also provides a living picture of the progress being made in brachiopod research.

During the last decade brachiopod embryology and development have been studied in detail in order to understand the origin and formation of certain organ systems like metanephridia, nerve system or mesoderm, and coelom. The results of these investigations clearly show that brachiopod anatomy can hardly be understood without knowledge of the developmental processes leading to observations of adult morphology. Additionally, morphological characters of larval and juvenile brachiopods may provide a reliable set of hitherto unused soft tissue character sets, which are invaluable for future analyses of brachiopod phylogeny. Here, Fritz MÜLLER's drawing from 1859 may be reminiscent of the beginning of brachiopod developmental research (Fig. 1500).

MANTLES AND BODY WALLS

MARGINAL (LARVAL AND ADULT) SETAE

The ultrastructural reinvestigation of marginal setae in subadult *Lingula anatina* and the subsequent comparison with and new findings on setae growing from setal sacs in lecithotrophic larvae of rhynchonelliforms and early developmental stages of *Discinisca* sp. cf. *tenuis* showed differences not only in diameter of the setae of larvae and adults (see WILLIAMS & others, 1997, p. 52), but also in their composition and the secretory regime of the chaetoblast (LÜTER, 1998b, 2000b, 2001a). While *Lingula anatina*, when in its planktonic stage, does not possess any marginal setae, setal growth in the lecithotrophic larvae of, for example, the rhynchonelliform brachiopods *Notosaria nigricans* and *Calloria inconspicua* commences after mantle lobe formation during their early larval phase. As outlined by many authors, the setae of these larvae are arranged in four setal bundles (a dorsal pair and a dorsolateral pair).

In general, the overall architecture of brachiopod setae is the same in both larvae and adults, but the origin of the setal material and the composition of the epidermal invagination housing these setae is different. In postmetamorphic stages of brachiopods (juveniles to adults), each seta (called adult seta hereafter) is located in an epidermal or ectodermal invagination of cells, called the setal follicle (Fig. 1501). At the bottom of this follicle, the cup-shaped chaetoblast secretes setal material at the basis of its apical microvilli. These microvilli are of almost identical length and serve as a template for the future inner structure of the growing seta. Distally, the adult seta is accompanied by several follicle cells (the epidermal cellular lining of the follicle), which are also involved in setal construction. Comparable to the invaginated apical cell surface of the chaetoblast, each follicle cell bears an apical row of microvilli. These microvilli are connected to the setal surface by intermediate filaments (Fig. 1502a), which are cytokeratin components of the cytoskeleton (not chitinous fibers as assumed by WILLIAMS & others, 1997). These intermediate filaments run from cell-matrix contacts

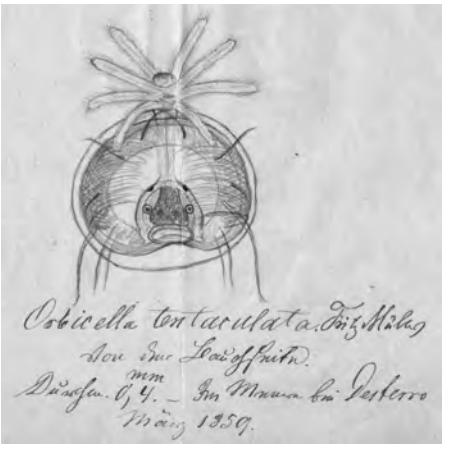

FIG. 1500. First picture of a brachiopod developmental stage, a pelagic juvenile of a discinid, drawn by Fritz Müller in a letter to his friend Max Schultze in March 1859; Müller wrote that the relationship to brachiopods is obvious, but he could not decide whether it was a larva of a brachiopod or not, mainly because he had not seen any adult brachiopods at the Desterro coast; provisionally, he named the new animal "*Orbicella tentaculata;*" in 1860 Müller described his new animal as the larva of a brachiopod, and his original lead pencil drawing was used as an illustration (Müller, 1860, taf. 1B,*2;* original letter courtesy of H. Lorenzen, Bovenden, Germany).

(hemidesmosomes) at each follicle cell's basal membrane through the cell body toward the tips of the microvilli, where they end in a hemidesmosome-like connective structure between the cell membrane and the extracellular setal material (Fig. 1502a). Due to their stiff texture, intermediate filaments provide a rather inelastic but strong connection between extracellular matrices and cells, so that the adult setae in *Lingula anatina* can be moved by contraction of well-developed muscle cells surrounding the setal follicle.

As stated correctly in volume 1 (WILLIAMS & others, 1997), the follicle cells are involved in the construction of each adult seta by secreting its outermost layer. In *Lingula anatina* this outermost layer consists of four sheets of setal material with differing electron density (Fig. 1502b; LÜTER, 2000b).

GUSTUS and CLONEY (1972) stated that the outermost setal layer, which they called enamel, is missing in brachiopod setae, but they were looking at lecithotrophic larvae of the rhynchonelliform brachiopod *Terebratalia transversa* and, similar to all other brachiopod larvae investigated so far, their larval setae indeed lack this outermost layer due to the differences in construction of brachiopod adult and larval setae (for definition of the term brachiopod larva, see Embryology and Development, p. 2339 herein).

With the exception of larvae of Thecideoidea and those of the terebratellides *Argyrotheca cistellula* (see GROBE & LÜTER, 1999) and *Macandrevia cranium* (see D'HONDT & FRANZEN, 2001) all brachiopod larval stages studied so far do have setae (called larval setae hereafter) of similar construction but differing arrangement. Early developmental stages of the linguliforms *Discinisca* sp. cf. *tenuis* from Namibia (LÜTER, 2001a) and *Discinisca strigata* from Panama (FREEMAN, 1999) have one pair of terminal bundles of larval setae, all rhynchonelliform brachiopod larvae (except those without setae) have two pairs of setal bundles (a dorsal and a dorsolateral pair), and those of the craniiform *Novocrania anomala* have three dorsal pairs of larval setae (NIELSEN, 1991).

Larval setae are exclusively produced by the chaetoblast. Several chaetoblasts are arranged in a cup-shaped invagination of the larval epidermis, the so-called setal sac. Either two (discinides), four (all rhynchonelliforms), or six (*Novocrania*) setal sacs can be found in the larvae. The process of production and release of setal material and the arrangement of the chaetoblast's apical microvilli forming a template for the inner setal structure are similar in both adults and larvae. The major difference is the lack of follicle cells in the larval epidermis. Larval setae in *Discinisca* sp. cf. *tenuis*, *Novocrania anomala*, *Notosaria nigricans,* and *Calloria inconspicua*, representing four Recent brachiopod superfamilies, have been observed to be accompanied only by a single epidermal cell (apart from the chaetoblast itself) before emerging from the larval body (Fig. 1503.1–1503.4; NIELSEN, 1991; LÜTER, 1998b, 2000b, 2001a; GROBE, 1999). This specialized epidermal cell looks like a thick-walled

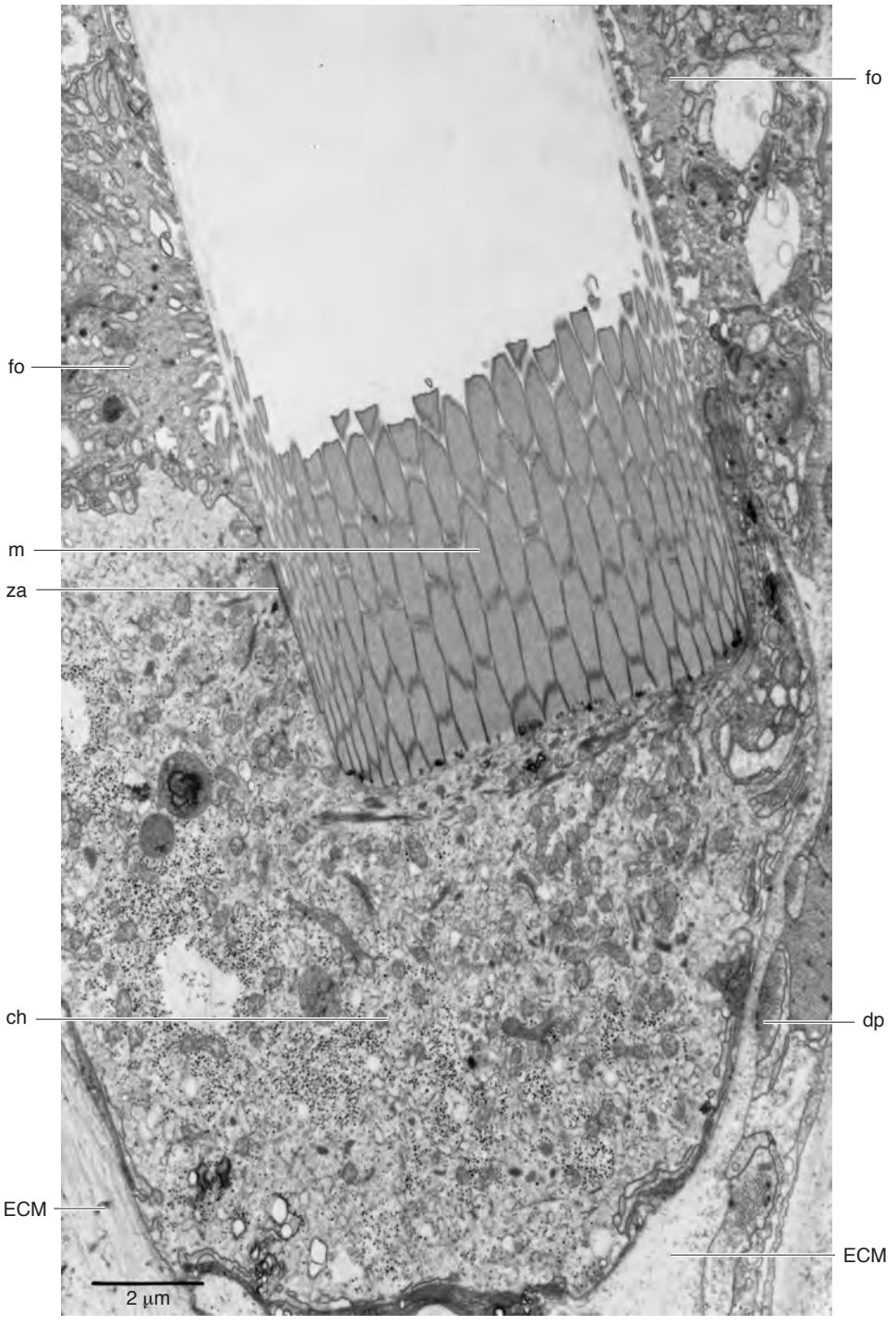

FIG. 1501. TEM micrograph of longitudinal section of setal follicle of *Lingula anatina*; chaetoblast (*ch*) is surrounded by collagenous extracellular matrix (*ECM*) and epithelial muscle cells connected to extracellular matrix by so-called dense plaques (*dp*); basal part of each setal canal filled with a microvillus (*m*). Adjacent to chaetoblast, follicle cells (*fo*) connect to setal surface through apical microvilli; *za*, zonula adhaerens (Lüter, 1998b).

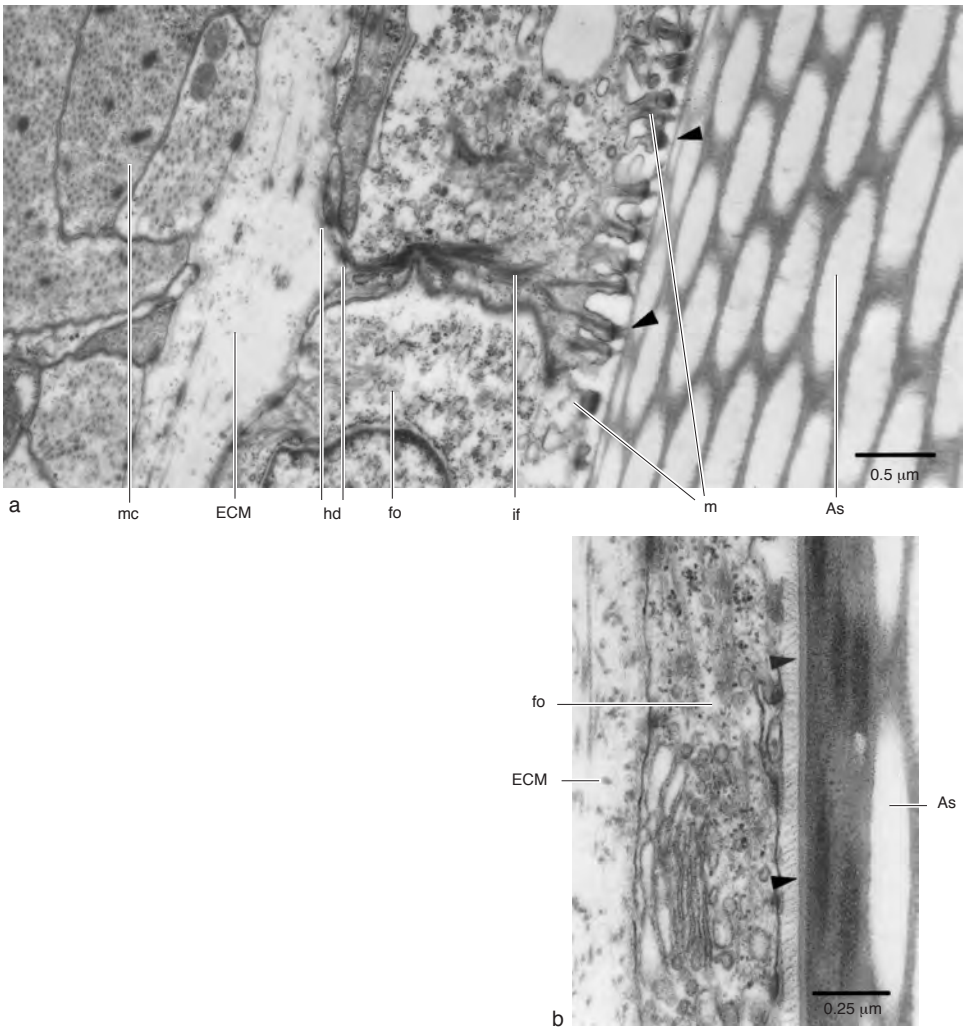

FIG. 1502. TEM micrographs of adult setae (*As*) of *Lingula anatina; a*, intermediate filaments (*if*) of follicle cells (*fo*) connect extracellular matrix and setal surface through basal hemidesmosomes (*hd*) and apical, hemidesmosomal-like contacts (*arrowheads*) at tips of follicle cell's microvilli (*m*); *b*, outer or enamel layer of adult seta consisting of four layers with differing electron density (*arrowheads*); *ECM*, extracellular matrix (Lüter, 2000b).

FIG. 1503. Reconstructions of brachiopod larval setae based on TEM cross sections; only two cells are involved, the chaetoblast and one specialized epidermal cell; *1*, larval seta (*ls*) of *Discinisca* sp. cf. *tenuis*; notice contact between specialized epidermal cell (*Epi*) and spine of larval seta (*arrow*) (Lüter, 2001a); *2*, larval seta of *Novocrania anomala*; the specialized epidermal cell (*Epi*) still produces a cilium (*Ci*), which runs parallel to larval seta through cell's tubelike canal; the microvilli of specialized epidermal cell do not contact larval setal surface (Grobe, 1999); *3*, larval seta (*Ls*) of *Notosaria nigricans;* setal spines (*sp*) of larval setae are made from setal material released by peripheral microvilli; *4*, larval seta (*Ls*) of *Calloria inconspicua*; next to specialized and invaginated epidermal cell (*inec*) a collar receptor cell (*co*) can be found; notice synaptic contact (*arrowhead*) of basal process of collar receptor cell to basiepidermal nerve cells (*nc*); *ch*, chaetoblast; *Coea*, cell of coelomic anlage; *ECM*, extracellular matrix; *mf*, myofilaments; *za*, zonula adhaerens (Lüter, 2000b).

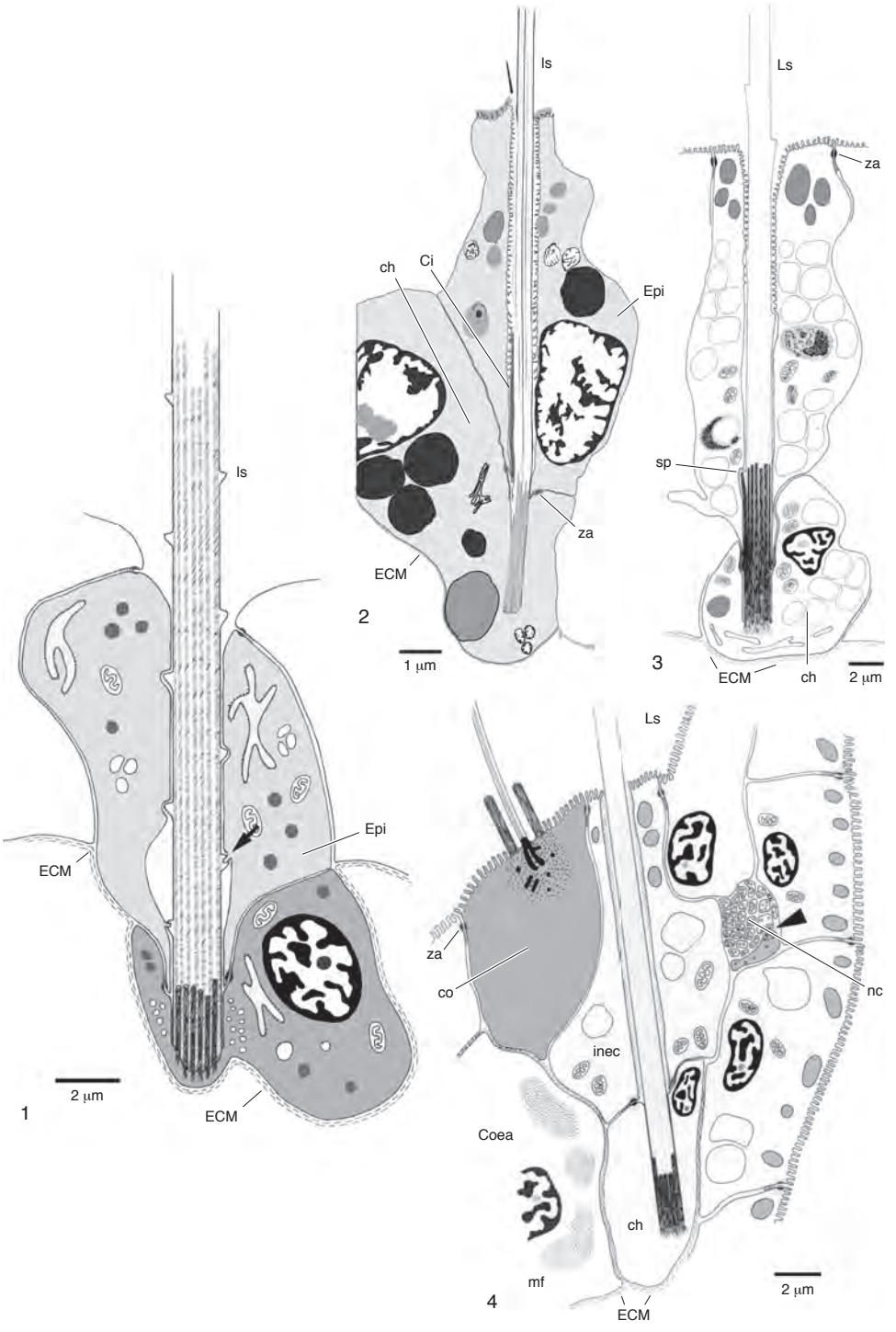

FIG. 1503. *For explanation, see facing page.*

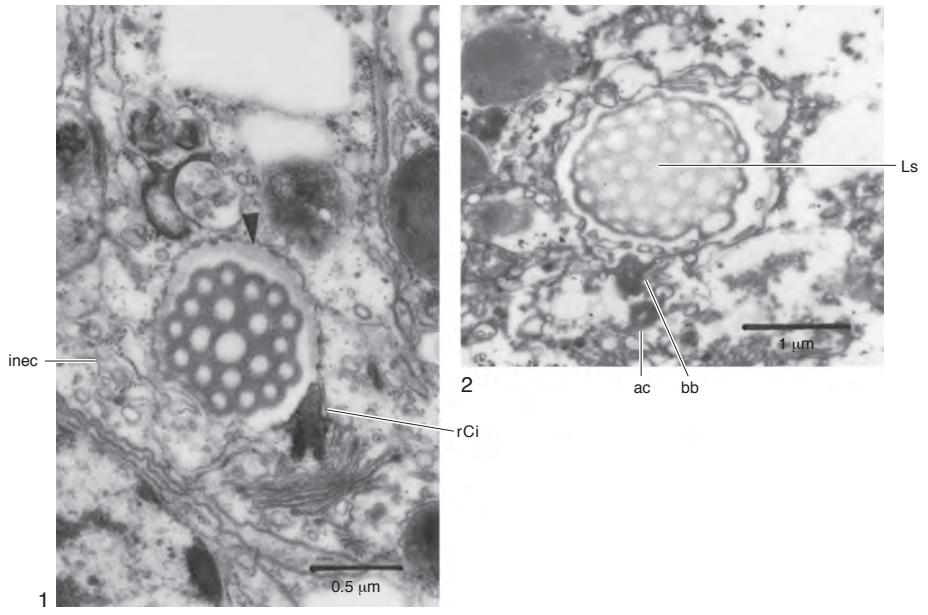

FIG. 1504. TEM micrographs of larval setae with accompanying rudimentary cilium; *1*, cross section of larval seta of *Calloria inconspicua*; specialized and invaginated epidermal cell (*inec*) bearing a rudimentary cilium (*rCi*); notice the glycocalyx (*arrowhead*) on cell surface; *2*, cross section of larval seta (*Ls*) of *Notosaria nigricans*; notice basal body (*bb*) and accessory centriole (*ac*) of rudimentary cilium (Lüter, 2000b).

tube, with its wall built by the cell soma. The longitudinal tubelike perforation enables the larval seta to pass through the cell toward the outside. In the tube the cell membrane of the specialized cell has no connection to the setal surface. Even if short microvilli are present, which in *Discinisca* sp. cf. *tenuis* can touch the setal surface, hemidesmosome-like connecting structures, as described for a setal follicle in adult brachiopods, cannot be observed. Additionally, each specialized cell surrounding a larval seta bears a rudimentary apical cilium, which projects into the tubelike perforation. Such a rudimentary cilium was already documented by NIELSEN (1991, fig. 12A–C) for the larva of *Novocrania anomala,* and its presence was confirmed by GROBE (1999). LÜTER (1998b, 2000b, 2001a) found this cilium also in the specialized cells of *Discinisca* sp. cf. *tenuis*, *Notosaria nigricans,* and *Calloria inconspicua* (Fig. 1504.1–1504.2).

Since follicle cells and their microvillous connection to the (adult) setal surface are responsible for production of the outermost setal layer, the latter is absent in brachiopod larval setae. In *Discinica* sp. cf. *tenuis* the specialized epidermal cell is folded around each larval seta so that a double cell membrane can be observed where the two sides of the cell are connected to each other. In rhynchonelliform brachiopod larvae and *Novocrania* (LÜTER, 2000b; GROBE, 1999), each larval seta runs through the cell, with the tube forming during setal growth as a subsequent invagination (from inside to outside) of the epidermal cell's membrane. In contrast to adult setae, the larval equivalent is not connected to the accompanying cells (except the basal connection to the chaetoblast), and therefore active movement of setae by muscle contraction is impossible. Spreading of larval setae, observed in all larvae as possible defending behavior, is provided by complete contraction of the animal's longitudinal muscles. The resulting pressure within the body cavity forces the deeply invaginated setal sacs to shift toward the body surface. The epidermal layer is thereby stretched out like the rubber

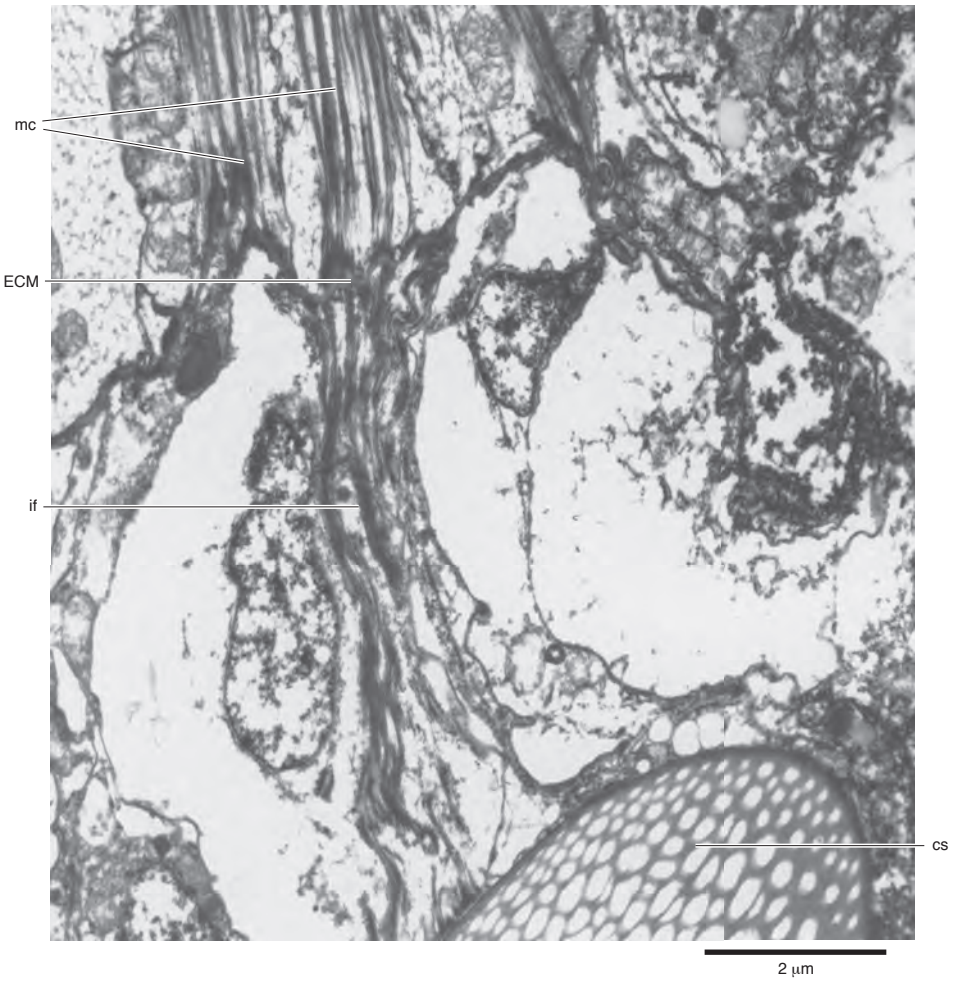

FIG. 1505. TEM micrograph of intermediate filaments (*if*) connecting curved seta (cs) of pelagic juvenile of *Discinisca* sp. cf. *tenuis* with extracellular matrix (*ECM*) surrounding setal follicle; notice close contact of follicle cell's intermediate filaments (*if*) and epithelial muscle cells (*mc*) (new).

membrane of a squeezed balloon, leading to a passive process of setal spreading.

In contrast to the pelagic juveniles of linguloid brachiopods, the bivalved developmental stages of *Discinisca* sp. cf. *tenuis* develop five pairs of special marginal setae, which outreach the setae of the usual marginal setal fringe in both length and diameter. They were called curved setae by CHUANG (1977) or juvenile setae in WILLIAMS and others (1997). CHUANG separated them, together with what he called flexible setae of the mantle margin, from the larval setae of the unshelled earlier stages. These curved setae are clearly adult setae (see above). They are built within a setal follicle consisting of a basal chaetoblast and an adjacent row of follicle cells. The follicle cells are connected to the setal surface by intermediate filaments (Fig. 1505), and the ultrastructure of these setae is identical with the ultrastructure of marginal setae of already sessile linguloid brachiopods.

The most prominent pair of these curved setae appears at the caudal margin of the mantle. In dorsal view these setae are

somewhat shaped like an inverted S. The tip of these setae has a prickly appearance in SEM pictures due to little spines covering the seta. These spines are products of peripheral microvilli of the chaetoblast, and they can also be found on larval setae of various groups and on the surface of adult setae of *Lingula anatina* for example. The growth process of adult setae is basically the same in all brachiopods: when the seta starts growing, the template for the first setal canals is built by only a few apical microvilli of the chaetoblast. Broadening the seta requires more microvilli in the periphery of the already-secreted setal material. In *Lingula anatina*, the chaetoblast's acquisition of peripheral microvilli is a highly coordinated process, which leads to a horsetail-like appearance of the setae, with peripheral setal canals ending up in a circle of spines (Fig. 1506; LÜTER, 1998b, 2000b). In the pelagic juvenile of *Discinisca* sp. cf. *tenuis,* every now and then a single peripheral microvillus is added to the chaetoblast's apical cell surface, having the effect that the spines on the curved setae are irregularly distributed over the setal surface. This has been shown for the adult marginal setae of *Discina striata* in WILLIAMS and others (1997, p. 53, fig. 47.2).

EXCRETORY SYSTEM

Brachiopods have one pair of metanephridia, except for rhynchonelloids, which have two pairs. In mature animals, the metanephridia additionally serve as gonoducts. Their excretory function can only be proven indirectly by ultrastructural details of the epithelial cells involved (LÜTER, 1995, 1998b). In principal, metanephridia are open canals connecting the secondary body cavity (coelom) and the outer medium. Such an open canal *per se* cannot work as an excretory organ. It directly depends on the process of ultrafiltration into the body cavity from an at least partly closed blood circulation system bounded by extracellular matrix (ECM). Blood pressure drives the filtration process by forcing low molecular waste molecules through the vessel-surrounding ECM. On the coelomic side, areas of filtration are characterized by a specialized coelomic epithelium with either gaps between single epithelial cells (fenestrated epithelium) or with podocytes. Both gaps and podocytes provide a direct neighborhood of blood vessels and the body cavity, separated only by a thin molecular sieve consisting of the fibrillar network of the ECM. So far, these filter structures have not been observed in brachiopods. It is therefore unclear whether metanephridia in brachiopods are functional excretory organs or not (LÜTER, 1995, 1998b).

On the other hand, the metanephridia show ultrastructural details typical for cells resorbing metabolites during excretion. Each metanephridium can be separated in two parts: a funnel-shaped nephrostome facing the body cavity and an outleading canal, open to the outer medium through a nephridiopore. In adult *Novocrania anomala* and *Terebratulina retusa*, one can observe a gradual change in the shape of the cells from the funnel toward the canal so that a distinction between funnel epithelium and canal epithelium is difficult (Fig. 1507; LÜTER, 1995). Pelagic juveniles of *Lingula anatina* (with six pairs of tentacles) already have fully developed metanephridia, and a distinction is possible. Five to seven cuboid nephrostome cells along the prospective funnel can be observed. In this early stage of development the funnel-like shape is not yet developed (Fig. 1508a). The prospective epithelial cells of the nephridial funnel can be distinguished from the coelomic epithelium by their lack of contractile filaments in the cytoplasm. In cross section, the prospective funnel is built by two nephrostome cells (Fig. 1508b). Additionally, the nephrostome cells have, if at all, very few, short microvilli extending into the lumen of the prospective funnel (Fig. 1508b). The cells of the canal epithelium look completely different. They are very large cells, with their cell apices extended into a dense row of very long microvilli (Fig. 1508c–1508d). At the base of these microvilli many coated pits and coated vesicles can be observed—a sign of active resorption from the lumen of the outleading

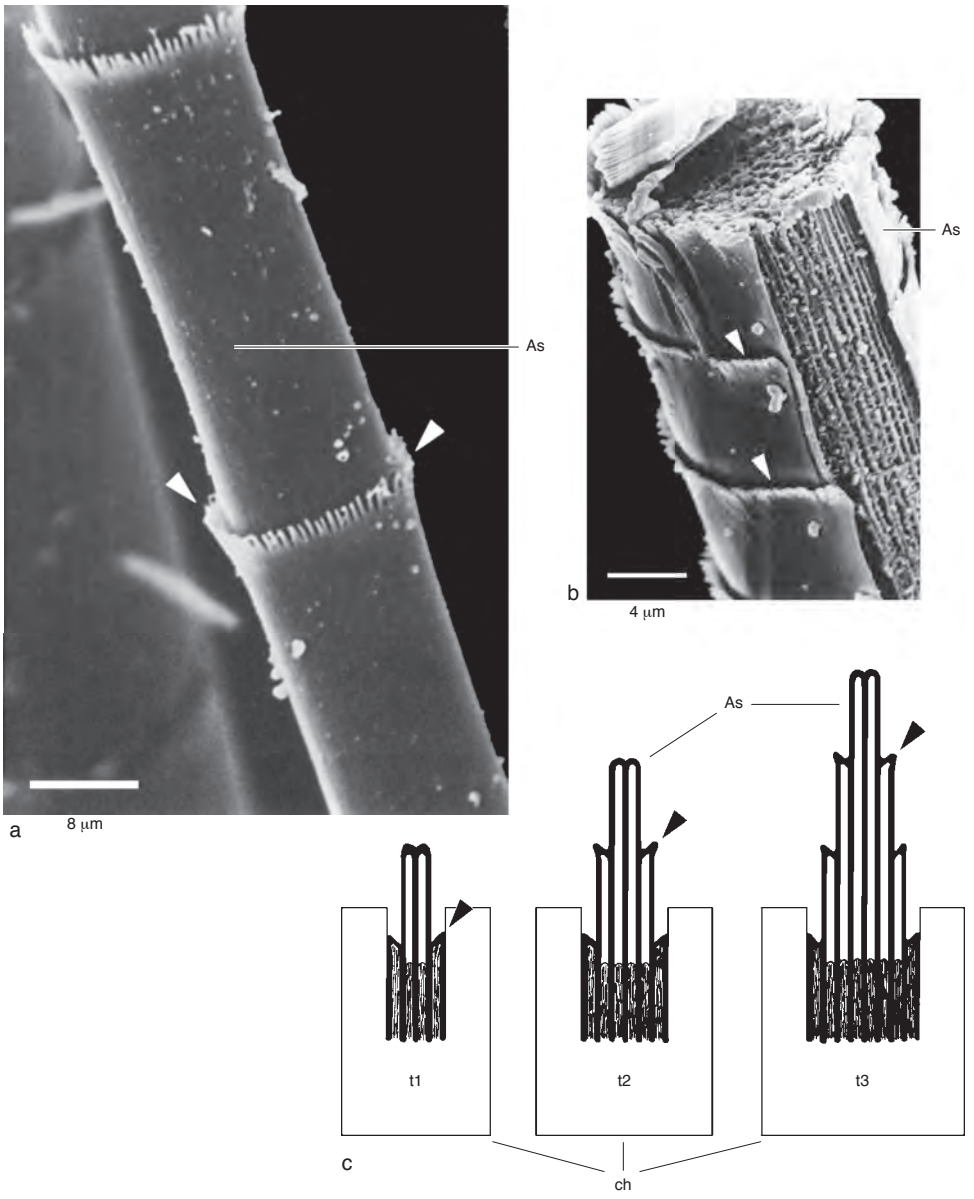

FIG. 1506. SEM micrographs and reconstruction of adult setae and their building process in *Lingula anatina*; *a*, detail of adult seta (*As*) showing its horsetail-like appearance due to regular circles of spines (*arrowheads*) produced by peripheral microvilli of the chaetoblast; *b,* fragment of an adult seta (*As*) illustrating architecture with each sheath of peripheral setal canals overlain by next younger layer (*arrowheads*); *c,* schematic reconstruction of growth process of adult seta (*As*) with chaetoblast (*ch*) shown at three different observation times (*t1*, *t2*, *t3*); simultaneously, new peripheral microvilli are built by chaetoblast, surrounding growing seta and secreting material for new peripheral layer of setal canals; *arrowheads* mark same setal canal at different times (Lüter, 2000b).

canal into the cells and a typical feature of a metanephridium at work (Fig. 1508c). According to these observations, brachiopod metanephridia are composed of two different cell types that may have originated from different epithelia. The nature of brachiopod metanephridia as heterogeneously assembled organs with a coelomic part (nephrostome)

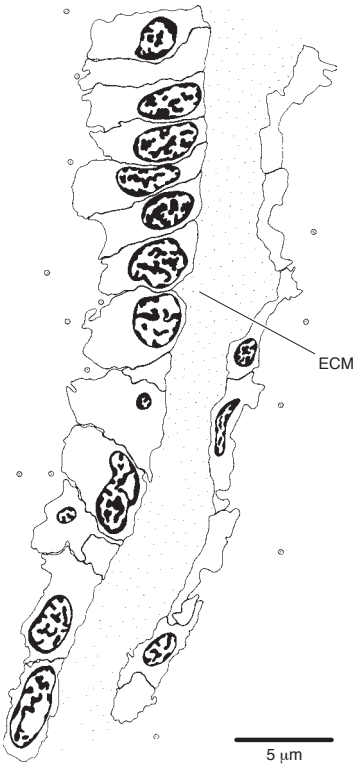

FIG. 1507. Reconstruction of gradually changing cells from funnel toward canal epithelium on left side of extracellular matrix (*ECM*) in metanephridium of *Terebratulina retusa*; a distinction between cells derived from either mesoderm or ectoderm is not possible (Lüter, 1995).

and an ectodermal part (canal) was anticipated very early (GOODRICH, 1945). This idea was corroborated by the results in *Lingula anatina* and could be demonstrated finally by studying the larval development of *Calloria inconspicua*.

The lecithotrophic larvae of *Calloria inconspicua* in their three-lobed stage have two symmetrically arranged canals leading from a pore in the outer epithelium toward the developing body cavity (Fig. 1509a–1509b). Both canals have blind ends (Fig. 1509b–1509c). A connection to the coelomic epithelium does not (yet) exist. The cells lining each canal are specialized epidermal cells that do not differ from typical cells lining a metanephridial canal in adult brachiopods. They already have the ability of metabolite resorption, clearly demonstrated by the presence of coated pits and coated vesicles (Fig. 1509d). Early postmetamorphic juveniles are different in having an open connection (a true metanephridium) from the body cavity to the outer medium. The invaginating cells of the metanephridial canal (Fig. 1510c–1510e), which had already been present in the pelagic larva, have broken through the ECM or basal lamina (Fig. 1510a–1510b) that separates ectoderm and mesoderm and made contact with the mesodermally derived future nephrostome cells (Fig. 1510a). This contradicts PERCIVAL's (1944) statements that in *Calloria inconspicua* the metanephridia are (1) coelomoducts, growing outwardly, and (2) that they are closed until sexual maturity. In contrast, metanephridia in *Calloria inconspicua* start growing during the pelagic larval phase and grow inwardly as an invaginating canal, which in a later stage connects to the coelomic epithelium, thereby forming a heterogeneously assembled organ, consisting of a nephrostome of mesodermal origin and an outleading canal of ectodermal origin. As long as ultrafiltration from the blood vessels into the body cavity is not confirmed in brachiopods, however, their metanephridia may primarily be regarded as gonoducts.

NERVOUS AND SENSORY SYSTEM

SETAE

Marginal setae in adult brachiopods as well as larval setae play an important role in protection and defence. Once the setae are mechanically stimulated, adult brachiopods close their shell with high speed. If a lecithotrophic brachiopod larva is disturbed mechanically or chemically, the animal contracts along its anterior-posterior axis, thereby spreading the larval setae beyond the outline of its body. This is interpreted as a behavior of defense, comparable to a curling hedgehog producing its spines in the presence of a potential predator. RUDWICK (1970)

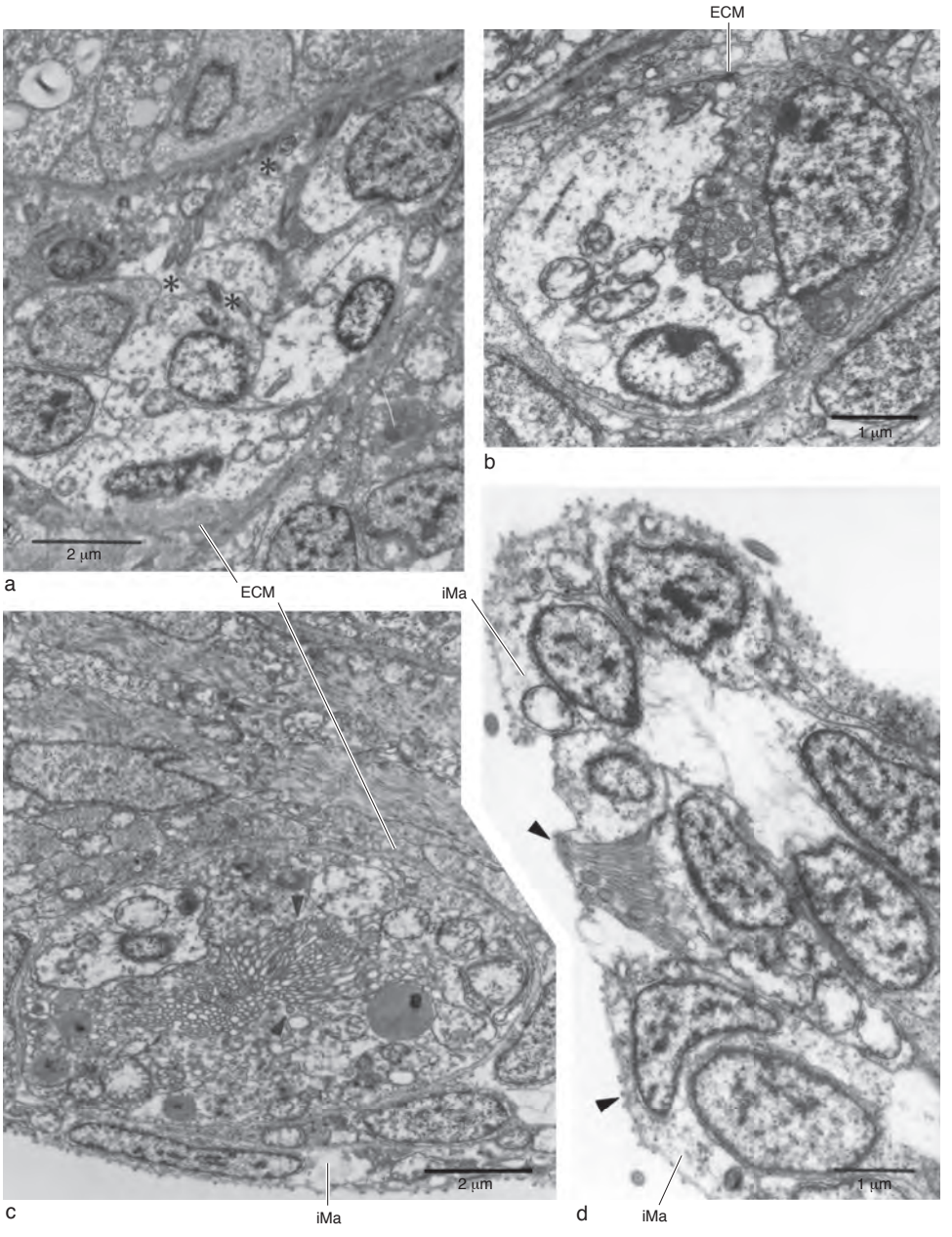

FIG. 1508. TEM micrographs of right metanephridium of pelagic juvenile (6 p.t. stage) of *Lingula anatina*; *a*, prospective nephrostome with first coelomic spaces (*asterisks*) between coelothelial cells; *b*, nephrostome further down metanephridium with only two nephrostome cells surrounding numerous cilia within prospective funnel lumen; *c*, cross section through metanephridial canal; notice long microvilli filling canal's lumen; presence of coated pits and coated vesicles (*arrowheads*) shows that canal cells are actively resorbing fluid from metanephridial lumen; *d*, nephridiopore with distalmost cell of metanephridial canal and surrounding cells of inner mantle epithelium (*iMa*). Notice length difference of microvilli of inner mantle epithelium and canal cells (*arrowheads*); *ECM*, extracellular matrix (Lüter, 1998b).

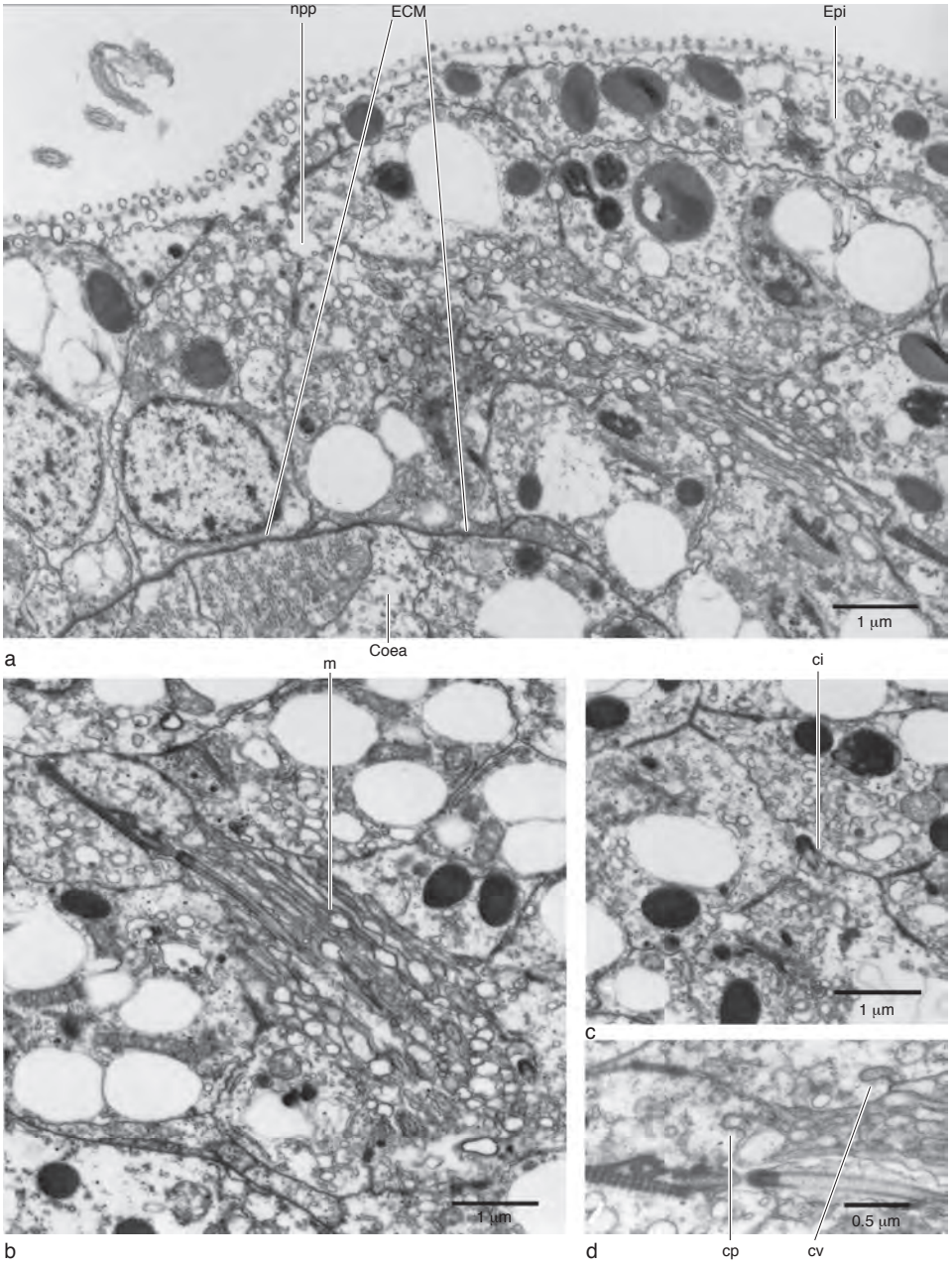

FIG. 1509. TEM micrographs of larval anlage of a metanephridium in a 3-lobed stage of *Calloria inconspicua*; *a*, nephridiopore (*npp*) opening to ventral side of larva; canal cells and epidermal cells (*Epi*) belong to same ectodermal epithelium, whereas coelomic anlage (*Coea*) is separated from ectoderm by extracellular matrix (*ECM*); *b*, lumen of metanephridial anlage with canal cells producing cilia (*ci*) and long microvilli (*m*); *c*, proximalmost canal cell of metanephridial anlage with cilium (*ci*); *d*, detail of two canal cells showing coated pits (*cp*) and coated vesicles (*cv*), indication of active resorption process (Lüter, 1998b).

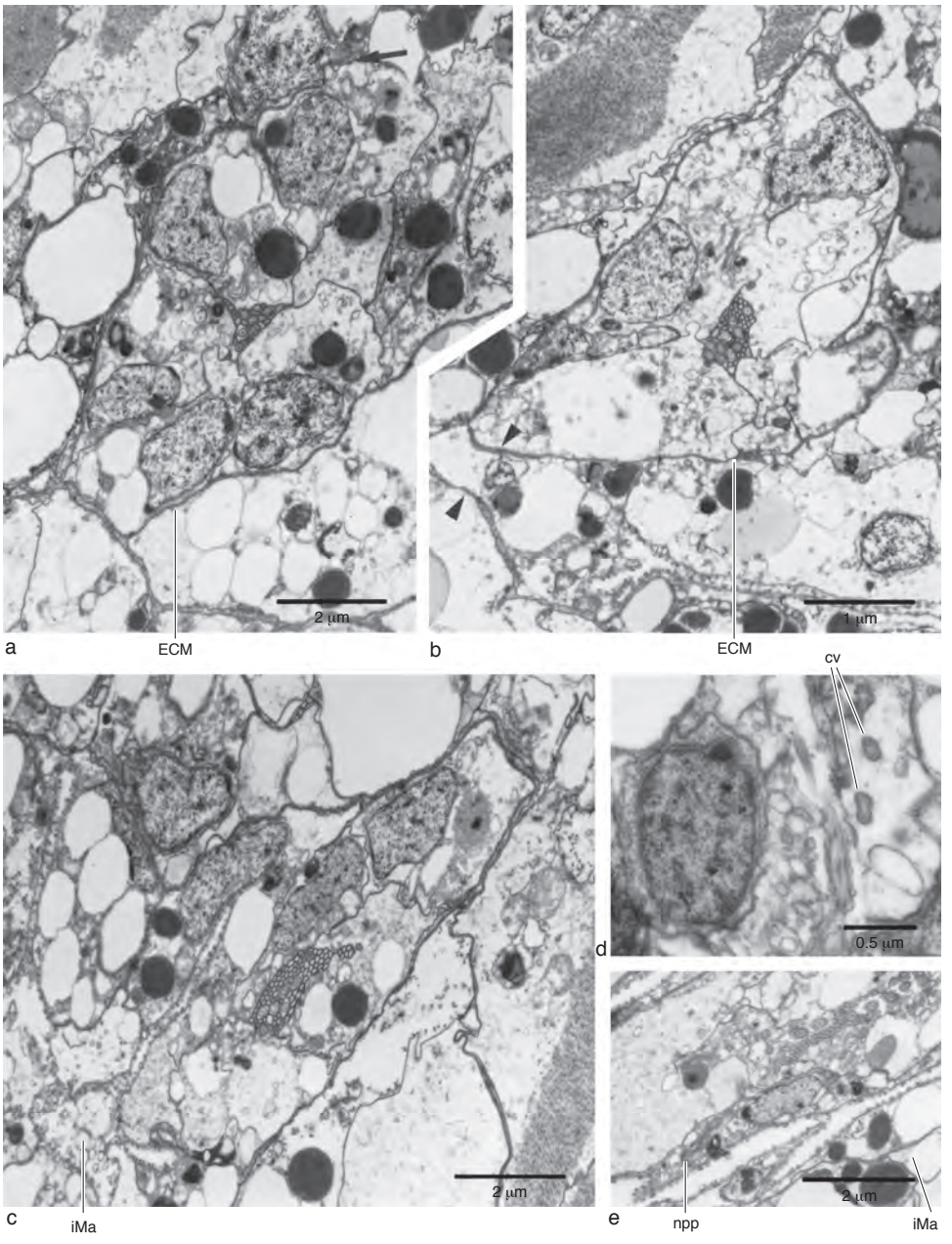

FIG. 1510. TEM micrographs of right metanephridium of postlarval *Calloria inconspicua* 9 days after metamorphosis; *a*, cross section through nephrostome with cilia filling lumen; where extracellular matrix (*ECM*) ends (*arrow*) nephrostome cells are in direct contact with myofilament-containing cells of coelomic lining; *b*, cross section of metanephridial canal showing prospective contact area (*top arrowhead*) of its surrounding extracellular matrix (*ECM*) with basal lamina (*bottom arrowhead*) of inner mantle epithelium; *c*, canal cells connect to inner mantle epithelium (*iMa*) a short distance from nephridiopore; *d*, coated vesicles (*cv*) in apical part of canal cells indicate activity of metanephridium; *e*, longitudinal section of distalmost part of metanephridial canal, showing nephridiopore (npp) in apical part of postlarval body; *iMa*, inner mantle epithelium (Lüter, 1998b).

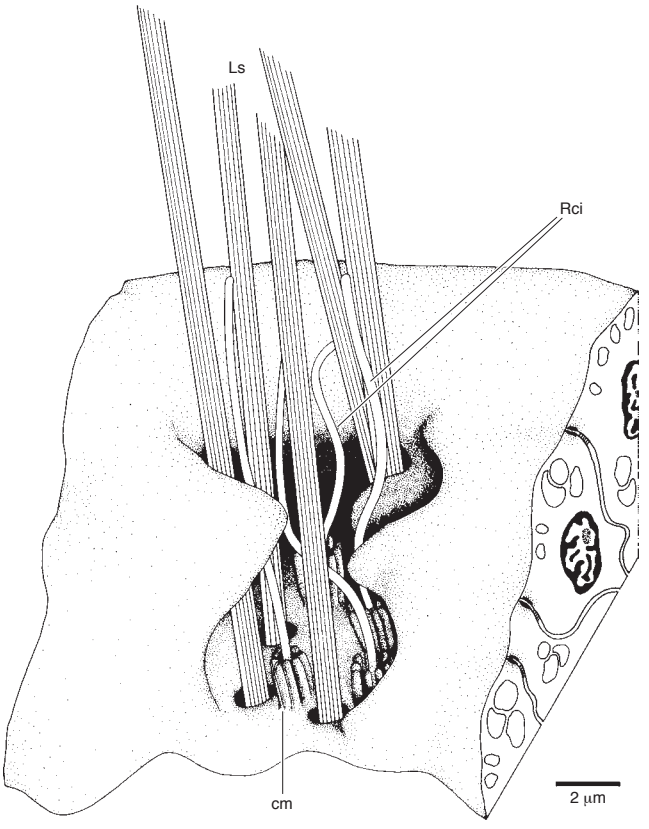

FIG. 1511. Reconstruction of sensory complex within left dorsolateral setal bundle, based on cross sections of three-lobed larva of *Calloria inconspicua* prior to metamorphosis, orientation upside down; notice receptive cilia (*Rci*) surrounded by circumciliary microvilli (*cm*) in direct neighborhood of larval setae (*Ls*) (Lüter, 2000b).

assumed a mechanical transmission of the setae's tactile properties to the mantle, since no direct connection of any seta and nerve cells had been observed and no specialized sense cells are known so far (JAMES & others, 1992). LÜTER (2000b) described a sensory complex of larval setae and collar receptor cells in the mantle anlage of three-lobed larvae of *Calloria inconspicua* (Fig. 1511; LÜTER, 2000b). As described above, larval setae of *Calloria inconspicua* are exclusively produced by a chaetoblast and accompanied by a single specialized epidermal cell, which itself has no direct connection to the setal surface. Within the setal sac of the primary receptor cells of full-grown *Calloria* larvae, so-called collar receptors can be observed in the direct neighborhood of the specialized epidermal cells. The receptor cell is monociliated, and the cilium is surrounded by a collar of nine thick and actin-filled microvilli (Fig. 1511, 1512a–1512b). The basal area of the receptor cell is filled with vesicles presumably containing a neurotransmitter, and here the collar receptor is separated from the neighboring nerve cell by a synaptic cleft (Fig. 1512c). Bending the larval setae obviously provides a mechanical stimulus transmitted onto the cilium of the receptor, and from there it travels to the nervous system, stimulating the larva to contract its longitudinal muscles. The sensory complex may also be present in *Terebratalia transversa*, as can be deduced from STRICKER and

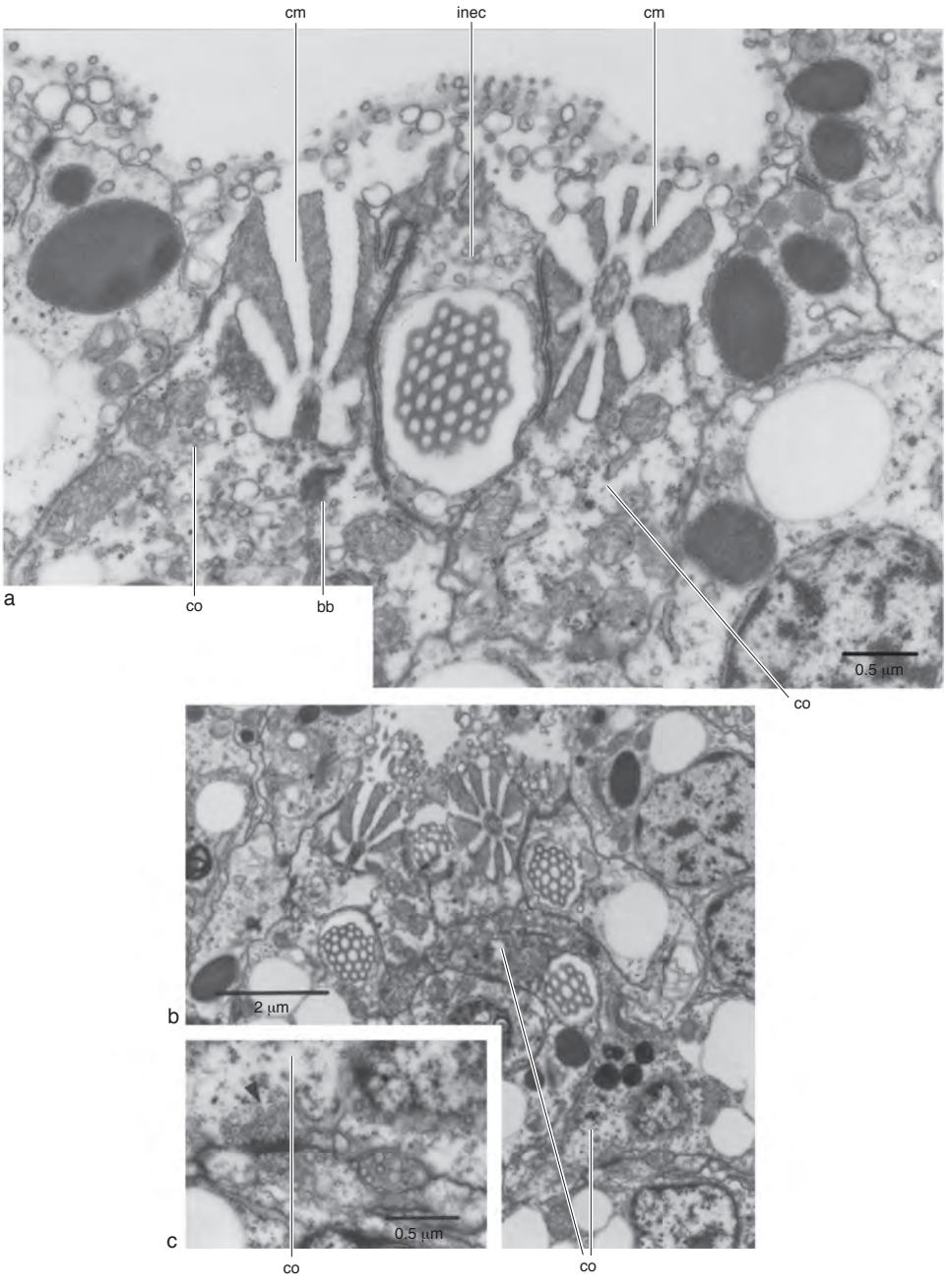

FIG. 1512. TEM micrographs of larval sensory complex in mantle lobe of three-lobed stages of *Calloria inconspicua*; *a*, alternating collar receptor cells (*co*) and specialized invaginated epidermal cells (*inec*); sensory cilium of receptor cell lacks ciliary rootlet and surrounded by a collar of 9 circumciliary microvilli (*cm*); *b*, collar receptor cells with a basal contact with nerve cells; *c*, detail of *b* showing a synaptic cleft between collar receptor (*co*) and nerve cell; notice transmitter vesicles (*arrowhead*) (Lüter 2000b).

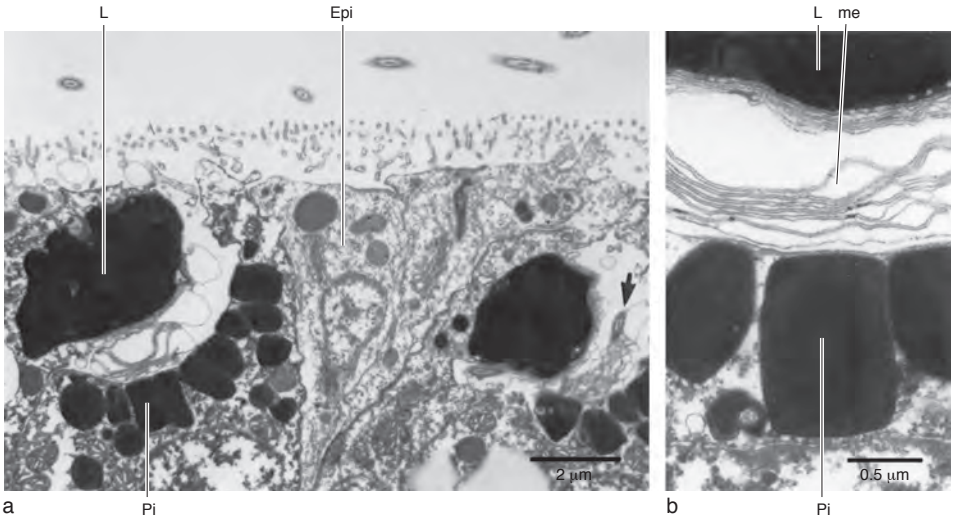

FIG. 1513. TEM micrographs of eyespots of three-lobed larval stages of *Terebratalia transversa*; *a*, eyespots embedded in epidermis (*Epi*) of apical lobe and consisting of pigment cell (*Pi*) and lens cell (*L*) with hollow space in between, filled by membrane staples from specialized cilium (*arrow*); *b*, details of pigment granules (*Pi*) in pigment cell, lens (*L*), and membrane (*me*) of cilium (Lüter, 1998b).

REED (1985a, fig. 6). This sensory complex consisting of larval setae and collar receptor cells may be an apomorphic character of terebratellid brachiopods.

EYESPOTS

Many authors report eyespots or pigment spots on apical lobes of lecithotrophic brachiopod larvae throughout the Recent superfamilies. In *Terebratalia transversa,* for example, 10 to 16 bilaterally arranged carmine-red eyespots are described. They form two rows that diverge in the anteroventral direction (LONG, 1964). Additionally, a defensive response to shading (retraction into the sediment) is reported for adult *Lingula anatina*. Their mantle margin shows numerous brownish spots that may serve as light-sensitive organs, but nothing is known about the ultrastructure of these spots.

Ultrastructural studies of larval eyespots in *Terebratalia transversa,* however, show that these eyespots are photosensitive organs composed of two specialized epidermal cells (Fig. 1513a). One sensory cell provides a cup-shaped arrangement of pigment granules (Fig. 1513a) and similarly acts as a receptor cell through a specialized, elongated cilium (Fig. 1513b) and a basal connection to the nervous system (not shown). The other cell has a bloblike apex containing a single large and electron-dark vesicle (Fig. 1513a). This cell presumably works as a lens (LÜTER, 1998b).

THE MEDIAN TENTACLE

Median tentacles only occur in lophophores of developmental stages of linguliform brachiopods (Fig. 1514a). Their occurence in lingulides and discinides has been observed many times. ROWELL (1960) and CHUANG (1974) also described a median tentacle in postsettlement stages of *Novocrania anomala*, but its occurrence in this species could not be confirmed by NIELSEN (1991). A sensory function of the median tentacle was assumed very early (YATSU, 1902; ASHWORTH, 1915; THOMSON, 1927) and was shown by LÜTER (1996) through ultrastructural studies of pelagic developmental stages of *Lingula anatina*.

The epidermal layer of the median tentacle in *Lingula anatina* contains numerous collar receptors (Fig. 1514b–1514d). They are primary receptor cells, divided in an apical cell body with a cilium surrounded by a

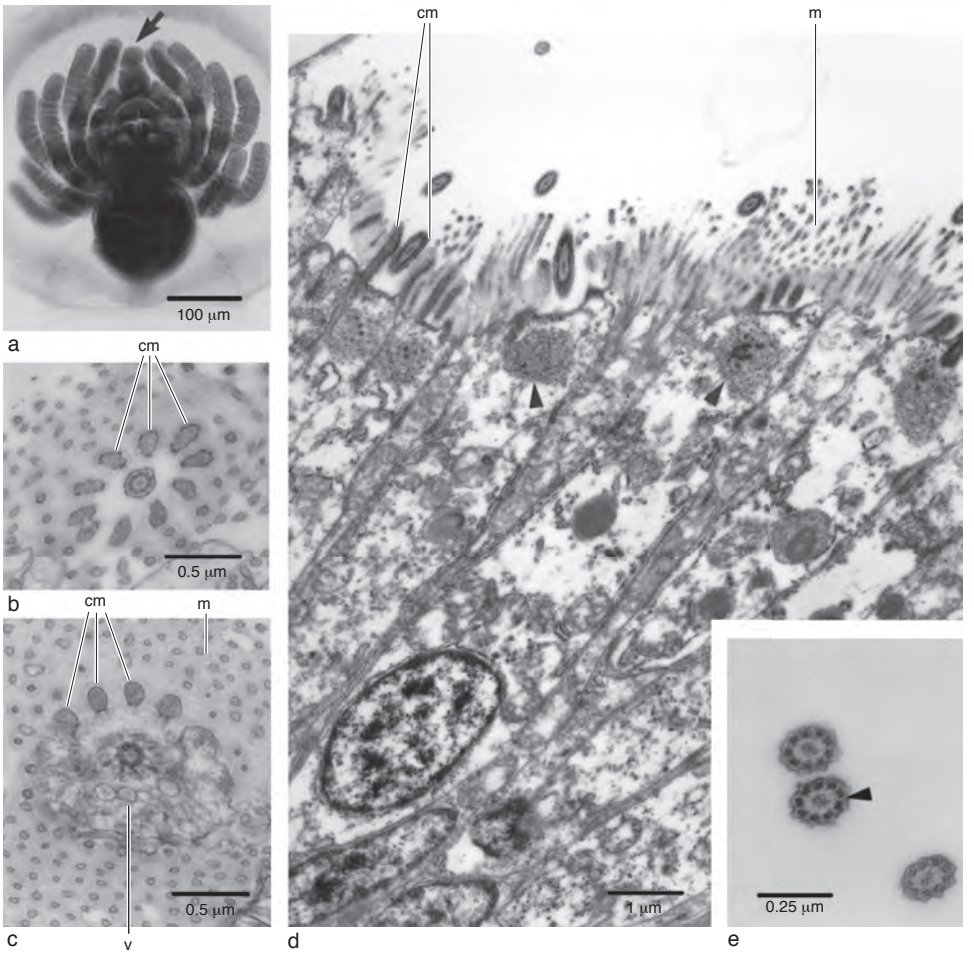

FIG. 1514. Light microscope and TEM micrographs of median tentacle of pelagic juveniles of *Lingula anatina*; *a*, light microscope micrograph of 7 p.t. stage with prominent median tentacle (*arrow*) in center of tentacle apparatus; *b–e*, TEM micrographs of 6 p.t. stage; *b*, collar of 10 circumciliary microvilli (*cm*) surrounding receptive cilium of collar receptor cells; *c*, basal body of cilium surrounded by electron vesicles (*v*); circumciliary microvilli (*cm*) conspicuously differ from normal microvilli (*m*); *d*, tip of median tentacle covered with collar receptor cells; their receptive cilia lack a ciliary rootlet, and their basal body is embedded in a ball-like structure of actin filaments (*arrowheads*); *e*, cilium of collar receptor cell with electron dark microtubuli (*arrowhead*) (Lüter, 1996, 1998b).

collar of 10 thick and actin-filled microvilli (Fig. 1514b–1514c, 1515a) and a basal axon (Fig. 1515b). The histology of these cells is unusual. The microtubules of the ciliary axoneme, apart from the central pair, are electron-dark in cross section (Fig. 1514e). This has also been observed in cilia of receptor cells in the tentacle epidermis of the Actinotroch-larva of *Phoronis muelleri*. Additionally, the sensory cilium has no rootlet. Its basal body is embedded in a ball-like structure of actin filaments (Fig. 1514d, 1515a). The basal axon is about one-tenth the diameter of the cell body and runs proximally toward the nervous system in the lophophore. The basalmost tip of the cell contains vesicles presumably filled with a neurotransmitter and is separated from the adjacent nerve cell by a synaptic cleft. Since the median tentacle is resorbed

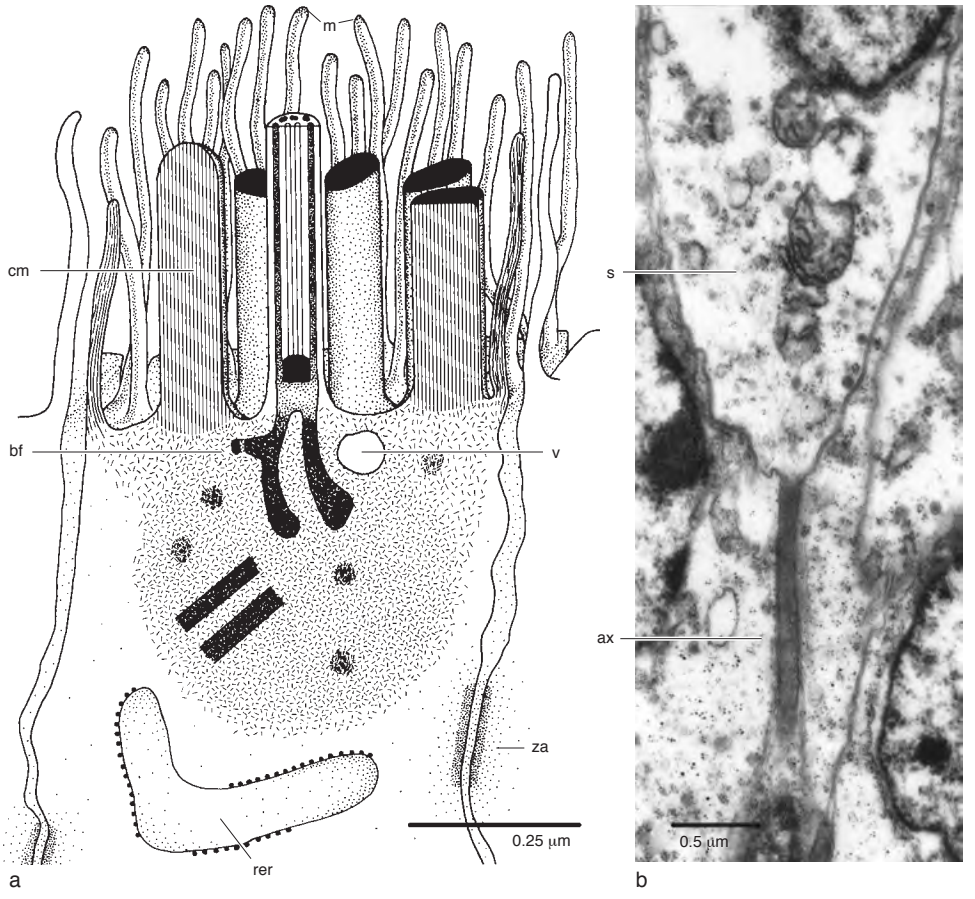

FIG. 1515. Reconstruction and TEM micrograph of receptor cell in median tentacle of 6 p.t. stage of *Lingula anatina*; *a*, reconstruction of apical part of receptor cell based on TEM cross sections; only half of cell shown; notice basal structure of receptive cilium; *b*, proximalmost part of collar receptor cell building an axon (*ax*), which connects receptor with basiepidermal nerve system; *bf*, basal foot; *cm*, circumciliary microvilli; *m*, microvilli; *rer*, rough endoplasmatic reticulum; *s*, cell soma; *v*, vesicle; *za,* zonula adhaerens (Lüter, 1996, 1998b).

in postsettlement stages of lingulides and discinides, its sensory function must be connected to the pelagic life habit of early free-swimming juveniles.

APICAL GANGLION

Studies of the development of the serotonergic system in pelagic developmental stages of *Glottidia* sp. have shown that brachiopods have an apical ganglion with numerous serotonergic neurons (HAY-SCHMIDT, 2000). The ganglion is located in the proximal half of the median tentacle and may, therefore, be a transitory morphological characteristic, since the median tentacle is resorbed during or after settlement of young linguloid brachiopods. Serotonergic cell bodies were absent along the ciliary band of the lophophore. Only two serotonergic tracts arise from the apical ganglion and project into the ciliary band. Since the concentration of serotonergic cell bodies in the apical ganglion seems to be a unique deuterostome character, HAY-SCHMIDT (2000) assumes that brachiopods (together with phoronids) are basal deuterostomes.

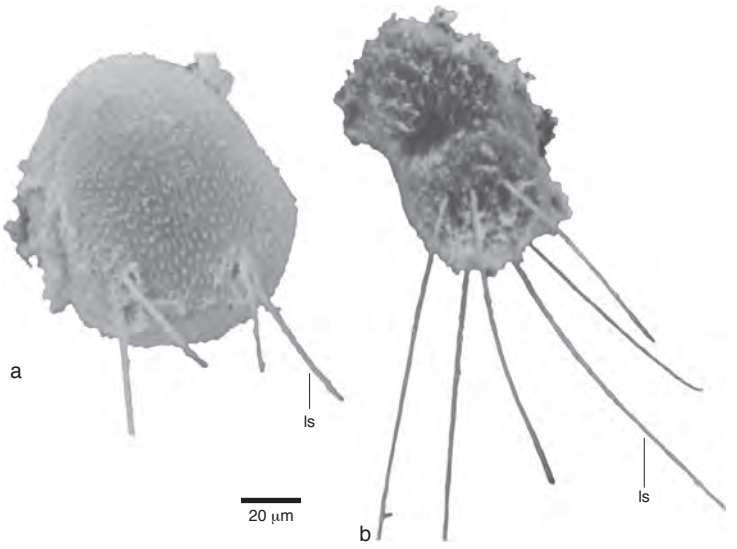

FIG. 1516. SEM micrographs of early developmental stages of *Discinisca* sp. cf. *tenuis*; *a*, embryo 20 h postinsemination, completely enclosed by vitelline membrane, with larval setae (*ls*) sticking out of egg shell; *b*, hatching stage ca. 27 h postinsemination resembling late wedge-shaped stage of rhynchonelliform brachiopods, with three larval setae (*ls*) on either side of larva (Lüter, 2001a).

EMBRYOLOGY AND DEVELOPMENT

GENERAL ASPECTS

WILLIAMS and others (1997, p. 153f.), in an attempt to standardize the terminology of brachiopod development and the corresponding developmental stages, mainly adopted the terminology of CHUANG (1990). According to CHUANG's account on brachiopod development and reproduction, all prehatching developmental stages when still surrounded by the vitelline membrane or egg shell should be named embryos. All posthatching stages, despite their obvious morphological differences in linguliform, craniiform, and rhynchonelliform brachiopods, are referred to as larvae. The postlarval or juvenile stage begins right after settlement; i.e., all juvenile stages are already immobilized through attachment on hard substrate. These definitions of developmental stages provided the basis for figure 158 in WILLIAMS and others (1997, p. 161). An extensive ultrastructural study of brachiopod development in *Lingula anatina*, *Discinisca* sp. cf. *tenuis*, *Notosaria nigricans,* and *Calloria inconspicua* (LÜTER, 1998a, 1998b, 2001a, unpublished data, 2001) led to a different conclusion. As already mentioned by LONG and STRICKER (1991), the bivalved, free-swimming stages of lingulid and discinid brachiopods resemble minute adults and therefore should be regarded as swimming juveniles rather than larvae. This is in accordance with LÜTER's results, the conclusion being that juveniles of *Lingula anatina* rather than larvae hatch from the egg shell. The stages corresponding to these free-swimming lingulid juveniles in rhynchonelliform brachiopods are their postsettlement stages. CHUANG's definition (1990) that all swimming stages are larvae and all sessile stages are juveniles or postlarvae puts too much weight on the ambient environment and the corresponding life habit of the developing brachiopods. Considering the morphology and especially the development of the excretory system (see below), CHUANG's definition does not apply. One possibility for measuring the stage of development is to count the number of pairs of lophophoral tentacles (LÜTER, 1998b). In rhynchonelliform brachiopods this is only possible in

already settled postlarvae. A comparison of these postlarvae with free-swimming juveniles of lingulides or discinides shows similar progress in development: shell valves, coelomic cavities, tentacles, and coelomoducts (metanephridia) are present, and even the size of the animals is comparable.

In contrast, rhynchonelliform brachiopods hatch as ciliated gastrulae and subsequently develop such typical larval characters as an apical lobe with an apical tuft, larval setae, or a prototroch-like ring of prolonged cilia around the apical lobe for movement. All these features are missing from posthatching stages in lingulides but not in discinides. Already the prehatching stage of *Discinisca* sp. cf. *tenuis* develops a pair of setal bundles, with two larval setae each. They pierce the vitelline membrane at the caudal end of the embryo (Fig. 1516a). Finally, the hatching stage of *Discinisca* sp. cf. *tenuis* is a two-lobed larva, with long cilia on what can be identified as the apical lobe and two bundles of larval setae protruding from the future mantle (Fig. 1516b). Their overall similarity to two-lobed stages of rhynchonelliform brachiopods is striking. This provoked the following theory: Embryonic development in brachiopods takes place within the egg shell (vitelline membrane) up to a group-specific time of release (hatching): all brachiopods with true lecithotrophic development hatch as very young developmental stages, whereas discinides hatch as two-lobed larvae with (some) typical larval characters and lingulides hatch as feeding juveniles or postlarvae. In the latter two groups embryonic and larval development is either partly or fully restricted to the life phase within the egg shell (Fig. 1517; see also Table 21 for new findings on brachiopod reproductive cycles).

GAMETE MATURATION

In brachiopods, oocytes develop in close association with follicle cells, the latter building a protective sheath around each maturing egg. Prior to fertilization the oocyte has to shed the follicle cells, a process called ovulation (Fig. 1518), and in most cases the breakdown of the follicle is accompanied by a breakdown of the germinal vesicle (nucleus), with the oocyte reaching fertility through meiotic maturation. Stricker and Folsom (1997) have shown that in *Terebratalia transversa* the follicle has to be detached from the ovaries to stimulate ovulation and meiotic maturation. This is also the case in *Novocrania anomala* (Freeman, 2000). Additionally, if oocytes in *Terebratalia transversa* are mechanically stripped of their follicle cells too early after detachment of the follicle from the genital lamella, the nucleus fails to break down and meiotic maturation does not occur (Stricker & Folsom, 1997). Once the follicle is detached, the follicle cells themselves induce maturation by transferring a trigger-substance via junctional complexes connecting the follicle cells and the oolemma (Fig. 1519). Similar junctions have been observed in *Lingula* (Williams & others, 1997, fig. 150). In *Glottidia pyramidata* detachment of follicles by mechanically disrupting the ovaries fails to induce oocyte maturation, but leads to oocyte lysis (Freeman, 1994). The same is obviously true for *Lingula anatina*, since artificial insemination experiments following recipes given in Reed (1987) failed to produce embryos (C. Lüter, unpublished data, 1995). However, oocyte maturation can be induced in *Glottidia pyramidata* by incubation of ovaries with a lophophore extract. Obviously, the lophophore releases a trigger-substance, which itself stimulates the follicle cells to release their chemical signal for oocyte maturation (Freeman, 1994). Treatment of premature oocytes with cAMP has the same effect; i.e., follicle cells in *Glottidia pyramidata* seem to have a cAMP–signalling pathway (Freeman, 1994). If oocytes in *Glottidia* are mechanically denuded or stripped of their follicle cells, treatment with the lophophore extract fails to induce maturation.

EMBRYOLOGY

Our knowledge about the embryology of brachiopods has been significantly increased through the work of Freeman (1993b, 1995,

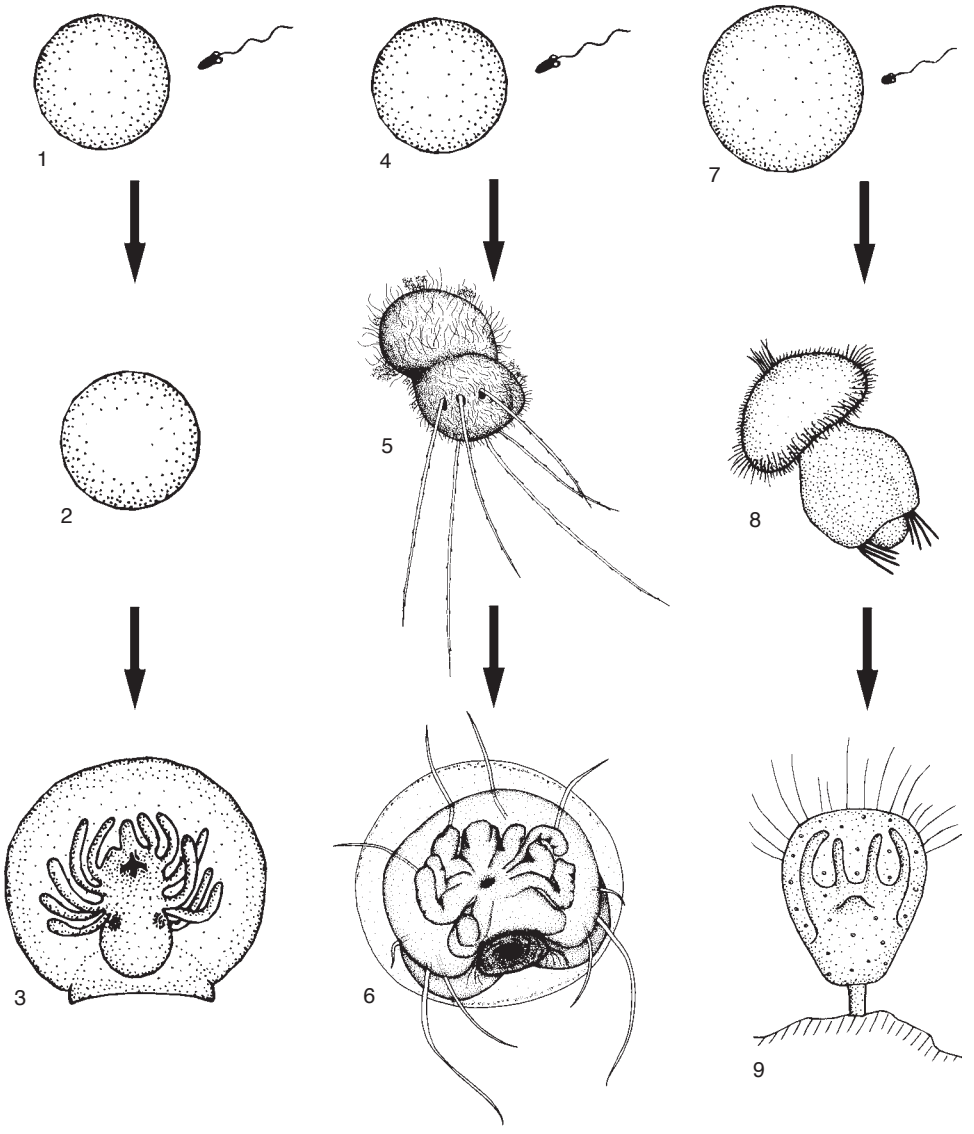

FIG. 1517. Comparison of developmental stages of lingulid (*1–3*), discinid (*4–5*) and rhynchonelliform (*6–9*) brachiopods. Comparable stages (semaphoronts, see definition in HENNIG, 1966, p. 6) are shown on same level. Rhynchonelliforms and discinids share a hatching stage with larval setae (*5, 8*), whereas lingulids hatch as juveniles without any setae (*3*). Additionally, pelagic juveniles of discinids (*6*) have adult setae comparable to postmetamorphic stages of rhynchonelliforms (*9*). The overall similarity in structural development (e.g., presence of valves, certain number of tentacles, fully developed metanephridia) makes pelagic juveniles of linguliforms and postmetamorphic rhynchonelliforms (*3*, *6*, *9*) comparable semaphoronts *sensu* HENNIG, 1966. This is in accordance with the free-swimming juvenile hypothesis of LONG and STRICKER, 1991. Drawing not to scale (new).

1999, 2000, 2001, 2003), who was able to construct fate maps for the development of *Glottidia pyramidata*, *Discinisca strigata*, *Novocrania anomala, Hemithiris psittacea*, *Terebratulina unguicula,* and *Terebratalia transversa*, thereby covering lingulides, discinides, craniides, and all rhynchonelliforms apart from thecideides. Experimental markings or destruction of blastomeres or parts of developing embryos led to

TABLE 21. Summary of brachiopod reproductive cycles. Table contains new findings that complement WILLIAMS and others (1997, p. 158, table 3); *RG,* ripe gonads; *SP,* spawning; *PH,* plankton hauls; *LR,* larval release; *BL,* brooded larvae (new).

Species	Author	Locality	Observation type	Month
Lingula anatina	Lüter, 1998b	Queensland, Australia	RG	Feb–Apr
Glottidia pyramidata	Freeman, 1995	Southern Florida	RG	May–June
Discinisca sp. cf. *tenuis*	Lüter, 2001a	Namibia	RG, PH	Feb–Apr
Discinisca strigata	Freeman, 1999	Panama, Pacific	RG	Dec–Feb
Notosaria nigricans	Lüter, 1998b	New Zealand	RG, SP	Apr–June
Tethyrhynchia mediterranea	Lüter, 2001b	Mediterranean Sea	BL	Jul[1]
Thecidellina blochmanni	Lüter, pers. obs., 2001	Christmas Island, Indian Ocean	BL	Feb
Kakanuiella chathamensis	Hoffmann, pers. obs., 2007	Chatham Rise, Southwestern Pacific	BL	Jan
Pajaudina atlantica	Hoffmann, pers. obs., 2007	La Palma, Canary Islands	BL	Jun
Ospreyella depressa	Lüter, pers. obs., 2000	Osprey Reef, Coral Sea, Australia	BL	Dec
Ospreyella maldiviana	Logan, 2005	South Male Atoll, Maldives	BL	Mar
Liothyrella neozelanica	Chuang, 1994	New Zealand	SP	Feb
Liothyrella uva	Peck & Holmes, 1989	Antarctica	SP, BL	Sept–Nov,[2] Jan–Feb
	Peck & Robinson, 1994	Antarctica	LR	Jan
	Peck, Meidlinger, & Tyler, 2001	Antarctica	LR	Dec–Feb
Macandrevia cranium	d'Hondt & Franzen, 2001	Western Sweden	SP	Nov
Calloria inconspicua	Chuang, 1996	New Zealand	SP	Feb–Apr
	Lüter, 1998a, 1998b	New Zealand	RG, SP	Apr–Jun
Argyrotheca cordata	Grobe & Lüter, 1999	Mediterranean Sea	RG, BL	all year
Argyrotheca cistellula	Grobe & Lüter, 1999	Mediterranean Sea	RG, BL	all year
Argyrotheca cuneata	Grobe & Lüter, 1999	Mediterranean Sea	RG, BL	all year[3]
Pumilus antiquatus	Lüter, pers. obs., 1996	New Zealand	RG	Apr–June

[1]almost constant environmental conditions possibly result in year-round reproduction; [2]indirect proof through tissue ash-free dry mass measurements; [3]uncertain due to small sample size.

differences in or failure of development of regions of embryos, having the effect that the responsibility of certain blastomeres for the construction of the epithelial layers like endoderm or mesoderm, for example, could be clarified. These experiments resulted in fate maps and developmental timetables (see Fig. 1520 and Table 22). Developmental timetables have been used by many authors (see JAMES & others, 1992; JAMES, 1997; WILLIAMS & others, 1997) to identify important steps in brachiopod development. However, larval development is temperature dependent and may also be influenced by the laboratory conditions under which all embryological investigations were conducted. The only direct comparison between two species from the same environment tested under similar conditions was documented by FREEMAN (2003). His results show that the terebratulid *Terebratulina unguicula* and the rhynchonellid *Hemithiris psittacea* differ significantly in their developmental times (see Table 22).

According to FREEMAN (2001) the assumption that embryogenesis takes place in a uniform manner in all brachiopods as implied by WILLIAMS and others (1997) is an oversimplification of the different developmental processes observed in the Recent brachiopod subphyla. Only the first two cleavages after oocyte fertilization are uniform in all brachiopods: The first cleavage occurs meridionally along the animal-vegetal axis of the egg, as does the second cleavage, but at 90 degrees from the plane of the first one. The third cleavage is equatorial in most cases, generating an embryo with four animal and four vegetal blastomeres. One can observe differences

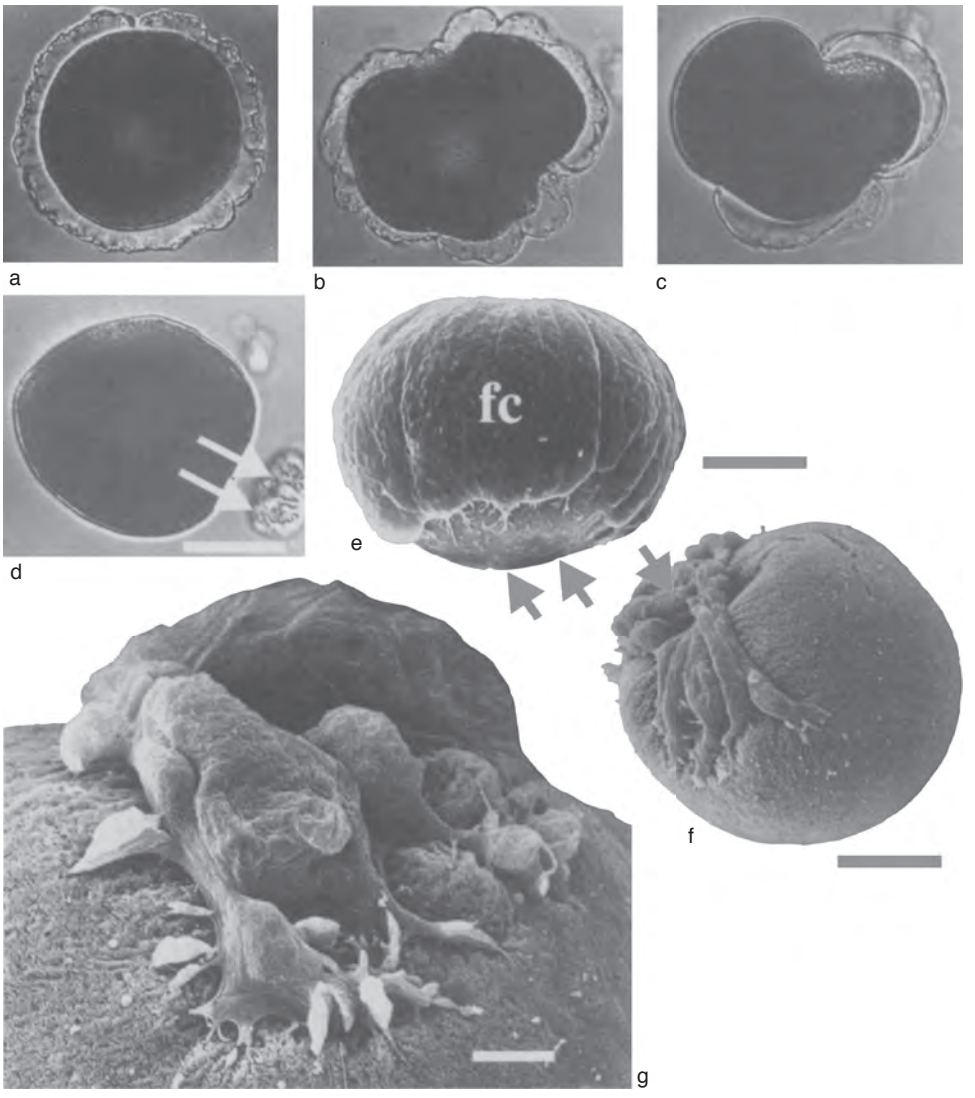

FIG. 1518. Ovulation of single oocyte of *Terebratalia transversa*; *a–d*, light microscope micrograph series of living oocyte, showing retraction of follicular sheath over about 90 min; follicular cells form cap of follicle cells (*arrows* in *d*), which eventually dislodges from oocyte; scale bar: 50 µm; *e–g,* SEM micrographs of oocytes retracting their follicular sheaths; *e*, oocyte 5 min after maceration of ovary with follicle cells (*fc*) covering most of oocyte except attachment site of oocyte to germinal epithelium (*arrows*), scale bar: 50 µm; *f*, oocyte 75 min after removal of ovary with nearly completed follicle cap (*arrow*), scale bar: 50 µm; *g*, detail of cap of follicle cells that form on one pole of oocyte during ovulation, scale bar: 10 µm (Stricker & Folsom, 1997).

between the brachiopod subgroups from the fourth cleavage on.

Lingulids and Discinids

The fourth cleavage occurs parallel to the plane of the first cleavage in the animal and vegetal blastomeres and generates a bricklike blastomere configuration that is four cells long (YATSU, 1902). Markings of the animal pole of the egg end up in the dorsal ectoderm of the embryo, whereas the apical part of the embryo originates largely from a lateral

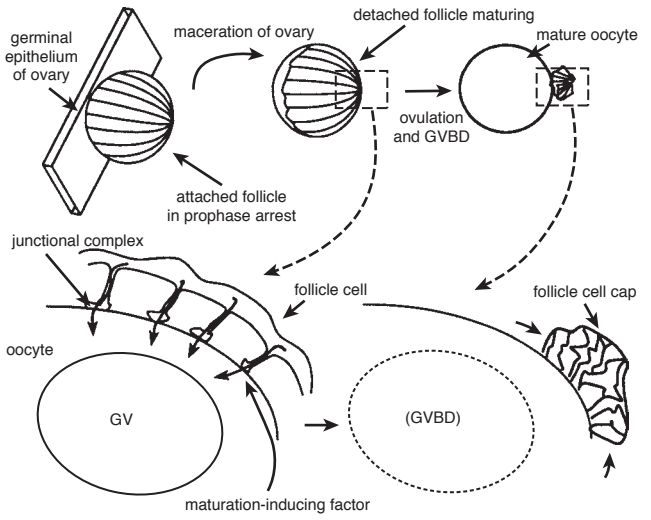

FIG. 1519. Diagram of key role that follicle cell-oocyte attachments are believed to play during oocyte maturation, based on video analyses and experiment manipulations; *GV*, germinal vesicle; *GVBD*, germinal versicle breakdown (Stricker & Folsom, 1997).

region of the egg. The vegetal part of the egg will in a later developmental stage represent the site of gastrulation. Although the anterior-posterior axis of the embryo can be detected very early, true bilateral symmetry becomes obvious through invagination of the archenteron. The plane of bilateral symmetry corresponds to the plane of the first cleavage, but it may already be fixed through anisotropy of the egg (FREEMAN, 1995, 1999, 2001).

Craniids and Rhynchonelliform Groups

Comparable to Linguliformea the fourth cleavage is meridional, but generates a morphologically different configuration of blastomeres, i.e., a double ring of cells enclosing a hollow space, referred to as a doughnut by LONG and STRICKER (1991). This was observed very early in rhynchonelliform brachiopod development (e.g., CONKLIN, 1902; LONG, 1964) but comprehensively illustrated through SEM studies of the embryogenesis of *Terebratalia transversa* by NISLOW (1994). By separating the blastomeres after the first cleavage, NISLOW was able to show normal development of each blastomere into half-size larvae of *Terebratalia transversa*. He already assumed regulative development rather than mosaic development in rhynchonelliform brachiopods, which was corroborated by FREEMAN's results. In *Novocrania anomala* a mark of the animal pole of the egg will end up in the anterior region of the apical lobe, whereas a marked vegetal pole will end up at the site of gastrulation. In contrast to Linguliformea, there is no correspondence between the plane of the first cleavage and the future anterior-posterior axis of the embryo (FREEMAN, 2000, 2001).

Apart from shell formation, the most examined developmental process in brachiopods is the formation of the mesoderm and the subsequent development of the coelom. Many authors have tried to identify mesoderm cells in gastrulae, for example, and have followed their individual fate using light microscopy. This resulted in very different and sometimes contradictory hypotheses. Through the work of FREEMAN we now know that the origin of the mesoderm is already manifest in the early development of the embryo. In *Novocrania anomala* the vegetal half of the egg will form the mesoderm, which becomes evident once the embryo starts gastrulation. In contrast to NIELSEN's (1991) observation that mesoderm cells are

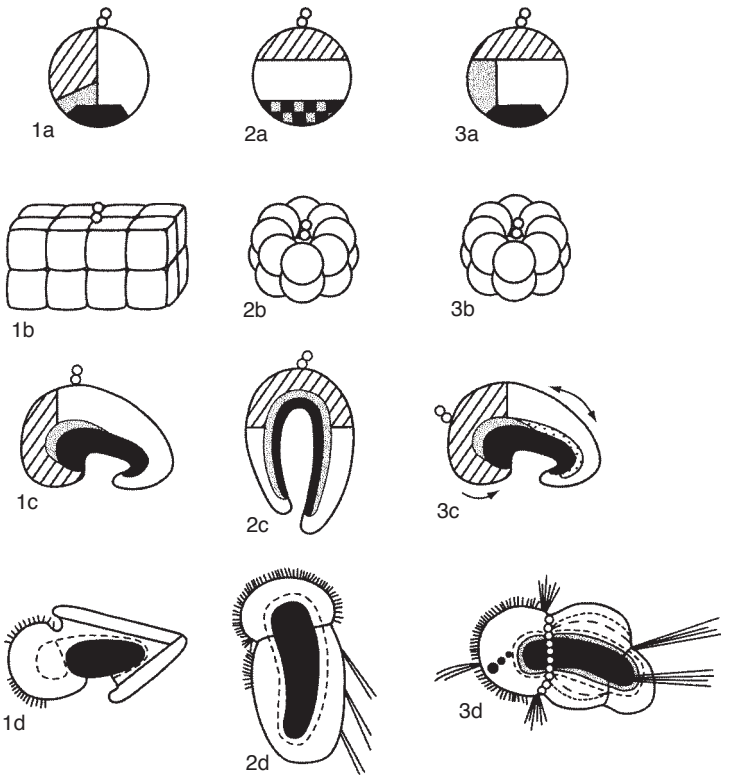

FIG. 1520. Fate maps of linguliform, craniiform, and rhynchonelliform brachiopods, showing different regions of uncleaved eggs (*1a*, *2a*, *3a*) and how they develop into endoderm, mesoderm, and anterior ectoderm, respectively, during ontogenesis; animal pole is marked by polar bodies, anterior is to left; *1b*, *2b*, *3b*, 16-cell embryos with anterior-posterior axis along plane of first cleavage in linguliforms (*1b*) and no relationship between plane of first cleavage and plane of bilateral symmetry in other two groups (*2b*, *3b*); *1c, 2c, 3c*, late gastrula stage, embryos oriented with blastopore (= vegetal pole) down; in linguliform brachiopods apical lobe on left (*1c–1d*) corresponding to placement of anterior ectoderm in fate map (*1a*). In craniiforms placement of anterior ectoderm is retained, whereas in rhynchonelliforms morphogenetic movements translocate apical lobe region (= anterior ectoderm) to left; *1d, 2d, 3d*, pre- (*1d*) and posthatching stages (*2d, 3d*) with orientation of apical lobe to left in linguliform and rhynchonelliform brachiopod developmental stages (Freeman, 2003).

built at the caudal part of the archenteron and subsequently grow forward by driving the endoderm and the ectoderm apart, FREEMAN (2000) postulated that the mesoderm in *Novocrania anomala* ingresses from multiple sites in the endodermal layer into the space between endoderm and ectoderm. Unfortunately, the youngest larval stage of *Novocrania anomala* so far investigated ultrastructurally is 64 hours old (GROBE, 1999). It has the full set of setae, and the blastopore is already closed. The archenteron is encircled by a mesodermal layer, the origin of which cannot be elucidated further at this stage. NIELSEN also described that by ingression of the three setal sacs on either side of the embryo, however, the coelomic anlage becomes divided in four parts: an unpaired anterior coelomic pouch and three paired posterior pouches. FREEMAN (2000) doubted the existence of the anterior coelomic pouch. The ultrastructural study of the larva of *Novocrania anomala* shows that neither of these pouches exists. Although the more-or-less compact mesodermal layer is to some extent compressed by the setal sacs, a continuous extracellular matrix surrounding the single pouches and separating them from other pouches does not exist. All mesodermal cells constitute a single coelomic

TABLE 22. Times of appearance of identifiable embryological features during development of brachiopods. Table contains new findings that complement WILLIAMS and others (1997, p. 180, table 5) (new).

Species	Egg diameter (µm)	Temperature (°C)	Time (h)	Developmental stage	Reference
Glottidia pyramidata	90	21–24	1	2-cell stage	Freeman, 1995
			2	8-cell stage	
			3	32-cell stage	
			6	blastula	
			10–12	gastrula	
			18	gut and valve formation	
			33	apical lobe and gut with cilia	
			48	hatching	
Discinisca sp. cf. *tenuis*	70	23–25	0.5–1	2-cell stage	Lüter, 2001a, unpub. data, 1998
			1	4-cell stage	
			18	gastrula	
			23	larval setae start growing	
			26	two-lobed stage, hatching	
			43	1 p.t. stage, median tentacle, functional gut	
			70	2 p.t. stage	
Discinisca strigata	65–70	29	1	2-cell stage	Freeman, 1999
			2	8-cell stage	
			3	32-cell stage	
			4	first cilia	
			5	blastula	
			9	early gastrula, invagination	
			11	apical tuft	
			18	setae, hatching	
			20	apical and mantle lobes	
			24	1 p.t. stage	
			26–27	2 p.t. stage	
			44	3 p.t. stage	
Novocrania anomala	130–135	11–14	2	2-cell stage	Freeman, 2000
			15–16	blastula, first cilia	
			27	gastrulation	
			36	embryo starts swimming	
			40	scattered mesodermal cells	
			55	constriction separates apical lobe from larval body	
			60–72	larval contraction (curling)	
			72	full-grown larva with 3 pairs of setal bundles	
Hemithiris psittacea	190–200	12–13	8	2-cell stage	Freeman, 2003
			47	ciliated blastula	
			57–72	gastrula	
			108[1]	3-lobed stage	
			150[1]	first setae	
Terebratulina unguicula	165–175	12–13	3, 5	2-cell stage	Freeman, 2003
			21	ciliated blastula	
			36–45	gastrula	
			70[1]	3-lobed stage	
			98[1]	first setae	

TABLE 22. *Continued.*

Species	Egg diameter (µm)	Temperature (°C)	Time (h)	Developmental stage	Reference
Liothyrella uva	–	0–2	24	gastrula	Peck & Robinson, 1994
			72	lobe formation starts	
			216	early 3-lobed stage	
			432	mantle lobe encircling pedicle lobe	
			936[2]	first larval setae	
			115–160 (days)[3]	settlement	
Terebratalia transversa	150	13	2	2-cell stage	Freeman, 1993b
			6–11	early blastula	
			11	first cilia	
			11–18	late blastula	
			18	invagination, beginning of gastrulation	
			25	apical tuft occurs	
			72	3-lobed stage, blastopore closed	
Terebratalia transversa	150	12	3	2-cell stage	Nislow, 1994
			4	4-cell stage	
			5	8-cell stage	
			7	16-cell stage	
			8–18	blastula	
			18	gastrulation	
			38	elongation of embryo	
			40–48	formation of larval mesoderm	
			48	mantle lobe formation	
			72–96	full-grown larva	
Laqueus californianus	130–140	10	3	2-cell stage	Pennington, Tamburri, & Barry, 1999
			4	4-cell stage	
			5	8-cell stage	
			6	16-cell stage	
			12–26	blastula	
			26–48	gastrula	
			48	wedge-shaped, elongation of blastopore, apical tuft	
			72	blastopore closed	
			80	mantle lobe formation, first setae	
			96	3-lobed stage	
			168	settlement	

[1]Time scale in Freeman (2003, fig. 4) slightly inconsistent. Between 84 and 108 hours of development, 12 h, 16 h, and 18 h intervals have the same scale. [2]In experiments of Peck, Meidlinger, and Tyler (2001), larval setae occured only after 1200 h. [3]Estimated from spawning time in October. Peck, Meidlinger, and Tyler (2001, p. 82) give "more than 80 days" as the "longest times to reach the competent larval stage."

anlage without any separation of compartments throughout early larval development in *Novocrania anomala* (see GROBE, 1999). A separation of an anterior and a posterior compartment only happens shortly before settlement, but the two coelomic pouches stay in contact through a ventral bundle of longitudinal muscles responsible for the presettlement curling of the larva. NIELSEN based his interpretation of coelom development exclusively on light microscopy investigations and could not see the delicate extracellular matrix and misinterpreted the very thin but still continuous mesodermal layer proximal to the setal sacs as true separations between coelomic pouches. These new findings are in accordance with embryological studies of rhynchonelliform brachiopod larvae. A single, undivided coelomic anlage has been described for *Terebratulina septentrionalis* (CONKLIN, 1902), *Terebratulina unguicula* and *Terebratalia transversa* (LONG, 1964), *Calloria inconspicua,* and *Notosaria nigricans* (LÜTER, 1998b, 2000a).

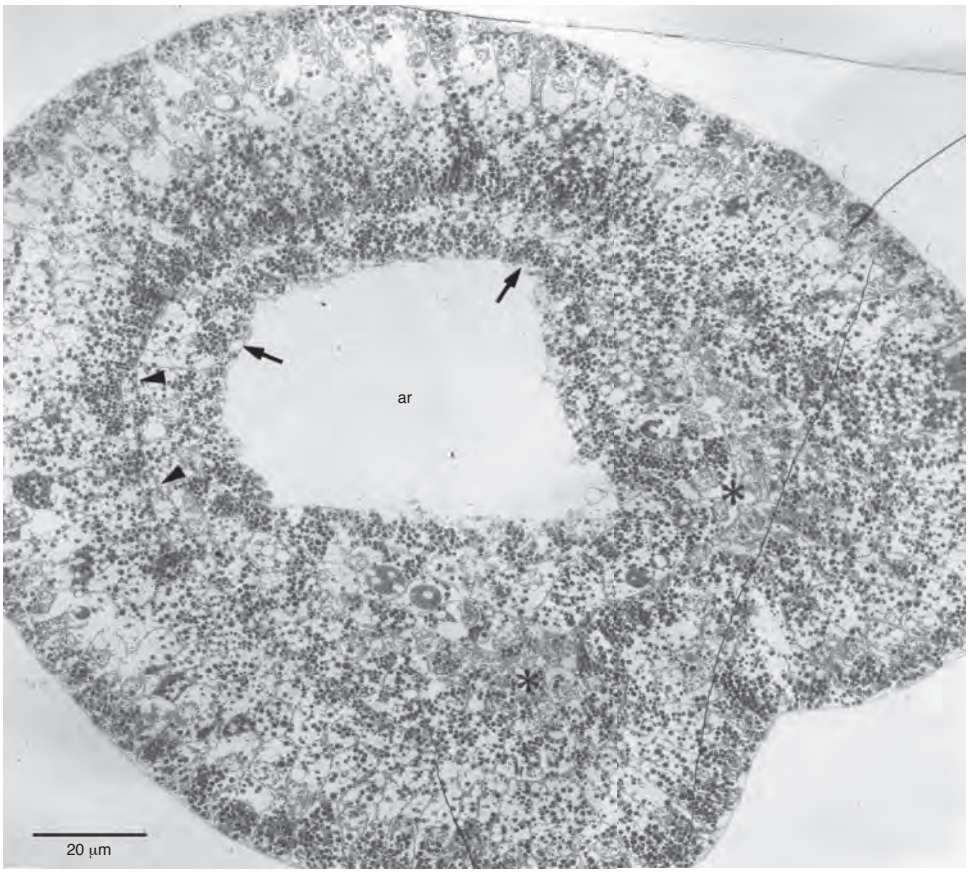

FIG. 1521. TEM micrograph of late wedge-shaped stage (~210 h postinsemination) of *Notosaria nigricans*; longitudinal section showing archenteron lined by a monolayered endoderm (*arrows*) and proliferating mesodermal cells (*asterisks*), which are beginning to be separated from endoderm through thin extracellular matrix (*arrowheads*) in frontal left area (right side of animal); *ar,* archenteron (Lüter, 2000a).

LARVAL DEVELOPMENT
Coelom formation

Secondary body cavities or coeloms in brachiopods are built by enterocoely, a process most extensively investigated and described in developing echinoderms. Echinoderm coelom formation is characterized by the formation of pouches of the archenteron in early larval stages. These pouches later become separated from the archenteron, thereby forming the tripartite arrangement of coelomic compartments. Each coelomic compartment consists of a membrane surrounding a monolayered coelomic epithelium (formerly archenteral epithelium), which itself encloses a fluid-filled chamber, the coelom (formerly archenteral lumen).

In brachiopods, coelom formation is basically the same. Invagination of the archenteron during gastrulation of the embryo displaces the blastocoel. In late wedge-shaped to early three-lobed larval stages of the rhynchonellid *Notosaria nigricans* and the terebratellid *Calloria inconspicua,* the prospective coelomic epithelium proliferates from the archenteral epithelium (Fig. 1521–1522). In *Notosaria nigricans* the cells proliferate from the caudolateral part of the archenteral wall, whereas in *Calloria inconspicua* it is the dorsolateral part of the archenteron (LÜTER, 1998b, 2000a). Growth of a so-called cellular curtain, as described

FIG. 1522. TEM micrograph of early three-lobed stage (~170 h postinsemination) of *Calloria inconspicua,* longitudinal section through midline of larva; mesodermal cells (*ms*) have proliferated from archenteral epithelium and are almost completely separated from future intestine (*in*) by extracellular matrix (*arrowheads*); *AL*, apical lobe; *Epi*, epidermis; *ML*, mantle lobe; *PL*, pedicle lobe (Lüter, 2000a).

for the mesoderm formation in *Terebratalia transversa* by LONG (1964, p. 59), could not be observed. In later stages, an extracellular matrix is secreted from the caudal end of the archenteron to the front, thereby separating the coelomic anlage from the archenteral epithelium.

The main difference from echinoderms is that in brachiopods the prospective coelomic epithelium proliferates as a compact cell mass. Initially, the prospective coelomic epithelium does not enclose a fluid-filled lumen. Throughout brachiopod larval life the coelomic anlage represents a solid

mesodermal cell mass, and only during metamorphosis will the mesodermal cells diverge, thereby opening a lumen, the coelom. According to definitions of mechanisms of coelom formation given by LÜTER (2000a), the development of secondary body cavities in brachiopods can be identified as enterocoely, because the prospective coelomic epithelium originates from archenteral cells (for a critique of these definitions, see JENNER, 2004).

The Trimeric Organization

Recent results on coelom formation in different brachiopod species (see above) demonstrate that it is obvious that a tripartite body organization cannot be found in brachiopods. Many authors have claimed that brachiopods, similar to phoronids (which are not tripartite either) or echinoderms, have a trimeric body with a prosoma, a mesosoma, and a metasoma. Discrimination of three parts of the body only makes sense if this is reflected in the inner organization of the animal; but in brachiopods this is not the case. All brachiopods studied thus far start with having only one coelomic cavity (see above), which may (craniides) or may not (all other brachiopods) be completely divided into two coelomic compartments (mesocoel and metacoel, respectively) during their postsettlement life phase. A prosoma (with a protocoel) has been assumed to exist in different places of the anterior part of the brachiopod body. PROSS (1980) identified the large arm sinus together with the epistome in *Lingula anatina* as the prosoma with protocoel, which corresponds to the epistome of the phoronid actinotroch larva. HAY-SCHMIDT (1992) suggested that the median tentacle of juvenile lingulides is the prosoma and contains a protocoel. Both hypotheses were contradicted by ultrastructural studies of the lophophore of *Lingula anatina*, which showed that all mesodermal cells in the tentacle apparatus form a continuous coelomic epithelium without any connective tissue separating the lophophore coelom (mesocoel) from some anterior protocoel-like compartment (LÜTER, 1996, 1998b). This was already shown by earlier brachiopod researchers, for example in the line drawings of YATSU (1902) and ASHWORTH (1915). The most promising suspect for containing a protocoel, however, was the epistomal region or upper lip above the mouth opening (Fig. 1523a). As has been shown for juvenile *Lingula anatina* (LÜTER, 1998b), the epistome contains single muscle cells that are embedded in a rather strong connective tissue (Fig. 1523b–1523c). These muscle cells are connected to each other and form a continuous epithelium with the mesodermally derived coelomic epithelium of the lophophore. Thus, there is no epithelialized coelomic space to be found in the epistome, which is separated from other such coelomic compartments by extracellular matrix; i.e., the epistome cannot be regarded as a prosoma with a protocoel. As a consequence, brachiopods cannot be regarded as trimeric organisms. Their secondary body cavity is only divided in two compartments, and this truly applies only to craniides, where mesocoel and metacoel are fully separated in adults (BLOCHMANN, 1892), whereas according to HYMAN (1959) all other brachiopods have life-long connections between the two coelomic compartments.

Larval Behavior

In *Discinisca* sp. cf. *tenuis* the curved setae (see above) play an important role in the brachiopod's behavior during both the pelagic phase and the settlement process. The function of the curved setae is two-fold. The long and curved setae enhance buoyancy, helping the brachiopod to drift with the ambient water currents. The specific weight of pelagic juveniles of *Discinisca* sp. cf. *tenuis* is higher than that of the surrounding water, however. To stay in the water column, the brachiopod must extend its lophophore out of the shell using the movement of the tentacle cilia to propel itself forward, thereby avoiding sinking. This was documented in the first drawing of a brachiopod developmental stage ever published (see Fig. 1500). The curved setae assist in this process. Once the lophophore is protected between the

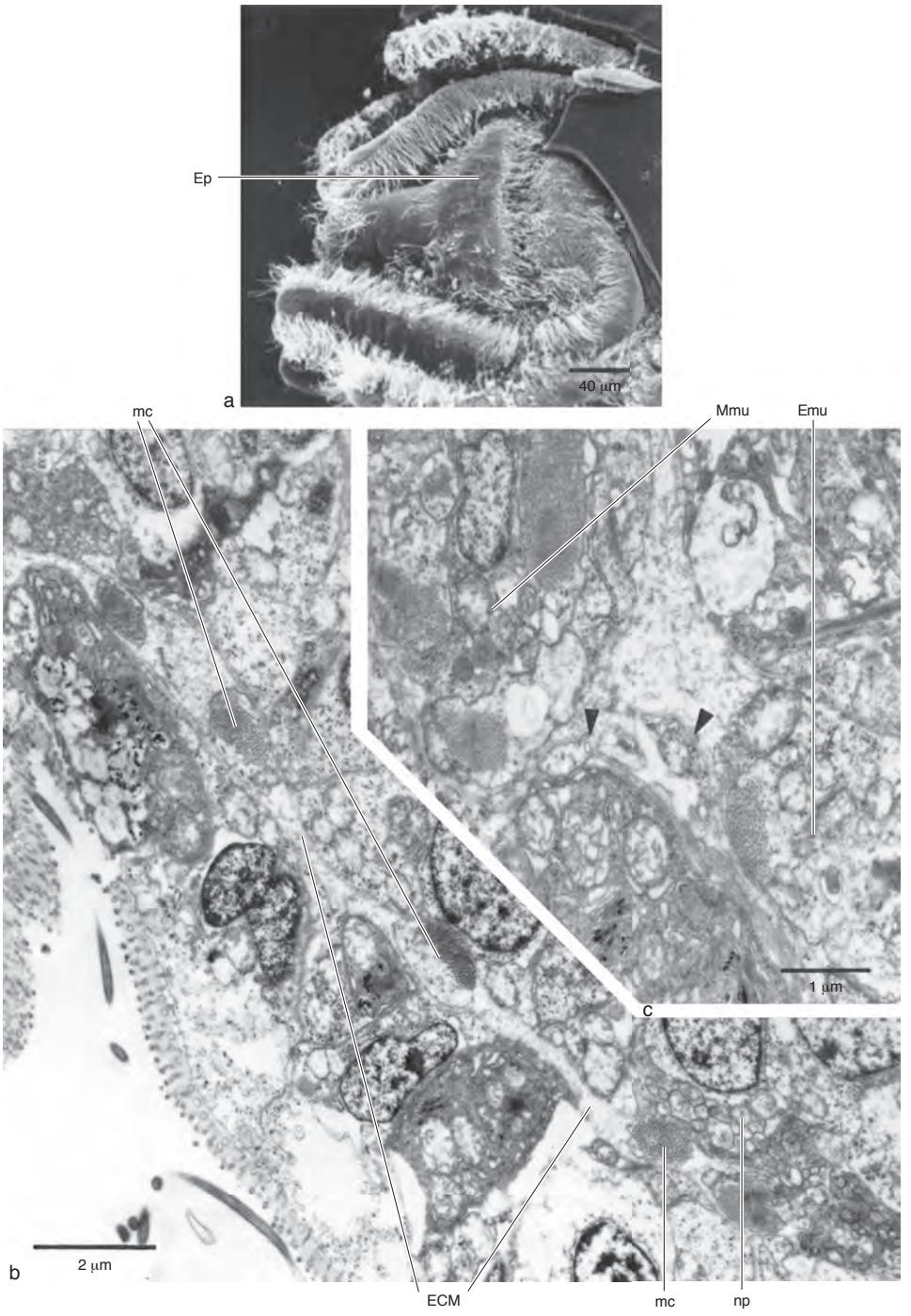

FIG. 1523. Epistome of pelagic juvenile of *Lingula anatina*; *a*, SEM of ventral side of epistome (*Ep*) or upper lip covering mouth opening of juvenile with 7 pairs of tentacles; *b*, TEM of longitudinal section through epistome of juvenile with 6 pairs of tentacles; muscle cells (*mc*) embedded in extracellular matrix (*ECM*) and in close contact to basiepidermal nerve cells (*np*); *c*, TEM micrograph of contact area (*arrowheads*) of epistomal muscle cells (*Emu*) and central musculature of median tentacle (*Mmu*) (Lüter, 1998b).

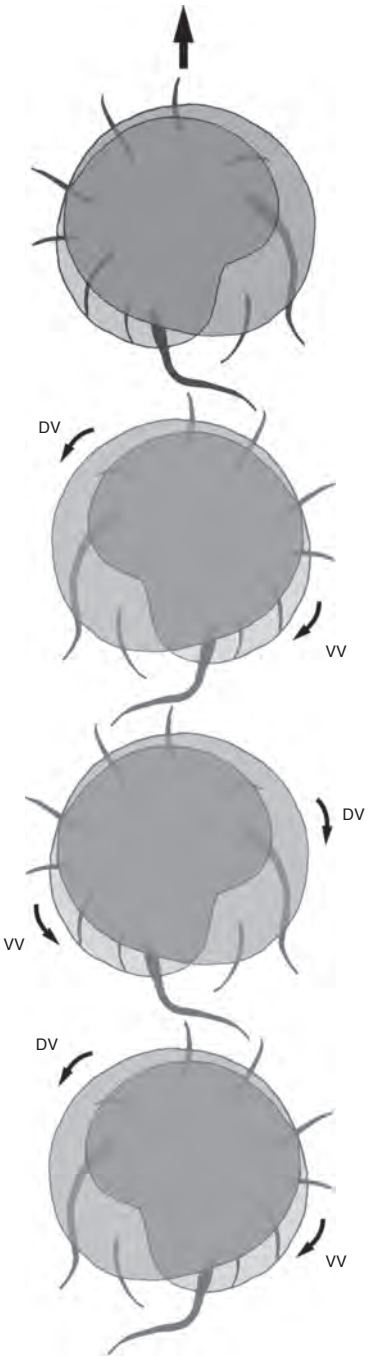

FIG. 1524. Schematic drawing of walking behavior of juvenile of *Discinisca* sp. cf. *tenuis* immediately prior to settlement; animal uses scissoring movements of dorsal (*DV*) and ventral valve (*VV*) against seafloor-touching curved setae to push itself forward in direction of *arrow* (new).

closed valves the young discinid immediately descends to the sea floor.

The second and more important function of the curved setae is to enable the juvenile discinid to move along the sea floor to search for a suitable attachment site. When the brachiopod leaves the plankton to start its benthic life phase, it sinks. Once it hits the sediment surface, the discinid performs a scissoring movement of the tiny valves. Adult linguloids use this type of valve movement in order to burrow into the soft sediment (EMIG, 1997b). Discinides live on hard substrates; i.e., the juvenile *Discinisca* has to find an attachment area, preferably on the upper valve of a conspecific specimen. The scissoring movement of the valves, together with the long and curved setae poking into the upper layer of the sediment allow the juvenile discinid to move in a walking-type motion. Functionally, the curved setae are stiff legs working against the scissoring movement of the valves (and the connected mantle). The discinides can thus walk to their final attachment site when they are ready to settle (Fig. 1524).

Larval Distribution and Survival

Lecithotrophic brachiopod larvae are characterized by a rather short pelagic phase. Accordingly, the dispersal ability of these larvae is said to be low. Brooded larvae are likely to settle in the vicinity of their parental stocks, since they leave the female's mantle cavity or brood pouch in an advanced developmental stage in which they may already have reached the competence to settle on hard substrates. In polar regions the speed of development is low due to ambient water temperatures. In the Antarctic species *Liothyrella uva,* development of brooded larvae is plastic, with larvae of different developmental stages present in brooding females and also differences among females in the same population (MEIDLINGER, TYLER, & PECK, 1998). Once the larvae are released they may take up to 160 days to develop into three-lobed stages competent to settle (see Table 22; PECK & ROBINSON, 1994). Obviously, these larvae are able to retard their

development after reaching the three-lobed stage until a suitable attachment site is available (PECK, MEIDLINGER, & TYLER, 2001). A prerequisite for this development is water temperatures below 4.5° C. Higher temperatures are lethal for these cold-adapted larvae. Most larvae released in large populations of *Liothyrella uva* settle on conspecifics (PECK, MEIDLINGER, & TYLER, 2001). This has also been shown for the Pacific species *Laqueus californianus* (PENNINGTON, TAMBURRI, & BARRY, 1999). Survival of *Laqueus* larvae was also shown to be temperature dependent. They died after one day in 25° C, but reached settlement competence after 5 to 9 days in temperatures between 15° C and 5° C. Many larvae survived in temperatures between 10–15° C for more than 70 days (see Table 22). Survival for more than 70 days or even 160 days, as in *Liothyrella uva*, enables these larvae to drift in water currents over long distances. Using the circumpolar Antarctic current, *Liothyrella* larvae may travel some 3000 km before they reach appropriate settlement sites. Long-term survival during such a long drift phase would certainly be an advantage. Brooding is obviously not necessarily combined with short-term survival of their lecithotrophic larvae, and dispersal over long distances, at least in some rhynchonelliform species, is possible.

BROODING

Larval brooding occurs in several subgroups of rhynchonelliform brachiopods and extends from simple storage of developing larvae in the lophophore to development in brood pouches, which are invaginations of either the ventral or the dorsal mantle. The most elaborate brood protection is found in thecideide brachiopods. Because of their small shell size, thecideides have often escaped the attention of collectors, and therefore their larval development has been rather enigmatic so far. The only reliable account on the morphology of the larvae and the brood protection in a thecideide brachiopod dates back to the middle of the 19th century (LACAZE-DUTHIERS, 1861). Dealing exclusively with *Lacazella mediterranea*, LACAZE-DUTHIERS's work represents only one out of five Recent thecideide genera: *Lacazella*, *Pajaudina*, *Ospreyella*, *Kakanuiella*, and *Thecidellina*. These five genera fall into two groups: *Lacazella*, *Pajaudina*, *Ospreyella,* and *Kakanuiella* have only one brood pouch to rear their larvae (LOGAN, 1988b, 2004, 2005; LÜTER, WÖRHEIDE, & REITNER, 2003; LÜTER, 2005). This pouch is situated medially in the ventral mantle (Fig. 1525c). Additionally, species within these genera have specialized tentacles, as described for *Lacazella* in volume 1 of the revised *Treatise* (WILLIAMS & others, 1997), and a marsupial notch in the calcified bridge of their brachidium supporting the specialized tentacles involved in brooding. Specialized tentacles, median ventral brood pouch, and larvae have only recently been studied in (ultrastructural) detail in *Ospreyella maldiviana* from the Indian Ocean (Fig. 1525a–1525b; LOGAN, 2005). The marsupial notch is only present in females so that sexual dimorphism is recognizable even when the soft tissue is not preserved (Fig. 1526).

In contrast, *Thecidellina* has two brood pouches in the dorsal mantle on either side of the brachidium's median ridge (Fig. 1527). These brood pouches are only present in specimens that carry developing eggs or larvae so that sex discrimination may be possible as well, but only in reproducing specimens (Hoffmann, unpublished data, 2007). WILLIAMS and others (1997, p. 177) mentioned that, "*Thecidellina* [is] known to deliver [its] eggs into brood pouches," erroneously citing the Anatomy chapter in the first edition of the *Treatise* (WILLIAMS & ROWELL, 1965a), which lacks a description of the breeding behavior of *Thecidellina*. PAJAUD (1970) gave a detailed description of the morphology of *Thecidellina*'s brachidium, including what he calls the sac interbrachial on either side of the median ridge. Obviously PAJAUD never encountered larvae or developing eggs in these sacs, so he was not aware that these are indeed the two brood pouches present in all *Thecidellina* species. Developing embryos plus 15 to 25 eggs can

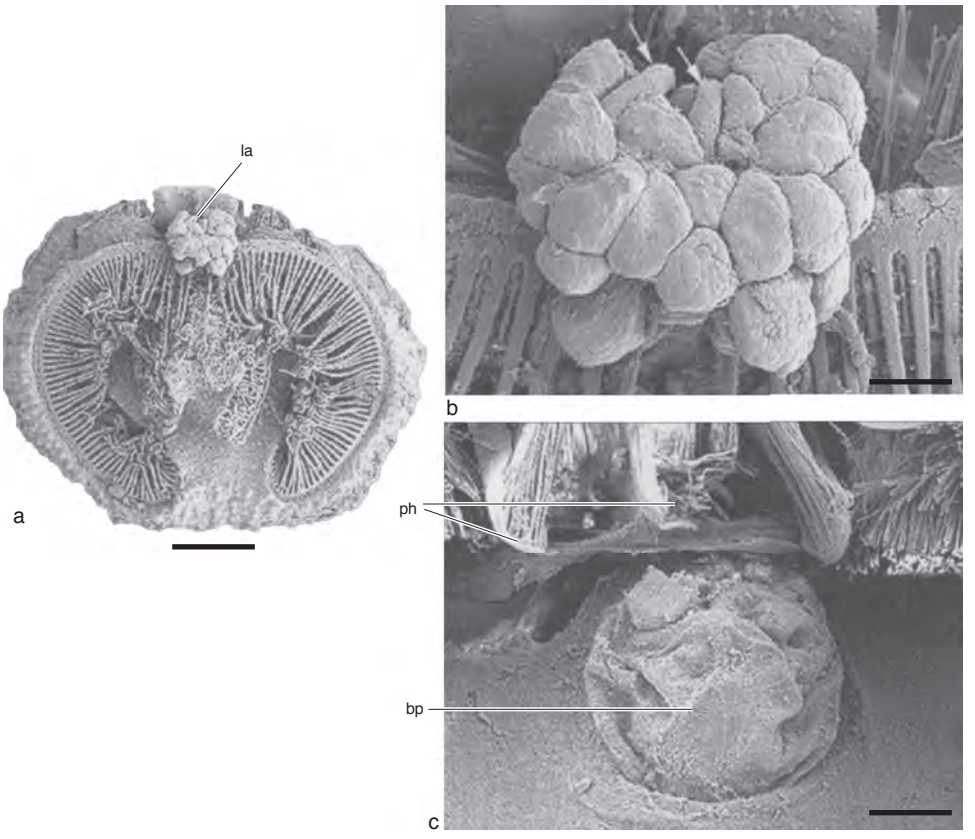

FIG. 1525. SEM micrographs of larvae of thecideide *Ospreyella maldiviana*; *a*, interior of dorsal valve with lophophore and several larvae (*la*) clinging to specialized pair of tentacles, scale bar: 1 mm; *b*, detail of *a* showing the larvae and parts of both specialized tentacles (*arrows*). In natural position tips of tentacles and larvae are situated in single brood pouch that is formed by ventral mantle; scale bar: 0.25 mm; *c*, empty brood pouch (*bp*) in ventral mantle of female below two prongs (*ph*) of hemispondylium; scale bar: 0.25 mm (Logan, 2005).

be found per brood pouch in large specimens of *Thecidellina blochmanni* from Christmas Island, Indian Ocean (C. LÜTER, personal observation, 2001), but the average number of embryos in brood pouches of *Thecidellina* spp. is much smaller (<10; Fig. 1527, indicating a yet undetermined *Thecidellina* sp. from Osprey Reef, Coral Sea, Australia). The brood pouches are invaginations of the dorsal mantle and can be covered by irregular calcitic spicules or tubercles. In some species the tubercles build an anastomosing network or even an almost solid calcitic plate. The morphology of this mantle calcification is highly variable on an individual level and cannot be used for species determination. The opening of each pouch is quite small and points backward toward the mouth opening. It is still unclear how the eggs enter the brood pouches, where they are fertilized, and how the fully grown larvae manage to escape from the pouch.

POSTLARVAL DEVELOPMENT

According to several authors (e.g., STRICKER & REED, 1985a), PERCIVAL (1944) mentioned shell secretion between the mantle lobes and the pedicle lobe in *Calloria inconspicua* during its late larval phase, but PERCIVAL's paper does not contain this statement. Instead he wrote that "during the later period of enclosure [of the apical lobe by the reversed mantle] … the outer surface of the mantle becomes glistening white and

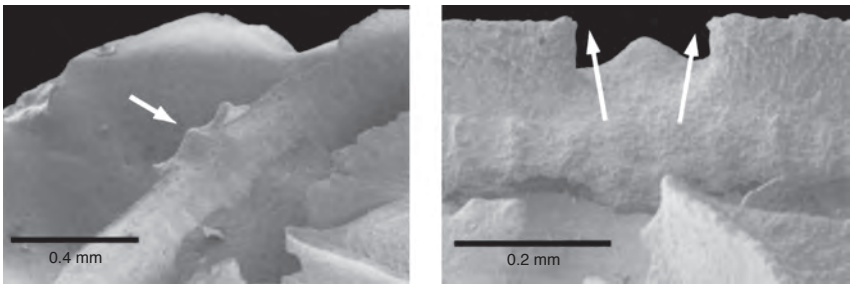

FIG. 1526. SEM micrographs of marsupial notch of thecideide *Ospreyella depressa*; *a*, ventral view of marsupial notch forming calcified plate (*arrow*) in center of posterior bridge; *b*, frontal view of marsupial notch with specialized tentacles (symbolized by *arrows*) reaching through central opening of bridge toward brood pouch in ventral mantle (Lüter, Wörheide, & Reitner, 2003).

smooth. The shape is no longer plastic and there is clear evidence of the formation of a hard shell" (PERCIVAL, 1944, p. 9–10). This happens only postsettlement, during or after metamorphosis and not while the animal is still in its pelagic, larval stage. The only material secreted between pedicle lobe and mantle lobe in rhynchonelliform brachiopod larvae is characterized as an amorphous substance (STRICKER & REED, 1985a, p. 248) followed by so-called multigranular bodies, observed in *Terebratalia transversa*. They may be precursors of the periostracum and were also found in premetamorphic stages of *Calloria inconspicua* (LÜTER, 1998b).

FREEMAN and LUNDELIUS (1999) suggested that fossil craniides had pelagic developmental stages comparable to discinides or lingulides. Examination of fossil craniid shells showed what FREEMAN and LUNDELIUS interpreted as larval shells, implying that through the Lower Jurassic all Craniidae possessed a larval mantle secreting a larval shell. According to the interpretation of lingulid and discinid bivalved developmental stages (see above; LONG & STRICKER, 1991) as pelagic juveniles, craniides would have also had a swimming planktotrophic juvenile (=postmetamorphic) stage. Within the craniides, several groups then may have evolved lecithotrophy during the Upper Jurassic, where "genera with a lecithotrophic larva that lacked a larval shell began to appear" (FREEMAN & LUNDELIUS, 1999, p. 197). The question remains whether these pelagic, shelled craniid developmental stages had a dorsal and a ventral valve. If this was the case, cementation of an already existing ventral valve on the substrate has to be explained. As far as is known from Recent craniides, the dorsal valve is always the first valve to appear. To provide suitable stability of attachment, it may be necessary for the postlarva to make sure that the developing ventral valve is in direct contact with the substrate from the very beginning of its appearance.

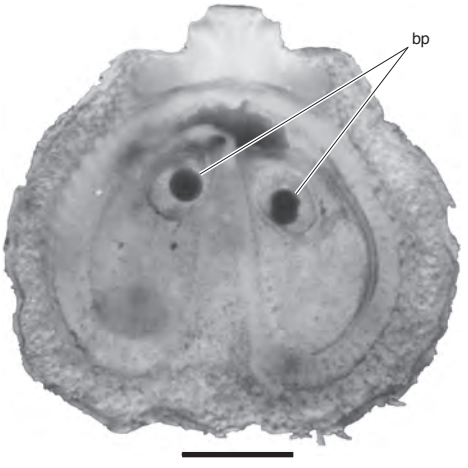

FIG. 1527. Interior of dorsal valve of *Thecidellina* sp. from Osprey Reef, Coral Sea, Australia, lophophore removed; on either side of median ridge dorsal mantle forming brood pouch (*bp*) containing one embryo each; scale bar: 1 mm (new).

THE BRACHIOPOD GENOME

BERNARD L. COHEN

[The University of Glasgow]

INTRODUCTION

The original chapter under this title was completed in August 1995. The most conspicuous advance since then, complete sequencing of nuclear genomes, has not involved brachiopods and is unlikely to do so unless a strong user community makes the case for it or data gathering becomes orders of magnitude less costly (as it shows signs of doing: BLAKESLEY & others, 2004). But smaller-scale progress can be reported, including the complete sequence of four mitochondrial genomes and a considerable quantity of taxonomically focused and phylogenetically valuable sequences derived from nuclear and mitochondrial genes.

The aim of the present chapter is to give an account of relevant work published since 1995 and to outline briefly what is known about work in progress or in press. It will start with an account of general progress and promise in phylogenetics. Then, relevant developments will be described under section headings derived from those used in the original chapter, following which additional new results will be described as far as possible in a descending systematic hierarchy, starting above the phylum level and following the general format of an earlier review (COHEN, 2001b). The reader is also referred to the molecular section of the Millennium Brachiopod Congress volume (BRUNTON, COCKS, & LONG, 2001, p. 119–159). Publications will be included only if they make a significant contribution to brachiopod (or phoronid) phylogeny; those that only incidentally include one or more of these organisms in a gene tree will be omitted, unless comment appears necessary.

General progress in phylogenetics is attributable first to the lower cost per nucleotide and increased throughput of automated DNA sequencing, second to the increased power of computers, and third to the development of new approaches and specialized software for phylogenetic analysis and hypothesis testing (see general accounts in PAGE & HOLMES, 1998; FELSENSTEIN, 2004). Large-scale comparative sequence analyses are in their infancy but have considerable promise and will grow rapidly in importance as more genome sequences are completed. One potential function of such genomic sequencing is to test the validity of phylogenetic inferences from individual or small numbers of genes (e.g., ROKAS & others, 2003; COPLEY & others, 2004; WOLF, ROGOZIN, & KOONIN, 2004). More surprisingly, even at this early stage, comparative genome analyses begin to allow the reconstruction of ancestral genomes (DANCHIN & PONTAROTTI, 2004). Smaller-scale analyses should be interpreted, as ever, with some caution, but large-scale analyses must also not be accepted uncritically, if only because most sequenced genes code for proteins that may be subject to divergent selection pressures in different lineages and at different times, while gene duplication and loss may result in unrecognized paralogy (TELFORD, 2002). There is some reason to expect that genes whose products are involved in complex intermolecular interactions (such as ribosomal RNAs and some proteins) may be among the more reliable indicators of phylogeny (e.g., ARIS-BROSOU, 2005).

STRUCTURE, COMPOSITION, AND ORGANIZATION OF THE NUCLEAR GENOME

COMPOSITION, SIZE, AND CHROMOSOME NUMBER

The only development under this heading has been the recent discovery of a thesis on the ontogeny of *Terebratalia transversa,*

which contains good images of meiosis in a dividing oocyte (FLAMMER, 1963). Seven distinct, small chromosomes are visible, with a hint of a possible eighth (Fig. 1528). The potential importance of chromosome number and organization as markers of evolutionary history has been enhanced by the recent recognition that successive, whole-genome duplications have occurred in the evolutionary history of chordates (MULLEY & HOLLAND, 2004, and references therein). The fact that both *Lingula* (YATSU, 1902) and *Terebratalia* have similar numbers of small chromosomes may indicate that brachiopod chromosomes have undergone little major architectural change since the Cambrian; this seems unlikely, but important if true.

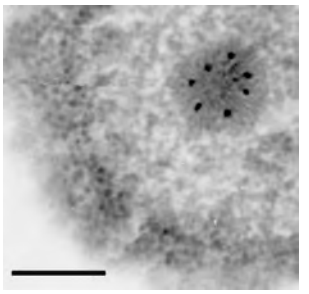

FIG. 1528. Chromosomes of *Terebratalia transversa*. Polar view of a meiotic second metaphase in an oocyte, showing seven clear chromosomes, with a suggestion of a possible eighth lying mostly out of the section plane. From a light-microscope histological study of embryology using stained, serial, 5 mm sections (Flammer, 1963). An inked label line on the left of the original illustration has been removed digitally, leaving a faint linear trace; scale bar, 10 mm (new).

STRUCTURE, COMPOSITION, AND ORGANIZATION OF MITOCHONDRIAL GENOME

In 1995, it was widely anticipated that complete mitochondrial genome sequences (mtDNAs) would prove to be a generally valuable source of phylogenetic information because in addition to straightforward evolution of maternally transmitted, homologous gene sequences, rare changes in gene order appeared to offer very strong phylogenetic characters (e.g., BOORE & others, 1995; BOORE, 1999). Broadly speaking, these hopes have been well satisfied within some groups (e.g., mammalian orders) from which a wide and representative selection of mtDNAs has been obtained, but results have not been so good where sampling has been narrower and at deep taxonomic levels. For example, gene order and sequence of mtDNAs only weakly resolves molluscan class-level relationships (ANDERSON, CORDOBA, & THOLLESON, 2004) and fails completely to resolve relationships between the major lophotrochozoan phyla. On the other hand, despite great morphological diversity, gene order appears to be relatively well conserved and informative among the major clades of annelids and in sipunculans (JENNINGS & HALANYCH, 2004). These and other examples show that the phylogenetic utility of complete mitochondrial sequences varies considerably; they are far from a panacea, and quite dense taxonomic sampling may be needed to obtain even modest resolution. Furthermore, accumulating evidence suggests that recombination of mitochondrial genomes of maternal and paternal origin may sometimes occur, though this should not affect phylogenetic inference above the population level (SLATE & GEMMELL, 2004). Despite these (and other) limitations, all published analyses of mitochondrial gene or genome sequences that include brachiopods and phoronids have strongly agreed that these taxa belong among the lophotrochozoan protostomes along with annelids and mollusks (COHEN, GAWTHROP, & CAVALIER-SMITH, 1998; STECHMANN & SCHLEGEL, 1999; NOGUCHI & others, 2000; BOORE & STATON, 2002; TOMITA & others, 2002; BOORE, MEDINA, & ROSENBERG, 2004; HELFENBEIN & others, 2004; PAPILLON & others, 2004; RUIZ-TRILLO & others, 2004; WOLF, ROGOZIN, & KOONIN, 2004).

No concerted program to obtain complete mtDNA sequences of taxonomically representative brachiopods and phoronids has been funded, and the four brachiopods so far sequenced appear to have been those

that could be most readily obtained by the workers concerned. Thus, complete mitochondrial genomes have been described from the cancellothyridid, *Terebratulina retusa* (Stechmann & Schlegel, 1999), the two terebratellids, *Laqueus rubellus* (Noguchi & others, 2000) and *Terebratalia transversa* (Helfenbein, Brown, & Boore, 2001), and from a lingulid, *Lingula anatina* (Endo & others, 2005), but no craniid, discinid, or rhynchonellide sequence has been seriously attempted. In addition, most of the mitochondrial genome of one phoronid has been reported (Helfenbein & Boore, 2004), and some work has been done on the mtDNA sequence of a second lingulid, *Glottidia* (K. Helfenbein and N. Tuross, personal communications, 2004). Not surprisingly, in view of the patchy taxonomic coverage, the resulting data have been relatively uninformative about brachiopod interrelationships, though they are of some molecular biological interest. Notable features of or inferences from the available brachiopod mtDNAs include the following.

The mitochondria of brachiopods use the same genetic code as most other protostomes (Saito, 1998; Stechmann & Schlegel, 1999; Saito, Kojima, & Endo, 2000).

Gene order in *Terebratulina* differs from that in a chiton (*Katharina*) by a single inversion. This was and probably still is the smallest difference between mitochondrial gene maps of any two metazoan phyla. The significance of this small difference remains uncertain, however (see below), as does the fact that in analyses of SSU rDNA sequences, a chiton was also found to be the closest outgroup to brachiopods and phoronids (Cohen & Gawthrop, 1996; Cohen, Gawthrop, & Cavalier-Smith, 1998). In *Terebratulina,* all the genes are transcribed from the same strand (Stechmann & Schlegel, 1999). This gene arrangement implies that transcription (i.e., synthesis of RNA complementary to DNA) is unidirectional, from a single origin. The significance of this is also uncertain (and see below), except that it may represent an evolutionary simplification.

The mitochondrial genome of *Laqueus* is small, with a compact organization in which overlaps of gene ends are prevalent. As in *Terebratulina*, all genes are coded in the same strand, but the overall gene arrangement differs from that of any other organism reported. Despite this, a number of short (2–3 gene) segments are arranged as in other mitochondrial genomes, including the chiton *Katharina* and the annelid *Lumbricus*, and hence may be interpreted as plesiomorphies (Noguchi & others, 2000).

The mitochondrial genome of *Terebratalia*, like that of *Laqueus*, is small for a metazoan (~1500 fewer nucleotides than *Terebratulina*), and again has all genes coded in the same strand, but with a radically different map order, though some gene junctions are shared with *Laqueus*. As expected from their consuperfamilial taxonomy, the *Laqueus* and *Terebratalia* genomes share features of base composition, codon usage pattern, and protein amino-acid composition, and differ from *Terebratulina* in these (related) properties. One laqueid noncoding (presumed replication start) region is the reverse complement of that in *Terebratulina*, suggesting that an inversion occurred in one lineage and that the origins of replication may be oppositely oriented. Comparison of gene junctions in all three brachiopod genomes and the chiton suggest that some are plesiomorphic and that the laqueid condition is derived (Helfenbein, Brown, & Boore, 2001), in keeping with other established gene sequence and morphological inferences. Although it is unfortunate that the brachiopod mitochondrial genome sample does not include all main lineages, the comparison of two laqueids with a cancellothyridid is useful.

For the phoronid, *Phoronis architecta*, the sequence of all but a small part of the mitochondrial genome has been reported. As in *Terebratulina*, there is remarkable similarity to the chiton, *Katharina*, with only 3 of 31

genes being differently arranged. Cladistic analysis of a gene adjacency matrix gives very strong support to the protostome, lophotrochozoan association of brachiopods and phoronids, and inversion of one particular gene junction suggests that lophotrochozoans are derived relative to deuterostomes. Again, however, there is insufficient information to resolve relationships between brachiopods and other lophotrochozoan phyla (HELFENBEIN & others, 2004).

The only mitochondrial complete sequence available from any inarticulated brachiopod, a specimen of *Lingula anatina*, is strikingly different in many respects from the metazoan norm, being unusually large (28.8 versus ~15 kb) with expanded genes that differ in nucleotide sequence from their homologues in other animals and also with much unassigned sequence and a highly divergent gene order (ENDO & others, 2005). This genome contains two major repeat regions and nested direct repeats of a complexity otherwise unparalleled in animal mtDNAs. Such a structure is not necessarily typical for lingulids, however, because unpublished data obtained by Southern blotting indicated that specimens of *Lingula* from other localities and of *Glottidia* appeared to have a more standard genome size (COHEN & GAWTHROP, cited in COHEN, 2001b). However, further examination of the blots has suggested that this conclusion may be unsafe (COHEN, unpublished observations, 2006).

The unusually large *Lingula* mtDNA could be explained by a model for mitochondrial gene rearrangement by duplication and nonrandom loss (LAVROV, BOORE, & BROWN, 2002), under which it might represent an intermediate evolutionary state between major duplication(s) and completed gene loss. This duplication or deletion model can also account for the (possibly independent) origin of mitochondrial lineages in which all genes are transcribed from the same strand, as in *Terebratulina*, *Laqueus,* and *Terebratalia* (LAVROV, BOORE, & BROWN, 2002).

Because the map order of most genes in the circular mitochondrial genome changes relatively slowly, high hopes have been entertained that map order comparisons would lead to strong phylogenetic inferences. This is a difficult problem when many maps are to be compared, made more difficult by ignorance of the full range of mechanisms by which these genomes become rearranged. A recent Bayesian analysis compared the full gene maps of 87 (and a limited set of 28) metazoan taxa (not including the incomplete phoronid sequence) using an admittedly oversimple evolutionary model in which inversion was the only allowed mechanism of change. Under this simplified model, and with the associated taxonomic priors, brachiopods, annelids, and mollusks group together with strong to moderate support, and brachiopods are a strongly supported sister group of annelids (LARGET & others, 2005). It is too early to know whether this result reflects the greater conservation of mitochondrial gene order in annelids than in mollusks or the relatively unrealistic evolutionary model used.

TOWARD A GENEALOGICAL CLASSIFICATION OF BRACHIOPODA

STUDIES ON PROTEIN AND NUCLEIC ACID SEQUENCES

The principles upon which molecular phylogenetic reconstructions proceed from protein (amino-acid) and nucleic acid (nucleotide base) sequences are generally well understood (e.g., PAGE & HOLMES, 1998; FELSENSTEIN, 2004), but until recently the accuracy of such reconstructions had been verified only indirectly. Strong, direct support has now been obtained in a biochemically defined, serial PCR (polymerase chain reaction) experiment (SANSON & others, 2002) in which all standard phylogenetic methods accurately reconstructed both known divergence times and ancestral sequences. This result strongly reinforces

the general confidence already placed in the molecular approach to phylogeny reconstruction; although limited to crown taxa, it provides the best available independent test of phylogenetic inferences from morphology. Of course, morphology itself depends on genes, but those used in phylogenetics neither modulate morphology nor are closely linked to those that do and thus (are assumed to) evolve independently. Various other assumptions about gene evolution underlie our confidence in metazoan molecular systematics, especially that lateral gene transfer (LGT) between distantly related taxa will rarely confuse. A microbial example shows how LGT might operate to distort a phylogeny based on the SSU rRNA gene (Miller & others, 2005).

The principles that should be adopted when comparing phylogenetic inferences based on molecular sequence data with the existing systematics of an extensively studied group like the Brachiopoda have not been the subject of much overt discussion. Those that the author favors are as follows.

1. As direct representations of the primary vehicle of inheritance, gene sequences provide the inherently most reliable evidence of evolutionary history, though as potential palimpsests, their interpretation may be difficult.

2. Molecular results must be replicable and preferably replicated, if possible from a genetically independent source; e.g., nuclear and mitochondrial genomes or closely related taxa or from nuclear genes of different functional classes.

3. Obvious sources of error such as paralogy or amplification of pseudogenes must be excluded.

4. Confidence in the validity of molecular results is enhanced by a large measure of congruence between molecular and nonmolecular systematics.

5. If all sources of molecular error have been excluded, residual discordance points to probable errors in nonmolecular data or their interpretation, e.g., caused by unrecognized homoplasy.

Above the Phylum Level: Protostomes or Deuterostomes?

The majority of post-1995 analyses of metazoan nuclear gene sequences that include at least one brachiopod and phoronid have involved the SSU rDNA gene, and these have confirmed earlier reports (Halanych & others, 1995; Cohen & Gawthrop, 1996, 1997; Cohen, Gawthrop, & Cavalier-Smith, 1998; Cohen, 2001b) that these taxa belong among the lophotrochozoan protostomes, not among deuterostomes, and that a (brachiopod + phoronid) clade is generally recovered. Given the limited resolution available from the SSU rDNA gene, particular interest attaches to analyses that add data from a new gene, especially if it gives concordant overall interphylum relationships while increasing resolution. The most convincing such work (Mallatt & Winchell, 2002) belongs to a series that shows that the LSU rDNA gene has these properties, improving basal, phylum-level resolution (but not enough) and confirming the protostome and deuterostome relationships already inferred from SSU rDNA sequences. Because both SSU and LSU genes specify ribosomal components, they are not evolutionarily independent, but many of the rDNA results have been independently confirmed by analysis of the amino-acid sequence of a gene coding for a protein whose function is unrelated to that of the ribosome (Anderson, Cordoba, & Thollesson, 2004).

Other protein-coding genes may be more problematical, however. For example, in an analysis of flagellar creatine kinase paralogues (i.e., a multigene family that originated by gene duplication and in which descendants of different copies form clades), not only was phylogenetic resolution low, but protostome and deuterostome sequences appear intermingled within a clade (Suzuki & others, 2004). The brachiopod sequence was close to one from a polychaete, but adjacent polychaete and deuterostome (echinoid) sequences were paraphyletic. These extraor-

dinary phylogenetic results probably reflect convergence of amino-acid sequences caused by natural selection acting via creatine kinase function. Problems also beset an analysis based on amino-acid sequences of a myosin subunit gene (Ruiz-Trillo & others, 2002), backed up by and combined with analyses of SSU rDNA sequences. The brachiopod myosin sequence came from a specimen of *Glottidia* sp. (identified by BLC from a specimen provided by I. Ruiz-Trillo, unpublished data, 2004), and it clustered well away from the phoronid, which appeared as the sister of a sipunculan, a relationship that has never emerged from SSU or LSU gene trees, in which available sipunculan sequences are divergent. The SSU analysis also widely separated the brachiopod (*Terebratalia*) and phoronid. Both unusual relationships probably result from inclusion in the alignment of highly divergent acoel sequences that necessitate the exclusion of many sites. Even in this analysis, however, the protostome affinities of brachiopods and phoronids were not in question.

Less comprehensive, but unambiguous reports of the protostome affinity of brachiopod genes, genome components, or gene products include the following: a brief account of 5S RNA (Küntzel, Piechulla, & Hahn, 1983) that escaped notice in our original chapter; an analysis of the phylogenetic distribution of structural forms of metazoan intermediate filament proteins that clearly distinguish protostomes from deuterostomes (Erber & others, 1998); a survey for the presence and phylogenetic relations of transposable elements (Arkhipova & Meselson, 2000); and a review that restated the already well-established protostome affinity based on *hox* and mitochondrial genes and genomes and went on strangely to discuss morphological and developmental characters based on information "mostly taken from classical zoological and developmental textbooks" (de Rosa, 2002, p. 855).

The number of independent lines of molecular evidence favoring a protostome affinity for brachiopods and phoronids is now too great for this to be discounted, which raises the matter of the current lack of congruence between inferences from molecules and from morphology. This is most strikingly demonstrated by a number of studies in which SSU rDNA alignments and morphological data have been combined in some sort of total evidence approach (e.g., Cavalier-Smith, 1998; Zrzavý & others, 1998; Peterson & Eernisse, 2001; Zrzavý, 2003; Glenner & others, 2004). In these analyses the molecular results on their own have given unqualified support to the position of brachiopods and phoronids within the lophotrochozoan protostomes, but the same cannot be said of the morphological results, in some of which, including one that explored differential morphological:molecular weighting (Zrzavý & others, 1998), the morphological characters clustered brachiopods and phoronids (and even ectoprocts) with deuterostomes. Traditional, noncladistic, morphological studies (e.g., Nielsen, 2002) also continue to favor a deuterostome affinity for brachiopods and phoronids, as do morphological cladistic analyses based on characters and codings that reflect similar assumptions (e.g., Nielsen, Scharff, & Eibye-Jacobsen, 1996; Sorensen & others, 2000).

It is at present unclear what features of the morphological characters or their analysis are responsible for the conflict. One possibility is that there may be too much morphological homoplasy for any analysis to retrieve a historically accurate evolutionary tree (Carlson, 1994), while weaknesses of character description and definition may also be involved (e.g., Jenner, 1999, 2000, 2001, 2002, 2004; Jenner & Schram, 1999), affecting both cladistic and traditional morphological studies. Evidence of the latter includes (1) an electron microscopical study that leads to revision of the traditional descriptions of a tripartite coelom in phoronids, suggesting that the light microscopy of stained tissue sections (the basis of most classical morphology) is not reliable for homology inference (Bartholomaeus,

2001); and (2) recent work on cell fate in a chiton, which sheds doubt on inferences based on the presence or absence of spiral cleavage (Henry, Okuso, & Martindale, 2004). A potential weakness specific to combined analyses of molecular and morphological characters is that while each nucleotide sequence difference probably corresponds (at least for moderately close relatives) to a single, fixed, evolutionary event, we do not know how many such events (between one and thousands) underlie typical morphological differences. Thus, it is questionable to accord equal weight to molecular and morphological data-matrix elements, as is commonly done (but see Sanderson & Donoghue, 1996), while the range of differential weighting so far explored may be inadequate. Thus, the supposed deuterostome affinity claimed by morphological analyses remains controversial, and it remains to be determined whether any characters that support it will survive critical reanalysis.

Monophyly of Lophophorates

Molecular evidence from the SSU rDNA gene has divided the four lophophorate phyla (pterobranchs, ectoproct bryozoans, phoronids, and brachiopods), putting pterobranchs into the deuterostome alliance alongside other hemichordates and the remainder among the lophotrochozoan protostomes (Halanych, 1995; Halanych & others, 1995). Until recently, only three ectoproct bryozoan SSU rDNA sequences were available, representing one gymnolaemate and two phylactolaemates, and in all analyses these fell among the lophotrochozoan protostomes but separate from brachiopods and phoronids (Halanych & others, 1995; Cohen & Gawthrop, 1997; Cohen, Gawthrop, & Cavalier-Smith, 1998; Giribet & others, 2000; Peterson & Eernisse, 2001). A further ten gymnolaemate and one stenolaemate sequence have since been deposited in GenBank (2006), so that all three ectoproct classes are now represented. When aligned with deuterostome and protostome sequences, the position remains as it was: ectoprocts are clearly lophotrochozoan protostomes, but there is no hint of support for a lophophorate or indeed an ectoproct clade (Cohen, unpublished data, 2005). A recent study of phylactolaemate interrelationships that involved a limited sample of other taxa arrived at similar conclusions (Wood & Lore, 2005). Thus, when the body plans of phyla are compared, lophophores are either plesiomorphic or convergent; lophophorates are not monophyletic (as they were considered to be from morphology, e.g., Hatschek, 1888 in 1888–1891; Emig, 1977).

Monophyly of Brachiopods, Position of Phoronids, and Relationships Between and Within Main Brachiopod Lineages

Whereas monophyly of brachiopods and phoronids has been supported by most SSU rDNA analyses that have included representatives of both taxa, their interrelationships have been less consistently reported, with an early SSU tree showing a (phoronid + articulated) but later ones a (phoronid + inarticulated) clade. This discrepancy was traced to the first phoronid sequence to be described (GenBank accession U12648, Halanych & others, 1995), which, by resequencing from the same nominate taxon, was inferred to be an artefactual chimaera, probably involving a phoronid and an articulated brachiopod (Cohen, Gawthrop, & Cavalier-Smith, 1998; Cohen, 2000). SSU analyses that exclude U12648 generally recover the (inarticulated + phoronid) clade, but depending on the alignment, phoronids may instead appear as the sister group of brachiopods (e.g., Peterson & Eernisse, 2001). Other analyses that have been misled by this sequence include Zrzavý and others (1998) and Wallberg and others (2004). The molecular monophyly of (brachiopods + phoronids) has led to three proposed reclassifications of brachiopods and phoronids: (1) as a new phylum, Phoronozoa (Zrzavý & others, 1998, with second thoughts noted in proof), (2) as a new phylum Brachiozoa

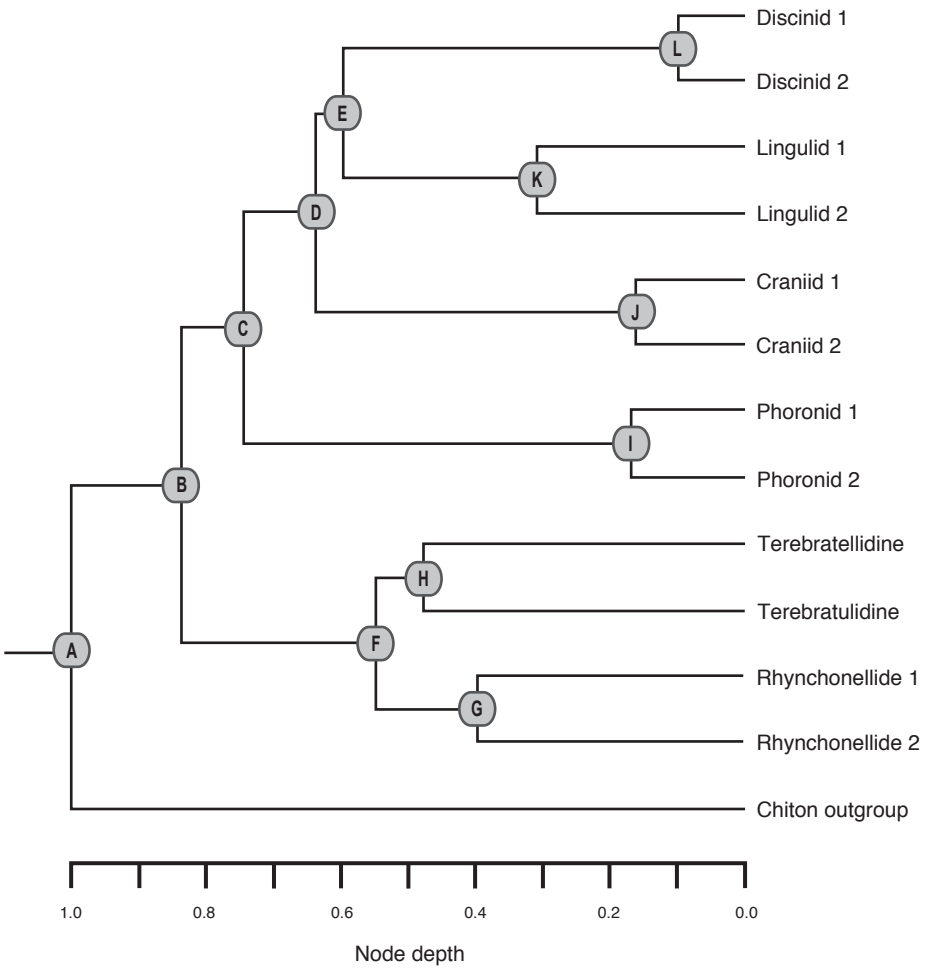

FIG. 1529. Phylogeny of brachiopods and phoronids. Nonparametric rate-smoothed maximum likelihood chronogram, with branch lengths proportionate to time depth. Node labels as in Cohen and Weydmann (2005) (new).

(CAVALIER-SMITH, 1998), or (3) phoronids as a subphylum Phoroniformea within a phylum Brachiopoda, redefined to include both shelled and tubiculous forms (COHEN, 2000). The last proposal was designed to fit into the supraordinal classification adopted in the present work (KAESLER, 1997, 2000, 2002, 2006; WILLIAMS & others, 1996), while avoiding the inconvenience of changing the name of a taxonomically rich phylum.

Following a demonstration that the LSU rDNA gene alone or in combination with SSU yields a well-resolved metazoan phylogeny congruent with other data (MALLATT & WINCHELL, 2002; WINCHELL & others, 2002), improved resolution of the (brachiopod + phoronid) clade and of the main brachiopod lineages has been sought by determining an informative portion of this gene in pairs of phoronids and of brachiopods from every main lineage except thecideidines. In the alignment analyzed, the SSU gene provided 170 and the LSU gene provided 377 variable sites, leading to greatly increased phylogenetic resolution (Fig. 1529). Analyses of these data, validated

by recovery of both previously reported distant outgroup relationships and ingroup indicator clades, strongly placed phoronids within brachiopods, as sister to the three inarticulated lineages, craniids, discinids, and lingulids. In a Bayesian likelihood analysis the posterior probability of all clades was 0.90–1.00, and this strongly supported result was used to propose a further amended classification (Cohen & Weydmann, 2005) in which the phylum Brachiopoda was again retained, but with its definition amended (as in Cohen, 2000) to include the shell-less, tubiculous phoronids. The subphyla Linguliformea and Rhynchonelliformea were retained, the former being amended to include phoronids, which became a new class, Phoronata (as anticipated, Cohen, 2000). In addition (and see below) the subphylum Craniiformea was reduced to a class, Craniata, within Linguliformea. In this analysis, molecular evolutionary rates in brachiopods, phoronids, and the chiton and pectinid molluscan outgroups were not ideally clocklike. Nevertheless, after rate smoothing, the data could be calibrated against the fossil record and used to estimate that chitons diverged from (brachiopods + phoronids) in the late Proterozoic, supporting the idea that much paleontologically invisible metazoan diversity originated long before the Lower Cambrian (Cohen & Weydmann, 2005).

The position of phoronids as the sister group of the other extant inarticulated brachiopods could result from a artefact that has been termed short branch exclusion, i.e., these taxa might be incorrectly drawn together by plesiomorphic similarities that are present because all have experienced atypically little evolutionary change (Stiller & Harrell, 2005). If this were so, the position of phoronids should be sensitive to taxon composition, changing when faster-evolving, long-branched taxa are added or removed. However, no such changes were observed when the taxon set was enlarged to include distant and long-branched outgroups, nor when severely pruned (Cohen & Weydmann, 2005). Short branch exclusion could potentially account for the repeated observation (e.g., Cohen & Gawthrop, 1997; Cohen, Gawthrop, & Cavalier-Smith, 1998; Cohen & Weydmann, 2005) that a chiton is the closest sister-taxon of (brachiopods + phoronids), but this possibility is also not currently supported by any evidence. One notable feature of this SSU+LSU rDNA analysis (Fig. 1529) is the presence, for the first time, of the (discinid + lingulid) clade that is strongly predicted by morphology but which has never emerged from analyses of the SSU rDNA gene alone. This tree also confirms earlier molecular evidence that calcite mineralization in craniids and in rhynchonelliforms must have originated independently or is plesiomorphic (Carlson, 1994, 1995); craniids do belong among inarticulated, not among articulated brachiopods (*contra* Gorjansky & Popov, 1986; Popov & others, 1993; Williams & Holmer, 2002; Li & Xiao, 2004). Indeed, this tree suggests that the old classification, with subphyla Articulata and Inarticulata, had considerable merit.

As noted, not all molecular analyses unambiguously recover a (brachiopod + phoronid) clade. One that did not is based on analysis of a large subset (~300 taxa) of what is probably the most wide-ranging alignment of metazoan SSU rDNA sequences yet published (over 600 taxa, Peterson & Eernisse, 2001). Absence of the (brachiopod + phoronid) clade in this analysis can probably be attributed to the exclusion of many ambiguously aligned sites necessitated by the alignment of so many sequences. Another heavily pruned SSU rDNA analysis also failed to recover a (brachiopod + phoronid) clade (Ruiz-Trillo & others, 2002), but it is less understandable that the protein-coding gene included in that work also recovered unusual relationships, as discussed above.

Two wide-ranging collections of sequence data bear on the relationships of the main brachiopod lineages, but both are unfinished and neither has yet been published in full. In Glasgow, the author has continued to

sequence SSU rDNA genes as and when new taxa arrive, and illustrative results from this data set are given in Figure 1530 (discussed below). Also, in view of the now-recognized limitations of SSU data, partial LSU sequences are being added as time and resources allow. In Japan, mitochondrial *cox1* sequences have been collected by Michiko SAITO, in some cases from the same individual DNAs used for rDNA gene amplification. The *cox1* data-set also includes closely related, especially laqueoid, species and genera that would not be appropriate candidates for rDNA sequencing, while the rDNA data set includes some taxa for which *cox1* sequences have not been obtained, either for want of opportunity and resources or because existing primers did not work well. Where they do overlap, there is a large measure of agreement between the two sources (COHEN, unpublished data, 2005, and see below). Separate and combined analyses of the SSU and *cox1* data will be presented elsewhere.

SSU rDNA Phylogeny of Brachiopods.—In general, the SSU rDNA gene clearly distinguishes animals from plants, and Radiata from Bilateria, and whether brachiopods belong in the protostome or deuterostome alliances, but it does not clearly resolve the interrelationships of the lophotrochozoan phyla nor the deepest (or shallowest) branchings of the extant brachiopod lineages. The failures probably reflect the duration and age of the cladogenetic events involved: a rapid sequence of divergence events will allow little phylogenetic signal to accumulate in such a slowly evolving gene, and the more ancient the divergence, the more likely the original signal will be overwritten (ADOUTTE & PHILIPPE, 1993). Moreover, resolution is further reduced because the most rapidly evolving gene regions are prone to length variation (necessitating the introduction of alignment gaps), and the wider the range of taxa involved the more must be excluded from analysis because gaps create alignment ambiguity. Figure 1530 is based on SSU rDNAs from 41 articulated brachiopods. The tree topology and clade support values were obtained by a Bayesian likelihood method, using a model of evolution and estimated parameters that best fitted the data, but without taking into account any differential rates applicable to base-paired and unpaired sites inferred from a secondary structure model. Note that Bayesian clade support values (posterior probabilities) are not directly comparable with bootstrap proportions (%).

The SSU rDNA results in Figure 1530 (which the reader might usefully compare with those in the original chapter, COHEN & GAWTHROP, 1997, fig. 180–188, p. 194, 196, 198, 200) illustrate the power and some pitfalls of molecular systematics. More detailed, but nonexhaustive discussion follows, group by group. The results shown generally satisfy the repeatability criteria noted above but reveal some disagreements with traditional, morphological systematics, of which some are dependent on the alignment and analysis method used, while others are taxon specific. The tree topology shown, while representative, is not definitive of the inferences available from the SSU rDNA gene and is deliberately incomplete; the craniid, discinid, and lingulid inarticulated lineages are omitted because this gene contains too few informative sites to reliably resolve their interrelationships (see Fig. 1529).

Molluscan Outgroups.—The chiton, *Acanthopleura*, was the designated outgroup (as discussed in COHEN, GAWTHROP, & CAVALIER-SMITH, 1998), and other short-branched mollusks were included to help indicate the reality of the (brachiopod + phoronid) clade.

Phoronids.—Resolution of the two phoronid genera is apparent, but otherwise the pattern of relationships resolved is unremarkable.

Rhynchonellides.—The five genera sequenced form two subclades, one containing members of the Basiliolidae (*Eohemithiris* and *Parasphenarina*), and one grouping together genera currently placed

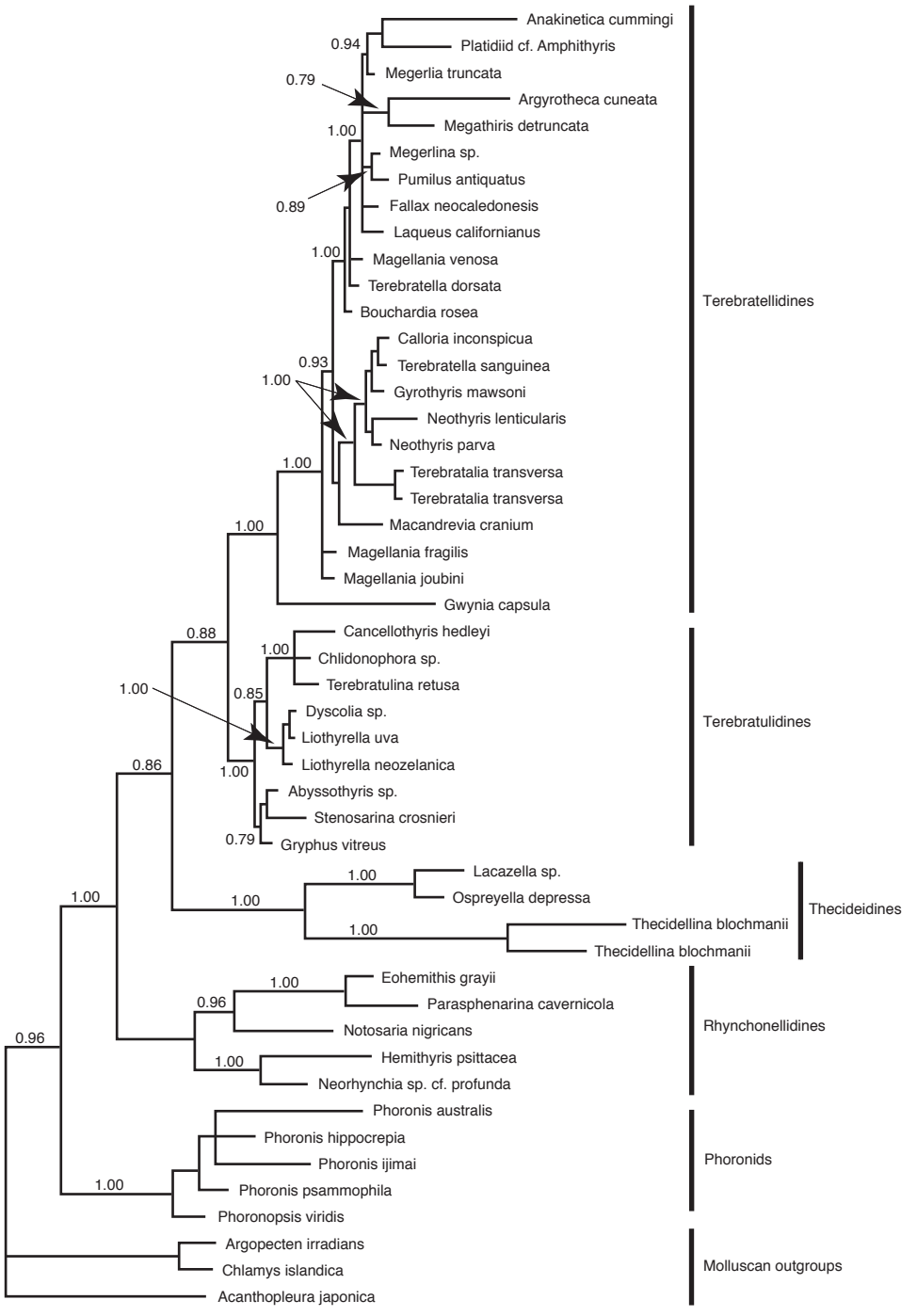

FIG. 1530. *For explanation, see facing page.*

in different superfamilies (*Hemithiris* and *Neorhynchia*). *Notosaria* is morphologically grouped with *Hemithiris*, but here joins the basiliolid clade with fairly strong support. These results both agree and disagree with the current classification (WILLIAMS, 2002). Rhynchonellides are undersampled and, as noted by WILLIAMS (2002), data from *Cryptopora* are awaited with interest. Unfortunately, first attempts to obtain SSU rDNA sequence from the only available specimen were not successful. A sample of the micromorph, *Tethyrhynchia* (LOGAN & ZIBROWIUS, 1994), also awaits analysis. The position of the rhynchonellides as the sister of loop-bearing extant rhynchonelliforms is compatible with the fossil record.

Thecideidines.—The phylogenetic position of thecideidines has long been enigmatic (e.g., BAKER, 1990; CARLSON, 1995; JAECKS & CARLSON, 2001, and references therein) and will evidently also be difficult for molecular data to resolve. When reliable sequence from *Lacazella* became available, our first sequence, supposedly from *Thecidellina* (COHEN, GAWTHROP, & CAVALIER-SMITH, 1998), was recognized as a PCR artefact and withdrawn (COHEN, 2001a). The four genuine SSU rDNA sequences now available clearly belong to and distinguish lacazellid and thecidellinid subclades (the two specimens of *Thecidellina* are from widely separated Pacific Ocean localities) and thereby agree with morphology, but they are on long branches, and in other analyses the whole clade behaves as a sister group of rhynchonellides (not shown). Bayesian clade support for the position shown in Figure 1530 is not very high, and it will be necessary to collect more slow-evolving data before a reasonably reliable position for thecideidines is identified; unfortunately, first attempts to obtain LSU rDNA sequences were not successful (COHEN, unpublished data, 2005). Although the results do suggest that thecideidines belong within the Terebratulida and are not relics of an otherwise extinct lineage, long-branch attraction between thecideidines and rhynchonellides is a possibility that cannot yet be excluded.

Terebratulidines.—It has long been recognized that relatively few useful morphological

FIG. 1530. Phylogeny of articulated brachiopods. SSU rDNA sequences were aligned using Clustal-X v. 1.81 (THOMPSON & others, 1997) with gap opening or extension penalties 10/0.5 and with local realignment of highly variable regions, giving a total of 1816 aligned sites. Ambiguously aligned regions were then removed using Gblocks 1.91 (CASTRESANA, 2000), with default parameters (which vary according to the number of taxa and using the conserved block size recommended for rRNA sequence) leaving 1655 aligned sites (91% of 1816 sites), which were analyzed using MrBayes 3.0. The autocorrelated gamma maximum likelihood model was used because it gave a slightly higher likelihood than the AIC-optimal model (6st+invgamma) identified by MrModeltest 2.0 (NYLANDER, 2004). The Bayesian likelihood analyses were run more than once with default priors in 4 chains for 10^5 generations, sampled every 10^2 generations. All relevant parameters stabilized within 10^4 generations and the consensus tree shown was obtained from the last 5000 generations. Clade support values (posterior probabilities) are attached to selected, nonterminal nodes. Support for all terminal nodes was 0.93–1.00. Branch lengths are proportional to the number of inferred substitutions per site. In the following list accession numbers are provided for sequences obtained from GenBank, and unpublished sequences from the author's laboratory are identified by a D number: *Anakinetica cummingi* D1307, Platidiid cf. *Amphithyris* D1302, *Megerlia truncata* U08321, *Argyrotheca cuneata* AF119078, *Megathiris detruncata* D1292, *Megerlina* sp. AF025943, *Pumilus antiquatus* D1482, *Fallax neocaledonesis* AF025939, *Laqueus californianus* U08323, *Magellania venosa* D1390, *Terebratella dorsata* D1432, *Bouchardia rosea, Calloria inconspicua* AF025938, *Terebratella sanguinea* U08326, *Gyrothyris mawsoni* AF025941, *Neothyris lenticularis* DNZ361, *Neothyris parva* AF025944, *Terebratalia transversa* AF025945, *Terebratalia transversa* D1494, *Macandrevia cranium* AF025942, *Magellania fragilis* AF202112, *Magellania joubini* D1295, *Gwynia capsula* AF025940, *Cancellothyris hedleyi* AF025929, *Chlidonophora* sp. AF025930, *Terebratulina retusa* U08324, *Dyscolia* sp. AF025931, *Liothyrella uva* U08330, *Liothyrella neozelanica* U08332, *Abyssothyris* sp. AF025028, *Stenosarina crosnieri* AF025934, *Gryphus vitreus* AF025932, *Lacazella* sp. D1340, *Ospreyella depressa* D1414, *Thecidellina blochmanii* D1440, *Thecidellina blochmanii* D1339, *Eohemithis grayii* AF025936, *Parasphenarina cavernicola* D1422, *Notosaria nigricans* U08335, *Hemithyris psittacea* U08322, *Neorhynchia* sp. cf. *profunda* AF025937, *Phoronis australis* AF202111, *Phoronis hippocrepia* AF202112, *Phoronis ijimai* AF202113, *Phoronis psammophila* AF025946, *Phoronopsis viridis* AF123308, *Argopecten irradians* L11265, *Chlamys islandica* L11232, *Acanthopleura japonica* X70210. The sequence from *Bouchardia rosea* was provided by M. G. SIMÕES (new).

characters are available among terebratulidines, so that sequence analyses should be particularly valuable, and this was reinforced by an analysis that showed that nuclear and mitochondrial genes gave congruent trees for a few members of this group (COHEN & others, 1998). Cancellothyridids apart, few new, morphologically identifiable terebratulidine specimens have been received, however [no longer as true as it was, but it will take much time before the work is done], and this potential remains unexplored. Cancellothyridids (COOPER, 1973c) are the best-established morphological subgroup, and SSU rDNA agrees (Fig. 1530), yielding a well-supported clade, as well as two other clades not predicted from morphology. Interestingly, analyses with mtDNA sequences within cancellothyridids revealed paraphyly (LÜTER & COHEN, 2002): *Cancellothyris* and *Chlidonophora* nested within Terebratulina, suggesting that cancellothyridids have been oversplit through the use of unreliable morphological characters (COOPER, 1973c). In our analysis (LÜTER & COHEN, 2002) with rather divergent outgroup sequences (none others then being available), *T. unguicula* from Alaska appeared to be the sister-group of the other taxa, but the polarity of this clade is now suspect and requires reinvestigation with closer outgroups. In this study it was suggested that brachiopod populations may retain evidence of ancestral migration through Mesozoic Tethys. This suggestion was also made on the basis of mitochondrial sequence evidence for well-supported clades uniting *Dyscolia* (but not *Gryphus*) with *Liothyrella* and Pacific *Stenosarina* with *Abyssothyris* (Fig. 1530 and COHEN & others, 1998), and it was also raised in speculations on the origin of *Glottidia* (WILLIAMS & others, 2000). Similar evidence appears to be emerging from a study of craniid interrelationships (COHEN, LONG, & SAITO, 2007). With their cosmopolitan distribution, lecithotrophic larvae, and modest rate of sequence evolution, cancellothyridids have considerable potential as model organisms for the study of post-Mesozoic evolution in the deep sea, and many specimens from Pacific locations, including the Norfolk Ridge seamounts, await analysis.

Terebratellidines.—There is good support in the SSU tree for a terebratellidine clade (Fig. 1530), confirming the utility of loop ontogeny and morphology as diagnostic characters, but within this clade there is little strongly supported resolution, consistent with a relatively recent radiation. The New Zealand endemic genera form a strongly supported subclade, suggesting that they differentiated in isolation and that ~80 myr is enough to allow clear divergence to be recorded by this gene. The sister-group relationship of *Terebratalia* with the New Zealand endemics seen in these trees is contradicted by new LSU and *cox1* sequence analyses, which agree that *Magellania* spp. are the sister-group of the New Zealand endemics. Comparison of analyses of SSU, LSU, and mitochondrial *cox1* sequence within the *Magellania* clade reveal disagreements, however, probably caused by base composition differences (M. A. Bitner, personal communication, 2005).

In the remainder of the terebratellidine SSU rDNA subtree some unsurprising terminal nodes are well supported, coupling *Argyrotheca* with *Megathiris, Megerlina* with *Pumilus*, and *Megerlia* with *Anakinetica* and a platidiid, while the unexpectedly close relationship between *Terebratella dorsata* and *Magellania venosa* can be explained if, as now seems likely, the former were juveniles of the latter, misidentified by the author. They were collected in the same locality.

Gwynia (currently *incertae sedis*) is another potentially problematic taxon, appearing as the sister-group of all other terebratellidine taxa, separate from the megathyridids with which it has been associated morphologically (LOGAN, MACKINNON, & PHORSON, 1997).

This result is as yet unreplicated, however, and awaits confirmation.

Apart from the terebratellidine SSU results just described, valuable analyses based on the relatively slow-evolving mitochondrial gene *cox1* have focused on relationships among the Laqueoidea, leading to the suggestion that some traditionally important morphological character states (especially adult loop characters) are prone to homoplasy, but that a previously overlooked loop ontogeny character (MacKinnon, 1993; MacKinnon & Gaspard, 1995) may be more reliable (Saito, 1996, 1998; Saito, Kojima, & Endo, 2000; Saito & Endo, 2001; Saito, Endo, & Cohen, 2001). As noted above, *cox1* disagrees markedly in some respects with SSU rDNA. In particular, it gave good support to a sister-group relationship between Antarctic *Magellania* spp. and the New Zealand endemic genera, and it united two *Terebratalia* spp. with other laqueoids (Saito, Endo, & Cohen, 2001). Both of these results are more consistent with traditional systematics than the relationships proposed by the SSU rDNA analyses, which are based on weaker phylogenetic signals.

Calibrated Rates of Molecular Evolution and Dates of Major Divergences

In recent years, use of a molecular clock hypothesis to estimate the ages of past divergence events has undergone considerable development. Evidence has accumulated from detailed examination of the distribution of changes within genes that each nucleotide site or domain may have its own rate of change, while relative rate tests have shown that the clock may tick at different rates in different lineages. Moreover, at different past times, the rate of evolution at a site, domain, or in a lineage may have fluctuated, and inevitably, the longer the time involved, the more likely it is that such changes will have occurred and that fixed mutations will be overwritten, obscuring phylogenetic signals. The molecular clock rate is therefore only approximately constant, and a variety of methods have been developed in attempts to escape from or cope with the various complications. Cautious and critical interpretation remains necessary for divergence times estimated with a molecular clock hypothesis.

For brachiopods, the first molecular clock analysis was based on a simple, graphical method of rate estimation from an SSU rDNA gene tree (fig. 7 in Cohen, Gawthrop, & Cavalier-Smith, 1998), using data that (with the test then employed) showed no significant rate heterogeneity. This analysis gave a range of rates that placed in the late Proterozoic the extrapolated time of divergence between brachiopods and a chiton, consistent with some other molecular analyses of the metazoan radiation (e.g., Wray, Levinton, & Shapiro, 1996) that imply considerable divergence well before the Cambrian explosion. This result has been reinforced by a new study based on much more rDNA sequence data from fewer taxa, which, when analyzed with more sophisticated methods, gave a closely similar range of dates for the brachiopod:chiton divergence (Cohen & Weydmann, 2005). The discordance between the Cambrian explosion as seen in the fossil record and the much earlier timing of metazoan divergence often inferred from molecular data has been addressed in a recent experimental analysis of molecular evolution rates, which concluded that unless rates were greatly accelerated during the Cambrian, divergence started ~100 myr earlier (Levinton, Dubb, & Wray, 2004), consistent with the results described above for brachiopods. Timing metazoan divergence by the correlation of molecular and paleontological data may be controversial (e.g., Graur & Martin, 2004; Hedges & Kumar, 2004), but new ideas that take into account effects of body size, metabolic flux, and temperature (Gillooly & others, 2005) have the potential to solve some of

the problems, and in doing so suggest that small brachiopods with low metabolic rates may be extremely suitable for the dating of ancient divergences.

A rate estimate has also been obtained for the SSU (12S) rDNA mitochondrial gene, calibrated by the likely time at which Antarctica and New Zealand *Liothyrella* sp. became isolated. This calibration gave a rate of mitochondrial sequence evolution (about 0.1% divergence per million years) several-fold slower than estimated for some other organisms. Since rate heterogeneity was absent, the *Liothyrella* rate was used to infer divergence times in *Terebratulina* sp., and it put the divergence between *T. unguicula* and the North Atlantic species *T. septentrionalis* and *T. retusa* at ~100 myr, and that between *T. septentrionalis* and *T. retusa* at ~60 myr. More recently, however, divergence between Antarctic and New Zealand craniids has been found to be greater than that between *Liothyrella* sp. (COHEN, unpublished data, 2005), which raises the possibility that effective separation of New Zealand and Antarctic *Liothyrella* populations may have been delayed by dispersal of long-lived larvae (PECK & ROBINSON, 1994). If so, and provided craniid and *Liothyrella* mitochondrial genes evolve at similar rates (unlikely!), the rate of evolution in *Liothyrella* may have been underestimated (by perhaps two-fold) and the divergence dates of *Terebratulina* sp. correspondingly overestimated. These questions are currently under review, and, in the light of the relationships shown in Figure 1530, it may also be necessary to reconsider the underlying assumption that isolation of the New Zealand brachiopod fauna dates from the time at which effective geographical isolation from Antarctica was established.

POPULATION DYNAMICS BELOW THE SPECIES LEVEL

In the only study under this heading since 1995, allozyme polymorphism was investigated in 10 population samples of *Terebratella sanguinea* in 5 New Zealand fjords (OSTROW & others, 2001). Most samples were in genetic equilibrium, but 2 from fjord-head sites were not. There was little evidence of large-scale genetic differentiation either within or between fjords, but some indications were obtained of small-scale differentiation between sample sites, with private alleles in single samples. Markers offering greater resolution than allozymes appear to be required for the resolution of brachiopod population structure and dynamics.

EVOLUTION AND DEVELOPMENT

Since 1995, the molecular analysis of animal development has greatly expanded, with further work on gene families such as *hox* (homeobox), *eng* (engrailed), and *wnt* (wingless) that encode signalling molecules with roles in the control of cell fate specification, proliferation, movement, and in segment polarity. The field has even acquired a nickname: EvoDevo (ARTHUR, 2002). A flavor of the complexity involved is given by the *wnt* gene family, of which one member has been isolated from a brachiopod (HOLLAND, WILLIAMS, & LANFEAR, 1991) but of which at least 9 (of 12 or more) subfamilies appear to have been present in the bilaterian common ancestor (PRUD'HOMME & others, 2002). Brachiopods and phoronids have been included in some genomic surveys for such genes (e.g., DE ROSA & others, 1999), but little or nothing has so far been published about their expression in development. Perhaps this is not such a major loss because co-option, co-evolution, and convergence are evidently implicated in the evolution of these genes (HOLLAND, 1990). For example, in some annelids, patterns of *eng* expression are unrelated to their clear segmentation (SEAVER & others, 2001, and references therein), and in echinoderms the roles of these genes evidently have been evolutionarily labile (LOWE & WRAY, 1997). Given such findings, it is perhaps not surprising that despite many detailed

advances and many new hypotheses, no grand new understanding of the evolution of developmental systems and body plans has so far emerged. Indeed, the only conclusion so far of direct significance to brachiopod studies is that such relatively inaccessible, marine creatures are not likely to be favored as candidate model organisms for this sort of work (TESSMAR-RAIBLE & ARENDT, 2003). Nevertheless, it is probably important to discover the expression patterns of developmentally important genes in brachiopods, even those potentially involved in segmentation. Even more than segmentation, left-right asymmetry is a developmental feature that has some potential to be discerned in fossils and, moreover, is ubiquitous in crown-group brachiopods. A small, core set of genes appears to be involved in the underlying symmetry-breaking process (PALMER, 2004), and perhaps these too would reward study.

Rather than attempt a comprehensive review of this field where so little is known that is directly relevant, the reader is referred to the discussion and bibliography in a recent, wide-ranging book (VALENTINE, 2004, especially chapter 3, p. 76–114).

ACHIEVEMENTS AND LIMITATIONS OF MOLECULAR SYSTEMATICS OF BRACHIOPODS

The main promise of molecular systematics, to provide a strong, independent test of morphological systematics, has been demonstrated and, in part, achieved. Monophyly of the Brachiopoda *s.s.* can no longer be in doubt, and accommodation of the Phoronida within Brachiopoda *s.l.,* though unanticipated, creates no known major conflict with morphotaxonomy. In addition, molecular data have revealed that brachiopods belong in the (morphologically unexpected) lophotrochozoan supraphylum alliance and have largely confirmed morphotaxonomic conclusions about the interrelationships of high-level brachiopod taxa, and confirmed the dual origins of calcitic mineralization. At lower levels and especially in phylogeography, insufficient work has been done to more than hint at gold waiting to be mined. Successes include the recognition of cancellothyridids as a clear clade and the distinction, in this family and in laqueoids, between some taxonomically reliable and unreliable morphological characters. For extant forms at least, the day of taxon-splitters is over, their bluff can be called.

The main limitations of molecular systematics reflect the cost, difficulty, and unpredictability of collecting, the cost of gene sequencing, the difficulty of distinguishing homoplasy from true evolutionary relationships, and the difficulty of knowing (when they disagree) which analytical method to trust. Because brachiopods are not perceived as model organisms and health-related connections are nonexistent, stable funding has been elusive and new workers scarce; except in paleontology, brachiopods do not appear to offer a safe basis on which to develop a research career. Thus, brachiopod molecular systematic and genomic analyses have not achieved a critical, self-sustaining mass and probably will not do so unless high-profile discoveries emerge, and because of the small size of the active, brachiopod-specific molecular research community these organisms are unlikely to win an early place in the comparative genomic sequencing roster. The case that needs to be made convincingly is that these creatures (especially craniids and discinids) may provide the clearest window into the state of the metazoan genome as it was in or before the Lower Cambrian, and they are therefore an essential component of comparative genomics.

GENE TREES AND IMMUNOTAXONOMY

Readers of the chapter on Shell Biochemistry: Immunology of Brachiopod Shell Macromolecules (CUSACK, WALTON, & CURRY, 1997, p. 261–266) inexplicably

were not alerted to discussions of the reliability of this approach and of its utility for the reconstruction of phylogeny (COHEN, 1992, 1994; CURRY & others, 1993). The latest of these papers concluded that while the method "… has a potentially important role in the extension of genealogical classification to fossils and empty shells, … in its current state [it] departs in several important respects from immuno-taxonomic norms," (COHEN, 1994, p. 910). No more recent publication gives cause to revise this assessment, and comparison of the relationships shown in CUSACK, WALTON, and CURRY (1997, fig. 219 and 220) reveals discordance with both morphology and with gene sequence-based trees (COHEN & GAWTHROP, 1997, fig. 180–188) and Figure 1530 (herein).

ACKNOWLEDGMENTS

Larry Flammer kindly supplied scanned images of illustrations from his thesis. M. G. Simões (University Estadual Paulista, São Paulo, Brazil) kindly provided the SSU rDNA sequence of *Bouchardia rosea*. Financial support for work on thecideidines was received from the University of Kansas Paleontological Institute, through Alwyn Williams. The author is particularly grateful to brachiopods (*s.l.*) for providing a fresh and stimulating research interest, and to Gordon Curry (University of Glasgow), who opened the door to it.

BIOCHEMISTRY AND DIVERSITY OF BRACHIOPOD SHELLS

Maggie Cusack and Alwyn Williams

[University of Glasgow; and deceased, formerly of University of Glasgow]

INRODUCTION

The Biochemistry section of Volume 1 (Cusack, Walton, & Curry, 1997, p. 243) introduced the complexity of the mineral-associated proteins of all three brachiopod subphyla. The mineral-associated proteins from modern brachiopods have been characterized in more detail (Williams & Cusack, 1999; Williams, Cusack, & Brown, 1999; Cusack & others, 2000; Cusack & Williams, 2001a, 2001b), and the complexity is now all the more apparent as is the rapid degradation of informative proteinaceous material (Williams & others, 1998). In the case of some modern brachiopods, the influence that these proteins have on crystallization *in vitro* has begun to be elucidated (Cusack & others, 2000; Lévêque & others, 2004). The catalysis of hydroxyapatite from amorphous calcium phosphate by proteins of *Lingula anatina* shells is unusual in that it is effected by proteins in solution (Lévêque & others, 2004). The discovery of siliceous tablets on the first-formed shell of discinids indicates major changes to biochemical regimes during ontogeny with a switch from the secretion of silica to that of apatite. The regularity of the shape and dimensions of the siliceous tablets suggests that they are produced intracellularly and secreted to the surface as intact, complete entities (Williams, Cusack, & Buckman, 1998) as confirmed by Lüter (2004; see section on discinoid juvenile shell in Chemicostructural Diversity Chapter, p. 2402 herein). The widely accepted description of rhynchonelliform brachiopod shell composition as low-Mg calcite is an oversimplification, since the concentration and distribution of magnesium varies considerably between species and even within species with a consistent species pattern in all cases. The magnesium content of the Craniiformea is uniformly high throughout the shell (England, Cusack, & Lee, 2007). The complexity of the magnesium distribution in brachiopod calcite must be understood fully in order for the Ca-Mg ratio to be exploited accurately as a paleothermometer (England, Cusack, & Lee, 2007).

ORGANOPHOSPHATIC SHELL CHEMISTRY

In the 1997 *Treatise* (Kaesler, 1997), the mineral component of the organophosphatic brachiopod shell was identified as a carbonate-containing fluorapatite (Watabe & Pan, 1984; LeGeros & others, 1985) with *Glottidia* containing higher concentrations of carbonate and thus having lower crystallinity than *Lingula*. Since then, there has been the discovery of intracellularly manufactured (Lüter, 2004) siliceous tablets on the larval surface of discinid valves (Williams & others, 1998; Williams & Cusack, 2001; see section on Lingulid Juvenile Shells in Chemicostructural Diversity, herein, p. 2409). The 1997 *Treatise* included details of proteins from valves of *Lingula anatina*, *Glottidia pyramidata,* and *Discinisca tenuis*, revealing different protein profiles in each case. More recent investigations of the organic components of organophosphatic shells have confirmed a wide diversity in the shell biochemistry of living lingulids. The ability of the proteins of *L. anatina* to catalyze the *in vitro* transformation from amorphous calcium phosphate to fluorapatite has been demonstrated (Lévêque & others, 2004). The rapid degradation of the organic components during fossilization has become apparent.

SHELL MINERALOGY

The basic apatitic unit of the discinid shell is a granule, 4–8 nm in diameter. The X-ray diffraction patterns of this biomineral in

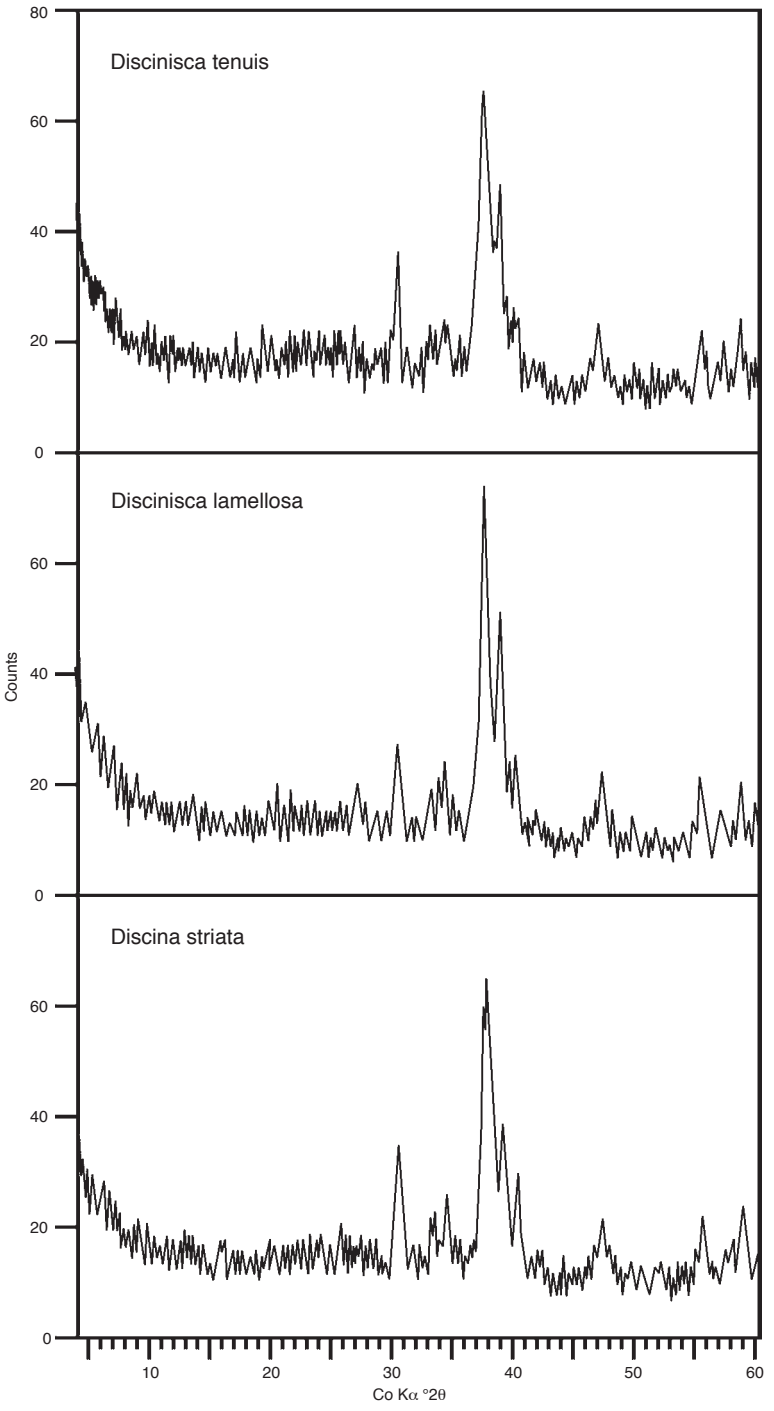

FIG. 1531. XRD line profiles of discinid shells. Shells powdered in acetone were poured over glass slides and XRD determinations made in a Philips PW 1050/35 XRD with a Co energy source (Williams, Cusack, & Buckman, 1998).

the shells of *D. tenuis*, *D. lamellosa,* and *D. striata* (Fig. 1531) are all comparable with those of *Glottidia pyramidata* and *Lingula anatina* obtained by LEGEROS and others (1985) who, using infrared (IR) absorption and fluorine analyses, described the mineral component of the two lingulids as "crystallo-chemically similar but not identical to marine phosphorite or mineral francolite, a carbonate-containing calcium fluorapatite" (LEGEROS & others, 1985, p. 99). PUURA and NEMLIHER (2001) examined the lattice parameters of Recent, subfossil, and fossil linguloid valves. They concluded that the lingulid shell mineral of ten specimens of *L. anatina* from the Philippines is a fluorine-containing carbonate-OH apatite, with lower OH and higher F content than in mammal teeth and bone. The range of lattice parameters within these ten specimens was a = 9.386–9.396Å and c = 6.859–6.864Å. In their study of ten subfossil valves of *Discinisca tenuis*, PUURA and NEMLIHER (2001) demonstrated that postmortem alteration processes partially replaced the *in vivo* shell apatite with apatite of lower OH content. In shells of fossil linguloids from the Upper Cambrian *Obolus* sandstone there was a mixture of diagenetically altered skeletal apatite and nonskeletal apatite that was precipitated during diagenesis. The range of lattice parameters of the fossil shells is a = 9.33–9.36Å and c = 6.87–6.89Å.

LIVING SHELL BIOCHEMISTRY

Shells of modern linguliform brachiopods, the lingulids and discinids, have a high organic and water content (Table 23). In *L. anatina* the organic components are concentrated in the shell anterior and lateral regions, while the posterior and median regions have a higher mineral content (CUSACK & WILLIAMS, 1996; LÉVÊQUE & others, 2004). *Lingula* and *Glottidia* shells have a higher organic and water content than discinid shells. The high level of organic material in lingulid shells relative to that of discinids (Table 23) is not reflected in the amino acid content, since the discinids have a higher concentration of amino acids than *Lingula* and *Glottidia* (Table 24). The high water content in *L. anatina* and *G. pyramidata* shells suggests a more hydrophilic organic component such as chitin or GAGs. Indeed, both glucosamine and galactosamine were detected after HCl dissolution of valves of *L. anatina* and *G. pyramidata* as well as *D. striata*. Failure to detect these amino sugars in *D. tenuis* and *D. lamellosa* is attributed to technical inadequacies, as amino sugars cannot be resolved from high levels of amino

TABLE 23. Water and organic content of three species of discinoid brachiopods as compared with linguloid brachiopods *Lingula anatina* and *Glottidia pyramidata*. Water content was determined at 30% relative humidity (new).

	Water	Organic (% wet weight)	Organic (% dry weight)
Discinisca tenuis	8.5	32.1	25.7
Discinisca lamellosa	6.8	31.5	26.5
Discina striata	6.1	41.1	37.3
Lingula anatina	9.7	42.2	35.9
Glottidia pyramidata	12.5	61.0	55.4

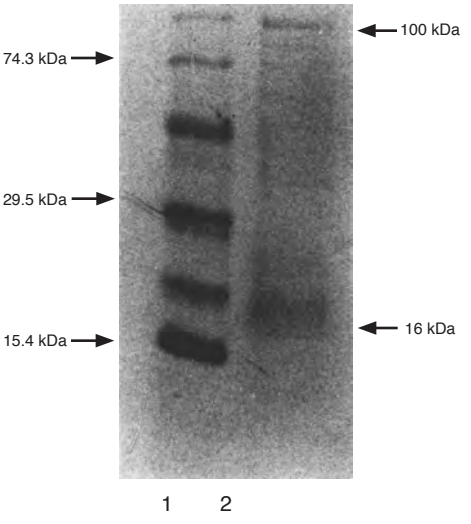

FIG. 1532. SDS PAGE of mineral-associated proteins of *D. tenuis* shells. EDTA-soluble proteins (equivalent to an extract from 1.1 g shell) were fractionated (*2*) in a 15% polyacrylamide gel alongside prestained proteins of known molecular weight (*1*). Proteins were revealed by staining with Coomassie Blue (Williams, Cusack, & Buckman, 1998).

TABLE 24. Amino acid content (pmoles/mg^{-1} shell) of three species of discinoid brachiopods as compared with linguloid brachiopods *Lingula anatina* and *Glottidia pyramidata* (new).

	Amino acid content
Discinisca tenuis	350 ± 48
Discinisca lamellosa	264 ± 35
Discina striata	257 ± 2
Lingula anatina	32 ± 4
Glottidia pyramidata	42 ± 8

acids. It is, therefore, likely that dilution of the amino acids from *D. tenuis* and *D. lamellosa* dilutes the amino sugars below the detection threshold (WILLIAMS, CUSACK, & BUCKMAN, 1998).

Proteins were extracted from shells of *D. tenuis* and *L. anatina* (WILLIAMS, CUSACK, & MACKAY, 1994) and fractionated on 15% polyacrylamide gels according to the method of SCHÄGGER and VON JAGOW (1987). Staining with Coomassie Blue reveals the most abundant proteins, while silver staining, which has much higher sensitivity, reveals those proteins present at lower concentrations. Protein glycosylation was determined by lectin binding using Concanavalin A-peroxidase (FAYE & CHRISPEELS, 1985). The EDTA-soluble mineral-associated proteins of *D. tenuis* are presented in Figure 1532, where Coomassie Blue staining reveals proteins in the molecular weight range of 16 to 100 kDa. Silver staining enlarges the lower range to 6.5 kDa (Fig. 1533). At least one of the proteins, molecular weight 13 kDa, is glycosylated (Fig. 1534). Coomassie Blue staining of proteins from *L. anatina* shells reveals relatively abundant proteins of molecular weight 21.5 and 24 kDa (Fig. 1535.2). Silver staining reveals the molecular weight range of 5 to 60 kDa (Fig. 1535.1). The two proteins of relatively high abundance and molecular weight 21.5 and 24 kDa are both glycosylated (Fig. 1535.3). The overall protein pattern is different for *D. tenuis* and *L. anatina* as is the pattern of glycosylation.

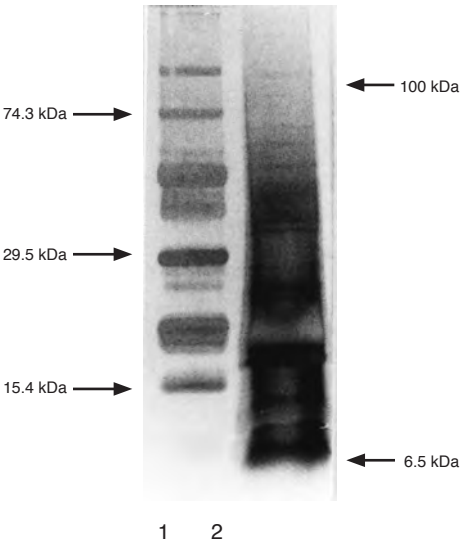

FIG. 1533. Silver staining of mineral-associated proteins of *D. tenuis* shells. EDTA-soluble proteins were fractionated by SDS PAGE and stained with silver (Morrisey, 1981) to reveal those proteins present at concentrations below the detection limit of Coomassie Blue; lanes (*1*) and (*2*) (Williams, Cusack, & Buckman, 1998).

The amino acid composition of the most abundant proteins extracted from *D. tenuis* and *L. anatina* is presented in Tables 25 and 26 respectively. Amino acid analysis does not distinguish between aspartic acid (D) and asparagine (N) nor glutamic acid (E) and glutamine (Q), and the total values for D+N and E+Q are here assumed to be acidic amino acids. In *D. tenuis*, the concentration of acidic residues is higher in the larger proteins, with mole% values of 26 for the proteins of molecular weight 100 kDa and 72 kDa. Although there is no information regarding the conformation of these proteins *in vivo*, comparison of the ratio of acidic to basic amino acid residues may indicate the overall charge of these proteins. The ratio of acidic (D, N, E, Q) to basic (H, R, K) residues is 4·2:1, 4·7:1, 2·6:1, 4·8:1, 3·1:1 and 4·4:1 for the 100, 72, 48, 34, 21, and 16 kDa proteins respectively. On this basis, the 34 kDa protein is the most acidic, and the 48 kDa protein the most basic.

The EDTA-soluble extract accounts for only a small proportion of the total shell

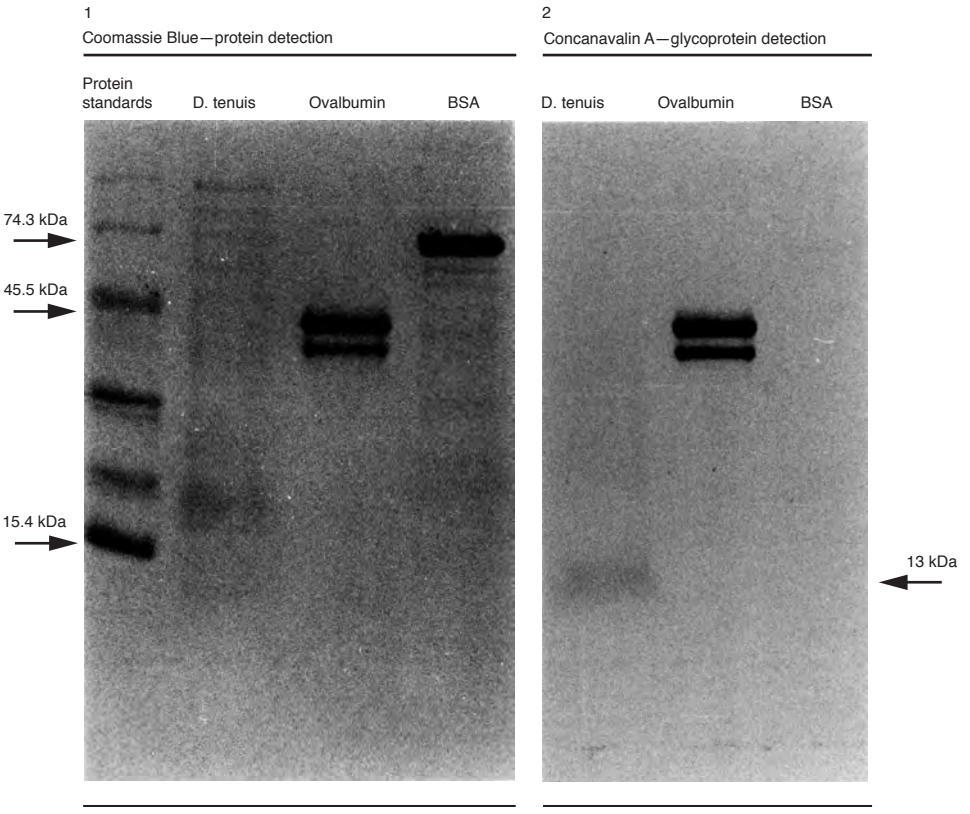

FIG. 1534. EDTA-soluble (glyco) proteins from *D. tenuis.* EDTA-soluble proteins of *D. tenuis* (equivalent to an extract from 1.1 g shell) were fractionated on SDS PAGE gels alongside proteins of known molecular weight and ovalbumin (3 µg), which is glycosylated, and bovine serum albumin (BSA; 5 µg), which is not. Duplicate samples were applied to the gel, and following electrophoresis, proteins were electroblotted onto ProBlott© membrane and the membrane halved; one portion (*1*) was stained with Coomassie Blue to reveal all proteins present; (*2*) the membrane was treated with the lectin, Concanavalin A to detect glycoproteins (Williams, Cusack, & Buckman, 1998).

protein (e.g., 0.016% of the total amino acid content of the shell of *D. tenuis*; WILLIAMS, CUSACK, & BUCKMAN, 1998), indicating that a large proportion of the shell protein is fibrous or at least insoluble to EDTA extraction. To extract information from the whole protein content, the total amino acid composition of the shells of four discinid species and those of *L. anatina* and *G. pyramidata* was determined by dissolving the shells with HCl (2N) and hydrolyzing all proteinaceous material released; the results are presented in Table 27.

As well as differences in the concentration of amino acids, which is higher in discinid than in lingulid shells (Table 24), some differences in amino acid composition between discinids and lingulids are also apparent. In the shells of living discinids, the average content of acidic amino acids (D/N and E/Q) is 14.5%, with *Pelagodiscus atlanticus* containing the highest concentration of acidic amino acids (16.9%) and *D. tenuis* the lowest (11.9%). For the basic amino acids (H, R, and K), the mean value is 13.2%, with *P. atlanticus* containing the highest concentration of basic amino acids (19.9%) and *D. tenuis* and *D. striata* the lowest, with 9.7% and 9.8% respectively. Glycine and alanine occur in large quantities. Glycine

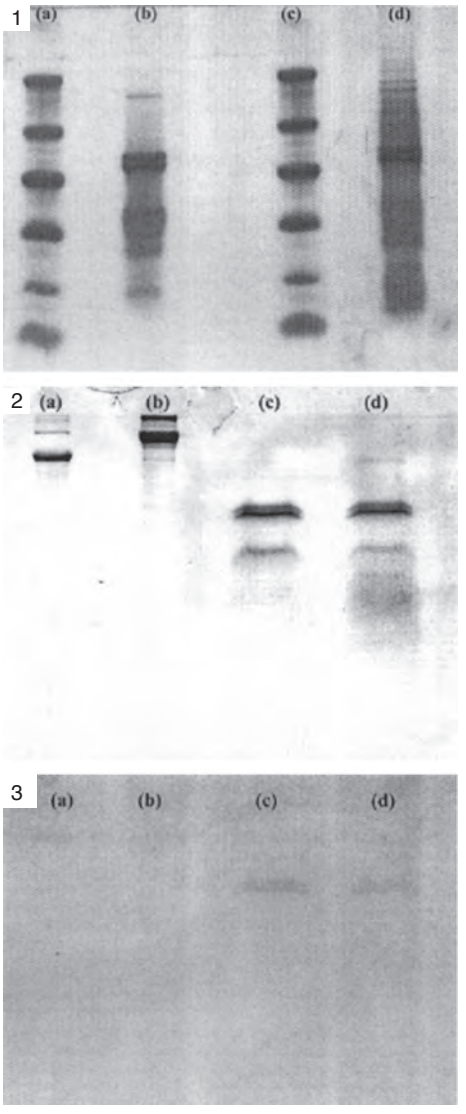

FIG. 1535. SDS PAGE gels and blot of protein extracts from *L. anatina* valves. *1,* SDS PAGE gels of (a and c) molecular weight markers corresponding to 44.7, 29.3, 20.2, 14.8, 5.7 and 2.9 kDa, (b) GnHCl-extracted proteins, and (d) EDTA-extracted proteins. Proteins were fractionated, fixed, and then silver stained; *2,* SDS PAGE gels of (a) ovalbumin (1 mg, 43 kDa), (b) bovine serum albumin (1 mg, 66 kDa), (c) GnHCl extract (3.9 mg protein), and (d) EDTA extract (3.9 mg protein); proteins were Coomassie stained; *3,* electroblot of duplicate gel as in *2,* probed for carbohydrate using Concanavalin-A (adapted from Lévêque & others, 2004).

has an average value of 24.3%, with *D. tenuis* containing the highest concentration (31.6%) and *P. atlanticus* the lowest (8.8%). For alanine, the mean value is 22.7%, and in this case, *D. tenuis* contains the highest concentration (29.3%) and *D. lamellosa* the lowest (24%).

The shells of living lingulids contain higher concentrations of acidic amino acids than those of discinids, with an average value of 21.1%. The levels of basic amino acids (H, R, and K), with a mean of 9.1%, are lower than that of the discinids (13.2%). Glycine and alanine also occur at high concentrations in lingulids, averaging 19.6% and 22.95% respectively for *L. anatina* and *G. pyramidata*, although these are still lower than those in discinids.

These total amino acid compositions were compared, along with those of *L. reevii, L. parva,* and *G. palmeri*, by Principal Components Analysis, the results of which are presented in a 2-D scatterplot where the two eigenvectors account for 70% of the variation between samples (Fig. 1536). Glycine, histidine, and leucine constitute the major differences along the first eigenvector U1 with proline and valine also contributing. Along vector U2, arginine is the major contributor with threonine, methionine, and cysteine also contributing. The three species of *Lingula* cluster together with high values for vector U2. Three discinid species, *D. lamellosa*, *D. striata,* and *D. tenuis* cluster together, while *P. atlanticus* plots away from all other linguliform brachiopods analyzed. Taking the three species, *D. lamellosa*, *D. striata,* and *D. tenuis*, as the discinid cluster, *Lingula* plots further from the discinids than does *Glottidia*. Indeed *Glottidia* occupies an intermediate position between *Lingula* and the discinids. This intermediate position may relate to the occurrence of baculation within shells of *Discina* and *Discinisca,* but it does not account for the fact that *Pelagodiscus* occupies a position distant from the other organophosphatic brachiopods

TABLE 25. Amino acid composition (mole%), using one- letter code for amino acids, of EDTA-soluble mineral-associated proteins of *Discinisca tenuis* (new).

Amino acid	100 kDa	72 kDa	48 kDa	34 kDa	21 kDa	16 kDa
D/N	15.1	14.9	11.9	11.2	10.2	10.8
E/Q	11.4	11.7	8.5	10.8	10.5	10.6
S	11.4	9.7	5.8	7.5	6.1	8.1
G	14.6	14.9	18.9	11.6	12.7	8.5
H	-	-	3.9	-	1.7	1.6
R	4.7	4.8	3.0	3.3	2.9	0.1
T	8.8	6.0	6.5	6.2	6.1	5.9
A	9.9	13.3	13.5	15.6	12.9	7.2
P	3.6	4.0	8.0	6.4	6.9	6.0
Y	-	-	-	1.1	0.9	2.3
V	5.7	2.4	3.7	5.2	4.2	5.6
M	-	3.6	3.5	2.1	2.3	3.6
C	0.5	-	-	-	0.4	6.2
I	4.7	5.2	4.8	6.3	6.7	5.6
L	6.2	6.4	5.0	7.3	8.1	7.4
F	3.1	3.6	3.5	4.6	4.9	7.3
K	1.6	0.8	0.8	1.3	2.1	3.1

analyzed, since the shell of *Pelagodiscus* is also baculate.

The valves, setae, and pedicles of organophosphatic valves contain chitin as determined by pyrolysis GC-MS, which revealed the presence of acetamidofuran, 3-acetamido-5-methylfuran, and 3-acetamido-*n*-pyrone (WILLIAMS, LÜTER, & CUSACK, 2001), all three of which are unequivocal markers for chitin (STANKIEWICZ & others, 1996).

LINGULA ANATINA SHELL PROTEINS AND *IN VITRO* CRYSTALLIZATION

The protein mixture extracted from *Lingula anatina* valves (Fig. 1535) was added to buffered calcium phosphate/fluoride metastable solutions at constant temperature. The induction period for FAP crystallization was reduced by approximately 24% for a protein

TABLE 26. Amino acid composition (mole%), using one- letter code for amino acids, of EDTA-soluble mineral-associated proteins of *Lingula anatina* (new).

Amino acid	46kDa	36kDa	24kDa	21.5kDa	10kDa	6kDa
D/N	6.08	9.68	8.98	7.38	9.88	9.65
E/Q	8.45	20.93	11.72	14.52	22.73	17.2
S	12.14	7.74	7.23	8.63	6.16	6.6
G	24.53	4.5	9.68	11.03	9.17	6.14
H	1.35	0.83	0.89	0	2.08	2.2
R	2.44	4.61	3.04	2.81	2.83	2.3
T	5.69	5.61	5.42	4.16	3.89	7.36
A	10.53	13.06	12.51	15.86	9.82	9.64
P	5.21	2.27	5.26	3.63	4.19	6.29
Y	1.47	4.08	1.29	1.38	1.59	2.04
V	7.26	6.26	12.09	10.65	7.13	7.22
M	0	0.27	0	0	0	0
I	5.04	5.73	6.78	7.33	5.22	7.46
L	4.38	8.89	6.43	5.92	5.42	5.54
F	2.66	1.76	4.15	2.94	4.96	5.8
K	2.74	6.74	4.49	3.75	4.88	4.31

TABLE 27. Amino acid composition (mole%), using one-letter code for amino acids, in valves of six species of organophosphatic brachiopods (new).

Amino acid	*D. tenuis*	*D. lamellosa*	*D. striata*	*P. atlanticus*	*L. anatina*	*G. pyramidata*
D/N	5.4	9.0	10.5	13.1	16.8	15.9
E/Q	6.5	4.2	5.6	3.8	6.5	2.9
S	4.3	4.9	2.5	6.3	4.2	3.5
G	31.6	27.0	30.0	8.8	16.3	23.0
H	-	0.2	-	0.7	0.7	-
R	8.6	12.0	8.7	18.5	4.9	6.7
T	3.6	3.5	3.1	14.2	4.4	2.7
A	29.3	24.0	28.0	9.6	22.9	23.0
P	4.6	6.2	5.1	7.9	8.0	6.4
Y	0.3	0.2	0.5	0.8	0.5	1.1
V	1.4	2.3	1.8	6.1	5.2	4.2
M	0.1	0.2	-	0.4	-	-
C	-	-	-	0.7	-	-
I	1.0	1.7	1.2	1.9	1.7	1.3
L	1.1	2.0	1.6	4.3	3.5	3.3
F	0.7	0.7	0.4	1.8	2.1	2.0
K	1.1	1.4	0.9	1.4	2.3	2.9

concentration of 0.5 μg/ml, with the consequence that needlelike crystals, rather than ACP granules, were observed in samples removed after 30 minutes (Fig. 1537). This catalysis of the formation of crystalline fluorapatite from amorphous calcium phosphate *in vitro* suggests an important role in shell formation (LÉVÊQUE & others, 2004).

FOSSIL SHELL BIOCHEMISTRY

The rapid degradation of proteins during the fossilization of linguliform shells is

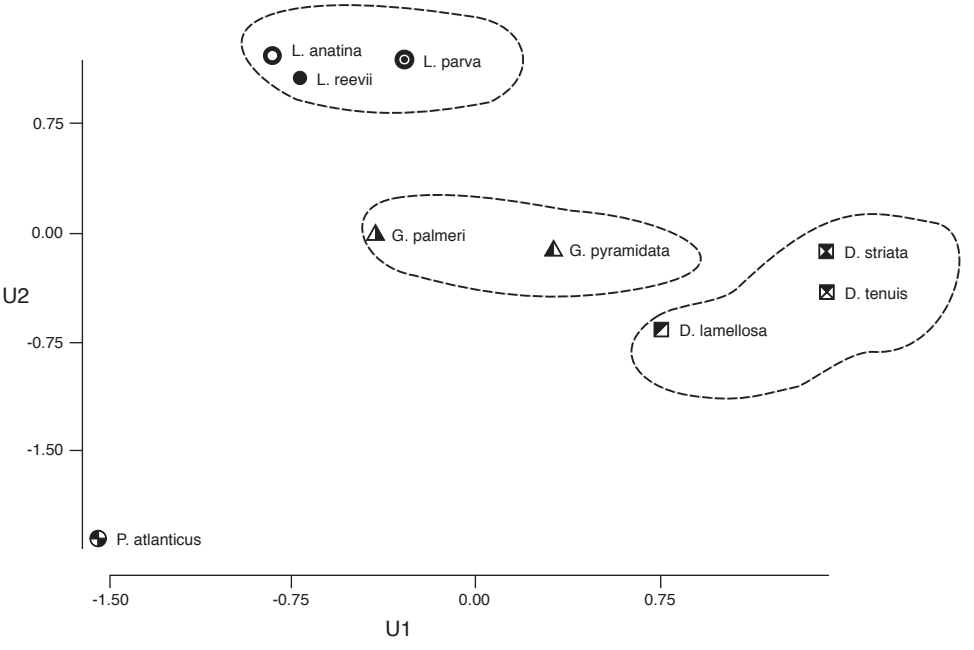

FIG. 1536. First two eigen vectors from principal component analysis of the amino acid content of valves of *L. anatina, L. reevii, L. parva, G. pyramidata, G. palmeri, D. striata, D. tenuis,* and *D. lamellosa* (data from Williams, Cusack, & Buckman, 1998 and Williams & others, 2000).

confirmed by comparing the amino acid suites of living *Discinisca* (Williams, Cusack, & Buckman, 1998, table 3) with that extracted from the Eocene *D. davisi* (Williams, Cusack, & Buckman, 1998, table 4). By the Carboniferous, amino acid suites surviving in lingulide shells are further reduced. Thus *Lingula squamiformis* retained low concentrations of some robust amino acids: aspartic acid/asparagine, glutamic acid/glutamine, glycine, alanine, tyrosine, and valine at total concentrations of 122 pmoles amino acid per mg of sample (Cusack & Williams, 1996). Moreover, shells of the contemporary discinid *Orbiculoidea nitida* retained the same suite of amino acids with the addition of alanine and threonine at a total concentration of 264 pmoles amino acid per mg of sample (Williams, Cusack, & Buckman, 1998). The residual amino acids extracted from the Ordovician shells of the discinoid *Schizotreta corrugata* and the linguloid *Pseudolingula*? spp. were essentially the same as those from the Carboniferous *O. nitida,* except for the absence of valine and the lower total concentration at 27 pmoles amino acid per mg sample (Williams, Cusack, & Buckman, 1998; Cusack, Williams, & Buckman, 1999). These examples serve to illustrate that degradation of proteins and polypeptides is thorough. In effect, fossilization results in the retention of only the most robust amino acids and the nullification of any taxonomic information that exists in amino acid suites of living lingulide shells. In modern *D. tenuis*, statistical analyses of amino acid shell extracts distinguish between the baculate ventral valve of *D. tenuis* and its nonbaculate dorsal counterpart (Cusack, Williams, & Buckman, 1999). Glutamic acid, glycine, alanine, arginine, and proline are associated with baculation and may be components of organic polymers involved in the formation of baculi. Such subtle differences, however, do not survive fossilization, so that amino acids retrieved from Paleozoic linguloid and discinoid shells are not statistically distinguishable (Cusack, Williams, & Buckman, 1999). Of course the shells of living linguloids and discinoids are chemicostructurally so close that some compositional convergence would have been inevitable among their Paleozoic ancestors, which would have distinguished them from contemporaneous linguliforms like paterinates and acrotretides. Amino acids survive in the earliest brachiopods, the paterinates with the suites extracted from the shells of the Cambrian *Askepasma* and *Micromitra,* and the Ordovician *Dictyonites* being the same as that recovered from the shell of the Carboniferous *L. squamiformis* except for the addition of serine and threonine (Williams, Popov, & others, 1998). The amino acid concentration in the *Dictyonites* shell was higher than those in the shells of Cambrian paterinates. The relative proportion of acidic amino acids, however, is much lower, which may be a consequence of the periodic reduction in the secretion of apatite that results in the perforations of the *Dictyonites* shell.

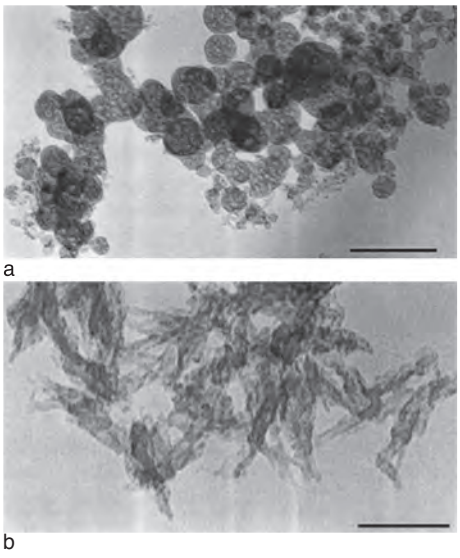

Fig. 1537. Catalysis of crystallization of fluorapatite by *L.anatina* shell proteins. TEM images of samples extracted after 30 min; *a,* control experiment showing spherical particles of hydrated ACP; *b,* fluorapatite crystals formed in the presence of *L. anatina* shell proteins at 0.5 µg/mL; scale bars, 100 nm (Lévêque & others, 2004).

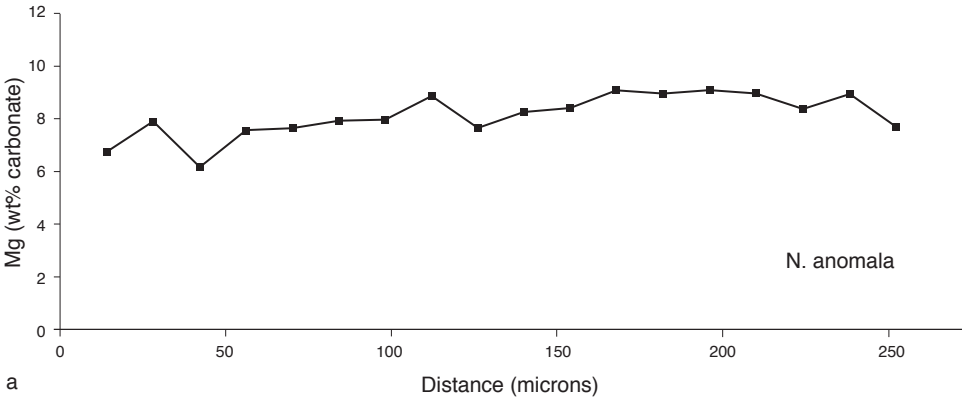

a

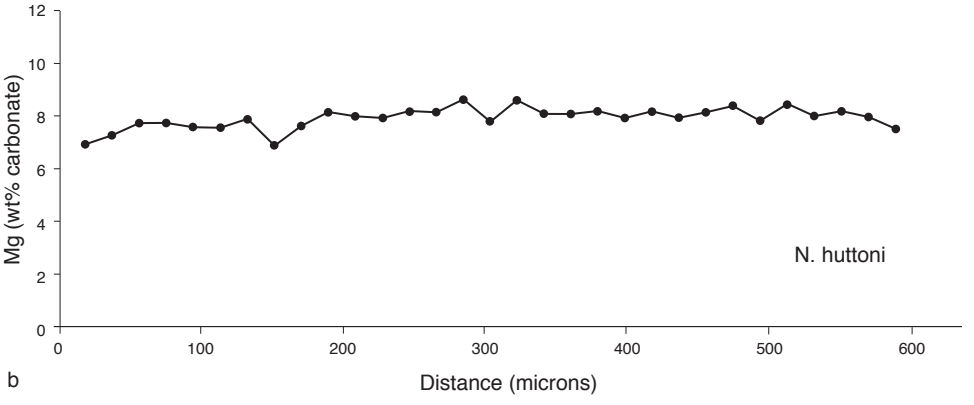

b

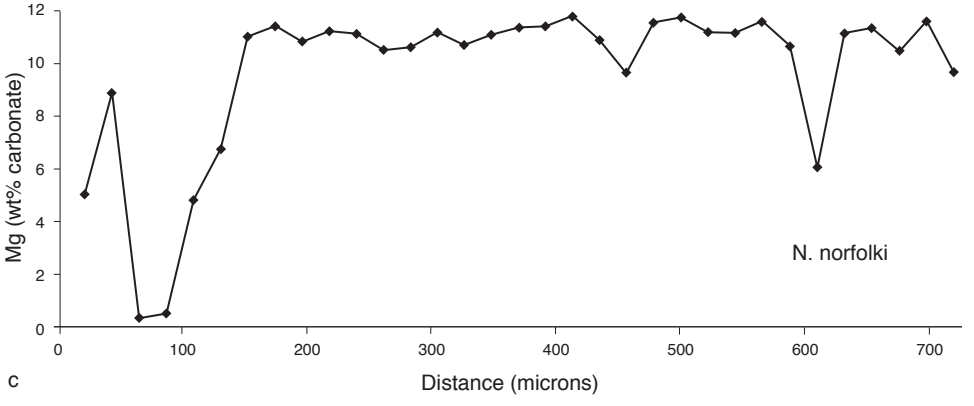

c

FIG. 1538. *For explanation, see facing page.*

SHELL CHEMISTRY OF CRANIIDS

The high concentration of magnesium in the calcite of craniid valves was noted in the 1997 *Treatise* (Cusack, Walton, & Curry, 1997, p. 243). The distribution of magnesium in living craniid shells has now been determined, and the replacement of magnesium by calcium in fossil craniids has been demonstrated. The proteins of the *Novocrania anomala* shell as described in the 1997 *Treatise* have been further characterized. The principal calcifying proteins have been identified (Cusack & others, 2000), and their location within the laminae of dorsal valves identified (Brown, 1998; Williams, Cusack, & Brown, 1999).

SHELL MINERALOGY

The high magnesium concentration is constant throughout the primary and secondary layers of such modern craniid shells (Fig. 1538) as those of *Novocrania anomala* from Scotland, *Novocrania huttoni* from New Zealand, and *Neoancistrocrania norfolki* from the South Pacific. In *N. anomala* (Fig. 1538a) the average magnesium concentration is 8.07 wt%, in *N. huttoni,* 7.87 wt%, and in *N. norfolki,* 9.61 wt%. The apparently low values at some points in the *N. norfolki* valve occur because of the numerous cavities within the valve. Removing the cavities from the analyses would increase the average Mg content to around 11 wt%. XRD analysis confirms that, in each case, magnesium occurs in the calcite lattice since there is no separate mineral phase. The magnesium concentration of these living craniids is significantly higher than in the calcite of most rhynchonelliform brachiopods. The solubility of calcite increases as the concentration of Mg within the lattice increases (Davies, Dove, & De Yoreo, 2000).

Table 28. Amino acid composition of the intracrystalline extracts from the dorsal and ventral valves of *N. anomala* (amino acids stated as residues per 100 amino acid residues) (new).

Amino acid	Dorsal	Ventral
D/N	32.6	18.9
E/Q	3.4	4.8
S	16.3	6.3
G	18.6	17.0
H	0.0	0.0
R	1.8	3.3
T	4.5	5.4
A	5.4	7.3
P	3.4	8.8
Y	0.4	0.7
V	3.2	6.4
M	0.0	0.0
C	0.0	0.1
I	1.5	3.9
L	2.9	5.9
F	1.1	3.0
K	3.5	8.1

LIVING SHELL BIOCHEMISTRY

Organic constituents account for 4.5% of the dry weight of *N. anomala* shells. The dorsal and ventral valves of *N. anomala* differ in their amino acid composition (Table 28), no less than their morphology and ultrastructure. The dorsal valves contain higher concentrations of aspartic acid/asparagine (D/N) and serine (S) and lower concentrations of all other amino acids except for glycine (G), hisidine (H), threonine (T), and

Fig. 1538. Magnesium concentration and distribution in calcite of craniiform shells. Shells of *a, N. anomala, b, N. huttoni,* and *c, N. norfolki* were sectioned from anterior to posterior, mounted in araldite blocks and carbon coated for electron microprobe analysis (EPMA). Electron microprobe spot analyses in a line perpendicular to the line of section (shell exterior to left) were determined for magnesium using a Cambax SX50 electron microprobe operating at 15KeV with a 10nA current and a 10 μm defocused electron beam for 30s counting time on each element. The instrument was calibrated for magnesium detection using a pure MgO standard. The totals for analysis varied between 98 wt% and 102 wt% and are within the acceptable error limit for carbonate analyses (Moberley, 1968). Since magnesium is substituting for calcium within the calcium carbonate and is not present as a separate phase, magnesium concentration is expressed as wt% carbonate throughout (new).

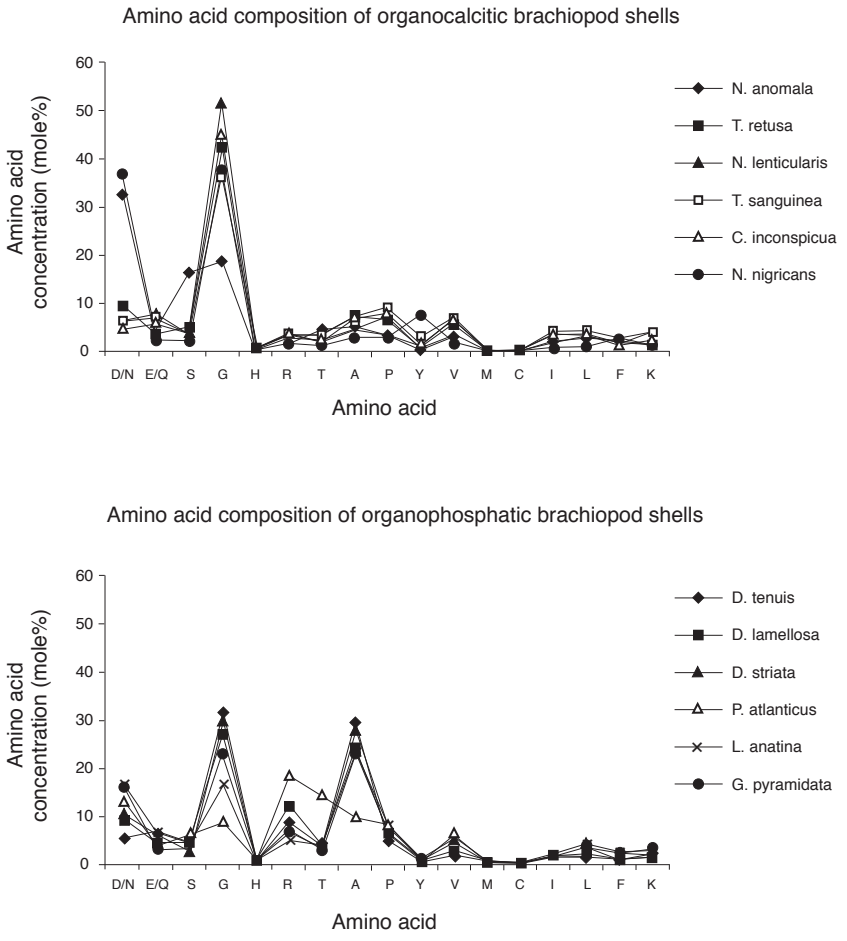

FIG. 1539. Amino acid composition of calcite and apatite brachiopod shells. Clean, powdered shells were dissolved in HCl (2N) at a ratio of 11 ml per mg shell. Following centrifugation, the amino acid composition of the supernatant was determined as follows. Supernatant samples were hydrolyzed by manual hydrolysis. Lyophilized samples in hydrolysis tubes were placed in hydrolysis vials containing 500 ml of HCl (6N). Vials were purged with argon at 2–3 psi for 30 sec, vials closed and heated at 165 °C for 1 hour for vapor-phase hydrolysis. Amino acid compositions were determined on a 420 amino acid analyzer from Perkin Elmer-Applied Biosystems (new).

methionine (M), which are within 80% of each other in both valves.

It is noteworthy that the amino acid composition of calcitic and apatitic shells of living craniiforms and linguliforms respectively is roughly similar (Fig. 1539). Apatitic valves contain 30% glycine and alanine, while calcitic valves contain higher concentrations of glycine (40%–50%) and much lower alanine concentrations (5%). The dorsal valve of *N. anomala*, however, contains a lower proportion of glycine (18%) than occurs in the calcitic shells of living rhynchonelliforms, which is closer to that of organophosphatic shells. The alanine content, in contrast, is like that of the shells of rhynchonelliforms.

Proteins, extracted from the dorsal valve of *N. anomala*, have been fractionated on 15% polyacrylamide gels according to the method of SCHÄGGER and VON JAGOW (1987). The EDTA-soluble extract from the dorsal valve of *N. anomala* contains two proteins of molecular weight 44 and 60 kDa

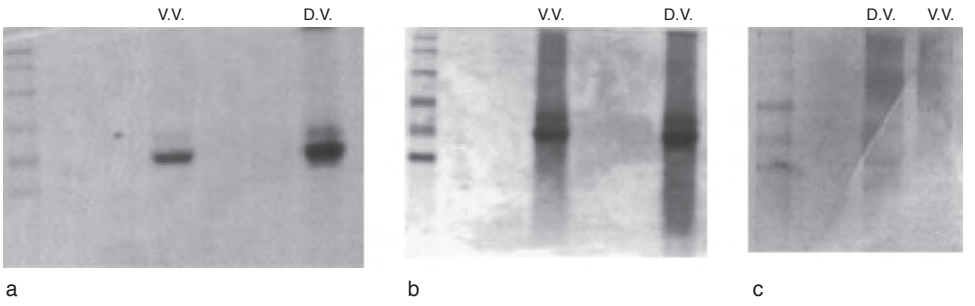

FIG. 1540. SDS PAGE gel and glyco-blot of protein extract from *N. anomala* valves. Digitized images of proteins extracted from the dorsal (*D.V.*) and ventral (*V.V.*) valves of *Neocrania anomala* and analyzed by SDS PAGE. Prestained proteins of apparent molecular weight 126, 102, 81, 53.5, 37, and 31 kDa were included in the left of each gel; *a,* proteins were fractionated by electrophoresis in a 15% polyacrylamide gel and then fixed and revealed using Coomassie-Blue; *b,* gel from *a* was then probed using silver staining; *c,* equivalent samples to those shown in *a* and *b* were electrophoresed on a 15% polyacrylamide gel and then electroblotted onto ProBlott membrane and probed with Concanavalin A to detect glycoproteins (Cusack & Williams, 2001a).

(Fig. 1540a). The 60 kDa protein is glycosylated (Fig. 1540c), as is a 30 kDa protein that is only evident using silver staining (Fig. 1540b) or by detection of the glycosylation (CUSACK & WILLIAMS, 2001a). The 44 kDa protein is present in both dorsal and ventral valves but is more abundant in dorsal valves. The 44 and 30 kDa proteins are present in both valves while only the 60 kDa protein is present in the dorsal valves. The amino acid composition of the most abundant protein, the 44 kDa protein, is presented in Table 29. The most striking features of this amino acid suite are the high proportion of acidic amino acids (aspartic acid and glutamic acid) and glycine and the low proportion of basic amino acids (histidine, arginine, and lysine).

This 44 kDa protein is the most abundant interlaminar polymer (BROWN, 1998). Induced degradation of laminae in craniid shells, including enzymic digestion, showed that calcite tablets were doped with proteins (WILLIAMS, CUSACK, & BROWN, 1999). Doping occurs by centripetal growth of the top granular layers of ramparts that trap the 44 kDa protein within tablets. The (0k.l) sites are doped mainly by the glycosylated 60 kDa protein (BROWN, 1998; WILLIAMS, CUSACK, & BROWN, 1999). The 44 and 60 kDa proteins react with Stains-All, indicating that these proteins are acidic (as confirmed by amino acid analysis) and suggesting that they are likely to be calcium binding (CUSACK & others, 2000).

NOVOCRANIA ANOMALA SHELL PROTEINS AND *IN VITRO* CRYSTALLIZATION

Synthetic calcite crystals were grown according to the method of ADDADI and WEINER (1985). The influence of *N. anomala* shell proteins on crystal growth was determined by introducing 10 µl of concentrated

TABLE 29. Amino acid composition (mole %), using the one letter code for amino acids, of the 44 kDa protein from *N. anomala* (new).

Amino acid	44 kDa
D/N	18.5
E/Q	13.9
S	7.6
G	9.1
H	6.0
R	3.9
T	4.5
A	3.4
P	4.9
Y	3.4
V	5.0
M	4.9
C	0.0
I	6.2
L	3.5
F	3.8
K	0.9

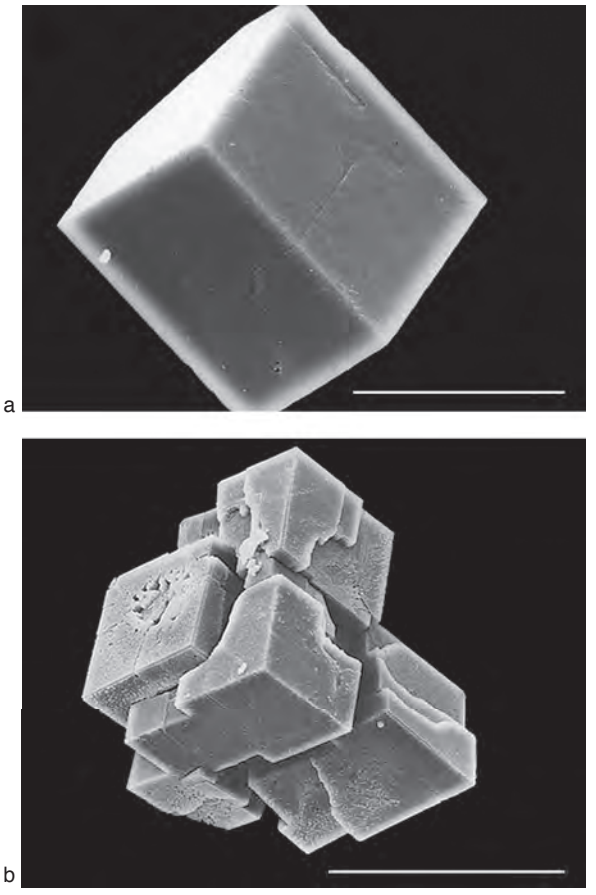

FIG. 1541. Influence of *N. anomala* shell proteins on calcite growth *in vitro*. Scanning electron micrographs of gold-coated calcite crystals grown *in vitro* according to the method of ADDADI and WEINER (1985) in the absence of any additives (*a*) and in the presence of 1.2 µg intracrystalline protein from *N. anomala* dorsal valves (*b*); scale bars: 20 µm and 50 µm (Cusack & others, 2000).

protein extract after 24 hours crystal growth. Controls were included in which only 18 MΩ water or nonmineral associated proteins such as serum albumin were added. Crystals grown in the absence of any protein had perfect rhombohedral morphology. The addition of intracrystalline proteins from *N. anomala* resulted in altered crystal morphology displaying intergrowth of crystals at final protein concentrations of 1.2 µg per ml (Fig. 1541). This effect is specific and is likely to result from the presence of the 44 and 60 kDa proteins, since at concentrations of 2 µg/ml, nonmineral associated proteins such as serum albumin had no effect on crystal morphology.

FOSSIL SHELL BIOCHEMISTRY

During fossilization, the magnesium in the calcite of the living craniid shell is replaced by calcium, and a high magnesium content is not diagnostic of fossil species (J. ENGLAND, personal communication, 2007). Magnesium distribution and concentration (Fig. 1542) was measured in the shells of the Ordovician *Petrocrania scabiosa*, the Carboniferous *Petrocrania modesta,* and the Cretaceous *Crania craniolaris*. None of the

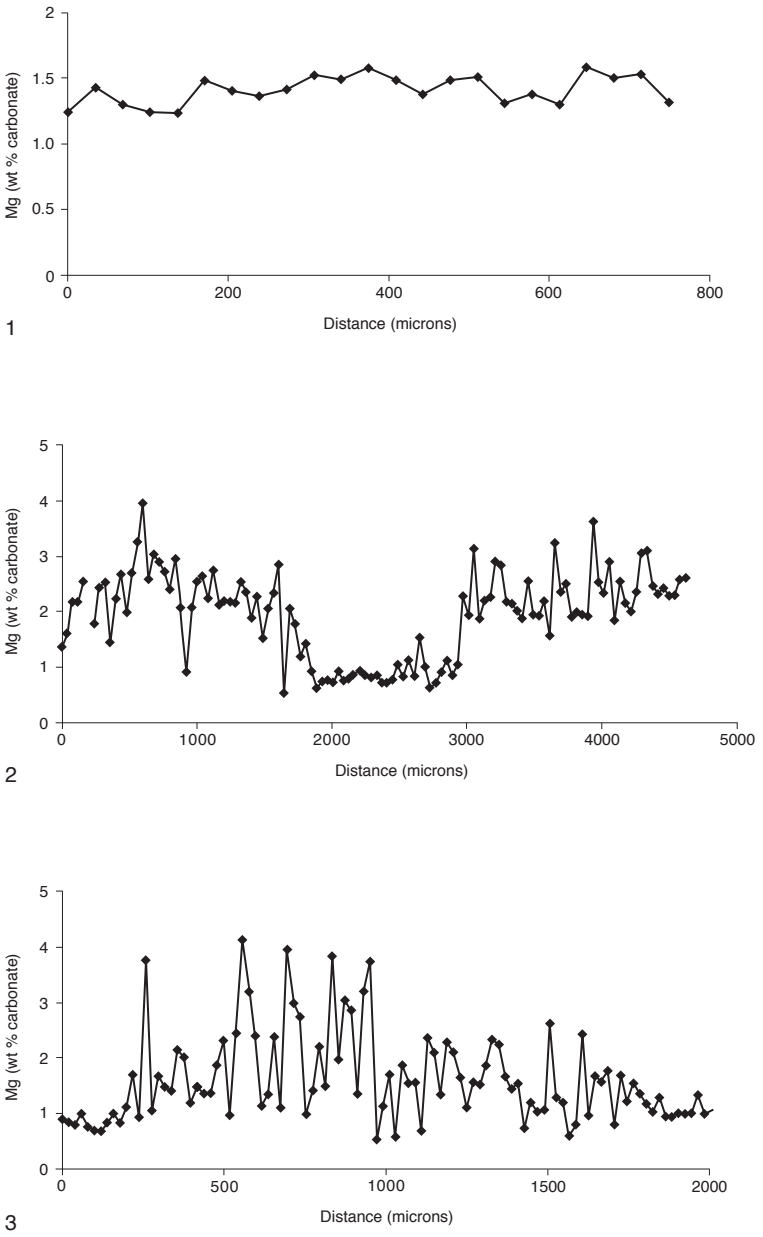

FIG. 1542. Magnesium concentration and distribution in calcite of fossil craniiform shells. Shells of *1, Crania craniolaris* (Cretaceous), *2, Petrocrania modesta* (Carboniferous), and *3, Petrocrania scabiosa* (Ordovician) were prepared and analyzed as described in Figure 1538 (new).

specimens had high magnesium concentrations.

In all fossil craniids examined by CUSACK and WILLIAMS (2001a), there is a reduction, with the increasing geological age of species, in the range and concentration of amino acids to a residue of acidic and aliphatic ones (Table 30). The acidic amino acids may be protected by interaction with calcite, while the other amino acids to survive are simple and robust like those preserved in other fossil brachiopods. Aspartic acid/asparagine,

TABLE 30. Amino acids extracted from shells of cranioid brachiopods; one-letter code for amino acids is used. Samples were dissolved in HCl. The values for modern valves are expressed as absolute quantities/mg shell and as mole% values; i.e., relative quantities if each valve contained 100 pmoles amino acid/mg shell. In all cases, values represent pmoles amino acid /mg sample (new).

Species	Age	Amino acids D	E	S	G	H	R	T	A	P	Y	V	M	I	L	F	K	Total
Novocrania anomala (dorsal)	modern	32.6	3.4	16.3	18.6	0	1.8	4.5	5.4	3.4	0.4	3.2	0	1.5	2.9	1.1	3.5	100
Novocrania anomala (ventral)		18.9	4.8	6.3	17.0	0	3.3	5.4	7.3	8.8	0.7	6 .4	0	3.9	5.9	3.0	8.1	100

Species	Age	Amino acids D	E	S	G	T	A	V	I	L	Total
Crania craniolaris (ventral)	Upper Cretaceous	4.2	5.1	4.4	15.1	2.0	11.3	4.5	4.1	2.7	53.4
Isocrania egnanbergensis (dorsal)	Upper Cretaceous	0.5	2.2	2.6	12.8	6.2	5.9	2.2	0	3.3	35.6
I. egnanbergensis (ventral)		0.3	2.1	2.2	11.6	6.4	5.8	2.3	1.5	2.7	34.8
Orthisocrania planissima (shell and matrix)	Upper Ordovician	7.8	2.2	1.0	5.3	0.8	1.1	0.5	0	1.0	19.7
O. planissima (shell)		0.6	1.6	3.0	8.5	1.2	2.5	1.2	0	0.8	19.4
matrix		0.5	0	0.6	3.3	0.6	0.9	0.4	0	0.7	7.0
Petrocrania scabiosa	Upper Ordovician	1.5	2.9	3.8	6.1	2.3	3.1	1.5	0	0.7	21.7
P. scabiosa Waynesville, Indiana		1.1	2.6	1.9	1.6	1.0	1.1	1.7	0	0.9	11.9
P. scabiosa Rafinesquina		0.9	1.8	3.8	12.4	2.8	3.1	3.5	0	1.0	29.3
P. scabiosa dalmanellid		1.0	0.7	1.3	5.3	0.5	1.1	0.5	0	1.3	11.8
Pseudocrania petropolitana (matrix)	Lower Ordovician	5.9	6.6	6.9	4.4	1.4	1.3	0.3	0	0.5	27.2
		0.4	0.3	1.5	3.2	1.3	1.7	0.9	0	0	9.3
Crania rhykholtiania (ventral, dorsal, and matrix)	Carboniferous	2.8	1.8	1.5	2.6	0	1.8	0	0	0	10.5
C. rhykholtiania (ventral and matrix)		2.2	0.9	0.8	3.9	0	2.3	0.8	0	0.8	11.7
matrix		3.3	1.6	1.5	3.4	0	1.7	0	0	0	11.5

serine, and glycine that occur in high concentrations in *Novocrania* shells survive in all fossil specimens from Upper Cretaceous and Carboniferous sediments. The ratio of D/N:S:G, however, bears no resemblance to that characterizing *Novocrania*. Basic amino acids (histidine, arginine, and lysine) and aromatic amino acids (tyrosine, proline, and phenylalanine) are not detected in the fossil samples.

ORGANOCARBONATE RHYNCHONELLIFORM SHELL CHEMISTRY

Since the 1997 *Treatise,* the distribution of magnesium in calcite of rhynchonelliform valves has been determined, and several of the proteins have been characterized further, identifying those that are glycosylated and those that have potential calcium-binding properties.

LIVING SHELL MINERALOGY

The mineral ultrastructure is consistent throughout the Rhynchonelliformea, with the primary layer of growth-banded calcite underlain by a secondary layer of calcite fibers as typified by living *Notosaria.* Most thecideidines vary from this theme with a shell comprised of primary layer throughout. The other variation occurs in *Liothyrella* where there is a tertiary layer of prismatic calcite (WILLIAMS, 1968a). Exceptions aside, the uniformity in ultrastructure is not registered in the concentration and distribution

of magnesium in the calcite of rhynchonelliform shells.

In marine biogenic carbonates, the Mg:Ca ratio increases with increasing temperature, providing a means of determining the temperature at which the carbonate was precipitated. Mg:Ca ratio is a proxy that, unlike skeletal $\delta^{18}O$, is unaffected by seawater salinity (Klein, Lohmann, & Thayer, 1996). This relationship between Mg:Ca ratio and temperature has been demonstrated in several such marine carbonate systems as benthic foraminifera (Lear, Elderfield, & Wilson, 2000), planktonic foraminifera (Elderfield & Ganssen, 2000), and coccoliths (Stoll & others, 2001). In 1996, Rao demonstrated that Tasmanian brachiopods recorded accurately the temperature of calcite deposition as expected by slow-growing low magnesium calcite.

England, Cusack, and Lee (2007) reported differences between the magnesium content and distribution in shells of *Terebratulina retusa* and *Novocrania anomala* when the specimens were collected from the same site and the calcite had therefore been precipitated at the same temperature. While *N. anomala* has 2.55 wt% magnesium throughout the shell, *T. retusa* shells have a lower overall magnesium content. In *T. retusa*, however, the magnesium is not evenly distributed, with the highest concentration (3.5 wt%) being in the primary layer and a maximum concentration of 1.5 wt% in the secondary layer, with an average secondary layer concentration of 1 wt%. The contrast in magnesium distribution is not restricted to intersubphyla comparisons but is evident within the subphylum Rhynchonelliformea. Buening and Carlson (1992) noted changes in magnesium content associated with ontogeny in *Terebratulina unguicula* and *Terebratalia transversa,* where the magnesium concentration in the umbo is at least double that in the shell anterior. In 1961, Lowenstam suggested that magnesium and strontium varies with brachiopod taxonomy. Buening and Carlson (1992) demonstrated that, in addition to ontogenetic influences, taxonomic differences do occur with the demonstration that *Terebratulina unguicula* has a higher magnesium content than *Terebratalia transversa*. Buening (1998) expanded the analyses to include the elements copper, zinc, manganese, and iron in two species of rhynchonelliform brachiopods from New Zealand: *Calloria inconspicua* and *Notosaria nigricans*. In both species, the elements Cu, Mn, Fe, and Zn were concentrated in the primary layer of the shell.

The distribution of magnesium through the shell layers of several species of the class Rhynchonellata, including members of the three extant orders, Rhynchonellida, Thecideida, and Terebratulida, is presented in Figure 1543. The umbonal region was avoided, and analyses were carried out in the median area of the shell, avoiding any regions of specialization. In *Liothyrella uva*, the Mg concentration is on average 1.1 wt%, but Mg concentration in the inner, tertiary layer is much higher than in the outer two-thirds of shell. This is not the case in *Liothyrella neozelanica* where the Mg concentration is low and effectively constant (mean = 0.35 wt%) throughout the shell. *Neothyris lenticularis* valves contain similar Mg concentrations to *L. neozelanica* with an average Mg content of 0.34 wt% distributed evenly throughout the shell. *Laqueus rubellus* and *Terebratella sanguinea* also have similar Mg contents (0.46 wt% and 0.49 wt% respectively), and in both cases the innermost and outermost regions of the shell have slightly elevated Mg concentrations. In *Calloria inconspicua* the average Mg concentration is 0.45 wt%, with a lower Mg concentration in the inner third of the shell. *Lacazella mediterranea* has the lowest Mg content of the brachiopods surveyed, with a mean value 0.03 wt% throughout the shell. In contrast, *Thecidellina barretti* has an overall Mg content (10.15 wt%), similar to the craniiform valves. The distribution of Mg in *Terebratulina retusa* and *Notosaria nigricans* are similar, with elevated Mg concentration in the primary layer

FIG. 1543. Magnesium concentration and distribution in calcite of rhynchonelliform shells. Shells were prepared and analyzed as described in Figure 1538. Note different scales on graphs (new).

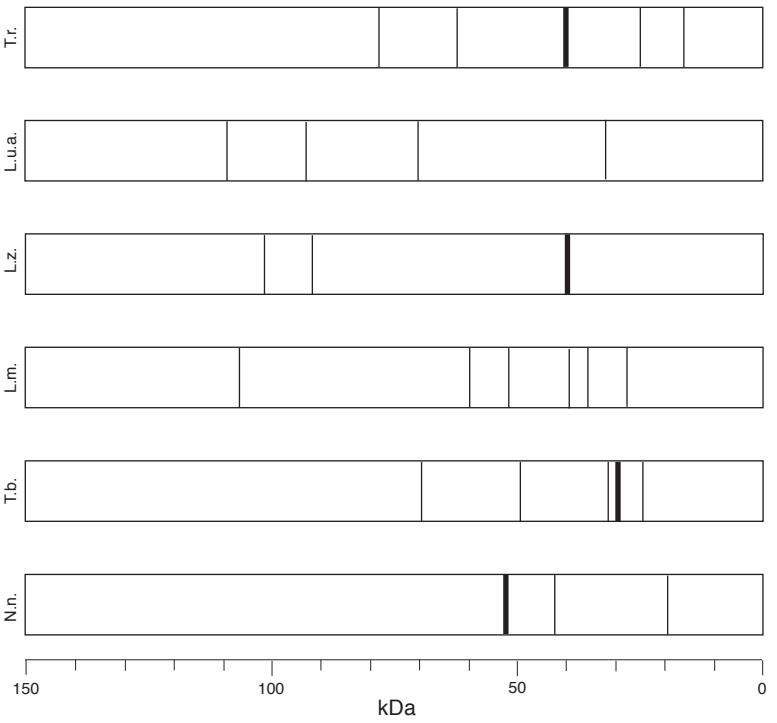

FIG. 1544. Diagrammatic representation of SDS PAGE analyses of proteins from rhynchonelliformean shells. Molecular weights (kDa) of the principal intracrystalline proteins, identified by SDS PAGE analysis in the shells of *Notosaria nigricans* (*N.n.*), *Thecidellina blochmanni* (*T.b.*), *Lacazella mediterranea* (*L.m.*), *Liothyrella neozelanica* (*L.z.*), *Liothyrella uva antarctica* (*L.u.a.*), and *Terebratulina retusa* (*T.r.*); thickened bars indicate proteins in comparatively high concentrations (Cusack & Williams, 2001b).

(1.2 wt% and 1.6 wt% respectively) and much lower and constant Mg concentrations throughout the rest of the shell (0.5 wt% and 0.3 wt% respectively). Overall, the Mg content of *T. retusa* is higher than that of *N. nigricans,* with mean values of 0.91 wt% and 0.66 wt% respectively.

LIVING SHELL BIOCHEMISTRY

Comparison of intracrystalline EDTA-soluble proteins from species of 3 ordinal groups revealed up to 21 proteins of molecular weight range 16 to 209 kDa (Fig 1544). None could be identified as specific to and therefore involved in the calcification of one or another of the layers of the rhynchonellate shell (CUSACK & WILLIAMS, 2001b). While the precise relationship between the organic and inorganic components is currently elusive, it is evident that not all of the proteins extracted need to play a calcifying role in the laminae. Indeed, some of these proteins could have arisen subsequent to the phylogenetic divergence of the terebratulides and thecideidines from their rhynchonellate sister group. Therefore, until those proteins involved in calcification are identified and their role understood, the protein chemistry of rhynchonellate shells is a less comprehensible guide than ultrastructure to ordinal genealogy (CUSACK & WILLIAMS, 2001b).

Organic content accounts for 3% of the dry weight of *T. retusa* shells. Proteins extracted and then fractionated using SDS PAGE had molecular weights of 16, 25,

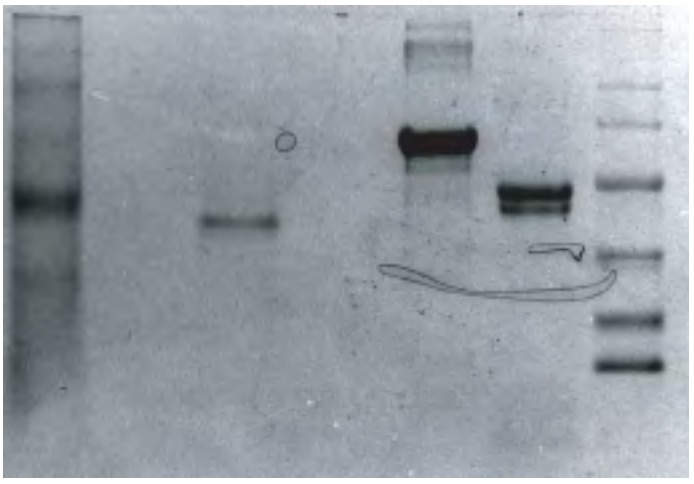

FIG. 1545. SDS PAGE of proteins from shells of *T. retusa.* SDS PAGE gel of EDTA-soluble intracrystalline extract of *T. retusa and N. anomala. Lane 1.* Prestained proteins of apparent molecular weight 97.4, 68, 43, 29, and 18.4 and 14.3 kDa. *2.* Ovalbumin (5 µg). *3.* BSA (5 µg). *4.* Blank. *5. N. anomala* shell extract (1 µg protein). *6.* Blank. 7. *T. retusa* shell extract (1.05 µg protein). Proteins fixed and visualized with Coomassie Brilliant Blue (CBB) (Cusack & others, 2000).

TABLE 31. Amino acid composition of the 40 kDa intracrystalline protein from shells of *T. retusa* (amino acids stated as residues per 100 amino acid residues). Values are the average of three analyses (new).

Amino acid	40 kDa
D/N	11.3
E/Q	12.2
S	8.5
G	13.7
H	0.0
R	4.4
T	6.4
A	9.2
P	0.0
Y	1.2
V	8.4
M	1.8
C	0.0
I	8.9
L	9.7
F	4.0
K	0.0

40, 62, and 78 kDa (Fig. 1545). The 40 kDa protein is the most abundant protein present; its amino acid composition is given in Table 31. This protein contains a high proportion of acidic amino acids (aspartic acid and glutamic acid) and glycine and a smaller proportion of basic amino acids (histidine, arginine, and lysine). Both this 40 kDa and the 62 kDa protein are glycosylated (Fig. 1546).

TEREBRATULINA RETUSA SHELL PROTEINS AND *IN VITRO* CRYSTALLIZATION

Synthetic calcite crystals were grown using the methods described for *N. anomala.* The addition of intracrystalline proteins from *T. retusa* resulted in altered crystal morphology displaying intergrowth of crystals at protein concentrations of 0.04 µg per ml for *T. retusa* (Fig. 1547). At concentrations of 2

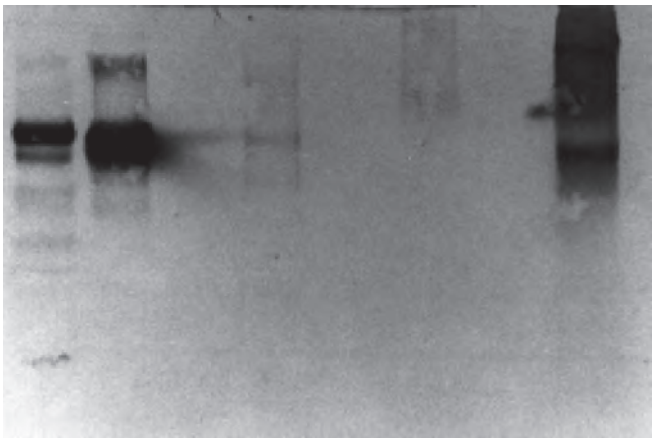

FIG. 1546. Electroblot of protein extract from *T. retusa* valves, reacted with Concanavalin-A to detect glycoproteins. Affinoblot of EDTA-soluble intracrystalline proteins from *T. retusa* and *N. anomala*, bovine serum albumin (BSA), and ovalbumin. Proteins fractionated by SDS PAGE, electrotransferred onto ProBlott membrane and reacted with Concanavalin A to detect glycoproteins (Faye & Chrispeels, 1985). *Lane 1.* Prestained proteins of apparent molecular weight 97.4, 68, 43, 29, 18.4, and 14.3 kDa. *2.* Ovalbumin (5 µg). *3.* BSA (5 µg). *4.* Osteonectin (0.6 µg). *5.* Blank. *6. N. anomala* shell extract (1 µg protein). *7.* Blank. *8. T. retusa* shell extract (1.05 µg protein) (Cusack & others, 2000).

µg/ml, nonmineral associated proteins such as serum albumin had no effect on crystal morphology. Crystal clustering occurs at much lower protein concentrations (0.04 µg/ml) with *T. retusa* shell proteins than with *N. anomala* proteins (1.2 µg/ml), suggesting that the *T. retusa* shell proteins or a component thereof is 30 times more potent than the *N. anomala* proteins.

FOSSIL SHELL BIOCHEMISTRY

Rapid and thorough degradation of proteins from Linguliformea and Craniformea shells strongly suggests that protein degradation would also be thorough in the Rhynchonelliformea, reducing the amino acids to a robust suite not representative of the diversity within the subphylum. One means of testing this assumption would be to carry out amino acid analyses from extracts of the same environment, perhaps using the well-preserved material of the Scottish Carboniferous.

CONCLUSIONS

Although rapid and almost complete protein degradation means that the rich source of information is lost in the fossil record, much information is to be gained regarding evolutionary relationships and biomineralization. In the three subphyla, the protein complement of the shells is complex and diverse. The characteristics of the proteins are specific to each subphylum. The role of these proteins in mineralization has been demonstrated for *L. anatina* and suggested for *N. anomala* and *T. retusa*. In order to progress these findings effectively, characterization of individual proteins and identification of their individual influence

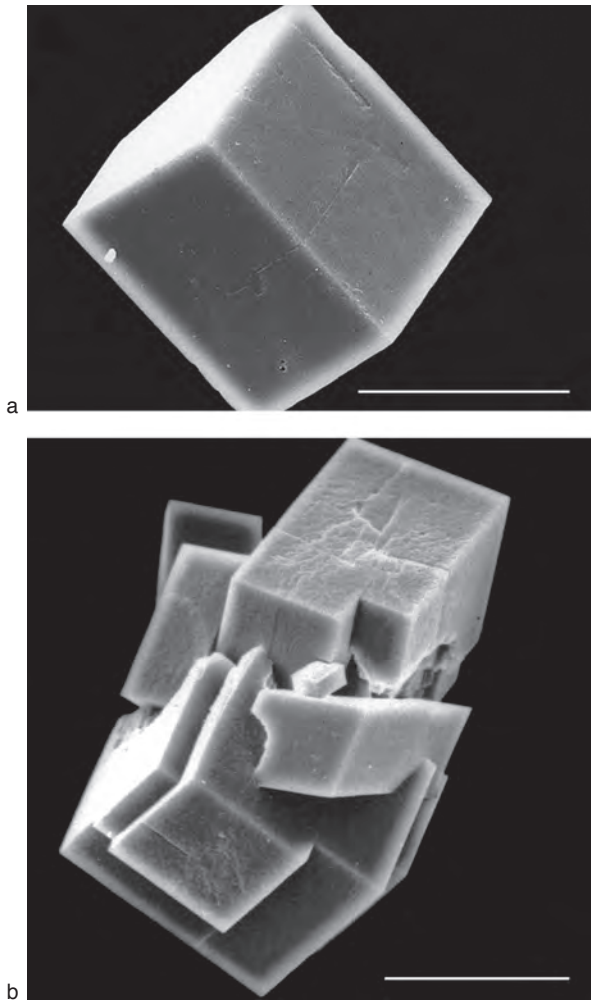

FIG. 1547. Influence of *T. retusa* shell proteins on calcite growth *in vitro*. Scanning electron micrographs of gold-coated calcite crystals grown *in vitro* according to the method of ADDADI and WEINER (1985) in the absence of any additives (*a*) and in the presence of 1.2 µg intracrystalline protein from *T. retusa* valves (*b*); scale bars: 20 µm (Cusack & others, 2000).

on mineral formation and thus their role in biomineralization would greatly advance our knowledge beyond the consideration of protein mixtures where there is always the possibility of the effect of one protein masking that of another. This approach of characterizing individual proteins has resulted in significant progress being made in other biominerals systems such as siliceous sponges (SHIMIZU & others, 1998) as well as other calcium carbonate marine invertebrates (MICHENFELDER & others, 2003; MARIN & others, 2005; KIM & others, 2006).

The observation that several of the brachiopod shell proteins are glycosylated should be pursued since the polysaccha-

ride moieties of glycoproteins influence calcium carbonate growth *in vitro* (Albeck, Weiner, & Addadi, 1996). The presence of carbohydrates in brachiopod shells has been noted by several workers (Jope, 1965; Pan & Watabe, 1988; 1989; Collins & others, 1991; Clegg, 1993; Cusack, Walton, & Curry, 1997). In addition, acidic sulphated sugars have been described in other marine invertebrate calcium carbonate biominerals including corals (Cuif & others, 2003) and bivalves (Dauphin & others, 2003, 2005). The widespread occurrence of these acidic polysaccharides suggests a fundamental role in biomineralisation that should be explored. The role of mucins in molluscan calcification (Marin & others, 1996, 2000) suggests that this should also be investigated in brachiopods.

The assertion that the shells of the Rhynchonelliformea and Craniiformea are composed of low magnesium calcite is not true in all cases. Even in instances where it is true, magnesium distribution is not even. This has important implications for the use of brachiopod shells as paleothermometers since the magnesium content is influenced by temperature, but this may be via kinetic influence that could be exerted by other factors such as organic components. Ultimately, it is necessary to determine whether magnesium is a true lattice component, since this is the basis of the Mg:Ca ratio proxy for water temperature.

ACKNOWLEDGMENTS

I would like to acknowledge my huge appreciation of all that the late Sir Alwyn Williams taught me, mostly by example, over the course of our 14-year collaboration. A dear friend and colleague, his enthusiasm, drive, and scientific rigor have been inspirational.

Sincere thanks to all those institutions and individuals who provided material used in the work referred to in this chapter. Daphne Lee (University of Otago) is thanked for arranging provision of *N. huttoni* specimens from the National Museum of New Zealand and Bernie Cohen (University of Glasgow) for providing specimens of *N. norfolki*. Jenny England is thanked for her major contribution to the microprobe analyses of magnesium.

Financial assistance from the NERC (GR 3/09604 and GR 9/02038), the Royal Society (RSR A/C 027 and RSS QG 16604), and the EPSRC (GR/R23107/01) is gratefully acknowledged.